The automatic optimization of metal forming processes

Inverse identification of constitutive parameters for tubular materials based on hydraulic bulge test

Zhang, Bin

DOI (link to publication from Publisher):
10.54337/aau468602757

Publication date:
2022

Document Version
Publisher's PDF, also known as Version of record

THE AUTOMATIC OPTIMIZATION OF METAL FORMING PROCESSES

– INVERSE IDENTIFICATION OF CONSTITUTIVE PARAMETERS FOR TUBULAR MATERIALS BASED ON HYDRAULIC BULGE TEST

BY
BIN ZHANG

DISSERTATION SUBMITTED 2022

AALBORG UNIVERSITY
DENMARK

The automatic optimization of metal forming processes

-Inverse identification of constitutive parameters for tubular materials based on hydraulic bulge test

Ph.D. Dissertation

by

Bin Zhang

Department of Materials and Production, Aalborg University
Fibigerstræde 16, 9220 Aalborg East, Denmark
E-mail: zb@mp.aau.dk

Dissertation submitted January 20, 2022

Dissertation submitted: January 20, 2022

PhD supervisor: Associate Professor Benny Endelt
Aalborg University

PhD Co-supervisor: R&D Lab Scientist Karl Brian Nielsen
Vestas aircoil A/S

PhD committee: Associate Professor Jens Henrik Andersen (chair)
Aalborg University, Denmark

Professor Cheng Lu
University of Wollongong, Australia

Associate Professor Jun Ma
Norwegian University of Science and Technology, Norway

PhD Series: Faculty of Engineering and Science, Aalborg University

Department: Department of Materials and Production

ISSN (online): 2446-1636
ISBN (online): 978-87-7573-950-9

Published by:
Aalborg University Press
Kroghstræde 3
DK – 9220 Aalborg Ø
Phone: +45 99407140
aauf@forlag.aau.dk
forlag.aau.dk

Printed in Denmark by Rosendahls, 2022

Abstract

Tube hydroforming process is an advanced manufacturing technology for complex thin-walled tubular components applied in the aerospace, aviation and automotive industries. The fluid medium is used as a pressure source to deform tubular materials into the desired shape in this process. Finite element model is a popular method to describe and analyze this innovative process. A successful tube hydroforming operation and reliable finite element simulation depend heavily on the accurate characterization of mechanical properties of the incoming tubular materials. As a result, it is critical to determine these material parameters utilizing suitable experimental tests and evaluation procedures.

This thesis presents the development of an automatic inverse parameter identification framework combining finite element models with gradient-based algorithms and its utilization in determining material parameters for thin-walled metallic tubes. The main principle of the inverse framework is the minimization of the objective function defined as the least square error between simulated results and experimental observations. Finite element methods are used to describe and analyze the experimental testing process and gradient-based optimization techniques adjust the input material parameters in the model until the calculated results have a good agreement with the experimental measurements.

The feasibility and performance of this proposed inverse framework are demonstrated through applying it to different tube hydraulic bulge tests with fixed and forced end-conditions to identify the flow stress data of thin-walled aluminium tubes. The bulge height, axial compressive force and pole thickness are measured during the experiment and input into the inverse strategy. Based on the obtained material values, finite element simulated models of hydroforming processes are established and used to predict the shape properties of final products. The comparison between simulated predictions and experimental data shows that the developed inverse strategy provide a robust and effective method to determine material properties for thin-walled metallic tubes.

Furthermore, a theoretical analysis is integrated into the inverse frame-

work, and the two are recombined into a hybrid strategy to avoid local minimums in the parameter identification process. The new strategy is tested by the experimental data from fixed and forced tube hydraulic bulge tests. As a result of this research, it is possible to conclude that the novel hybrid strategy does not depend heavily on the initial points and can improve the computation robustness and identify more accurate constitutive parameters for tubular materials.

Resumé

Tube hydroformingsproces er en avanceret fremstillingsteknologi til komplekse tyndvæggede rørformede komponenter, der anvendes inden for rum-, luftfarts- og bilindustrien. Væskemediet bruges som en trykkilde til at deformere rørformede materialer til den ønskede form i denne proces. Endeligt element model er en populær metode til at beskrive og analysere denne innovative proces. En vellykket rørhydroformningsoperation og pålidelig simulering af endelige elementer afhænger i høj grad af den nøjagtige karakterisering af de indkommende rørformede materialers mekaniske egenskaber. Som et resultat er det afgørende at bestemme disse materialeparametre ved hjælp af egnede eksperimentelle test og evalueringsprocedurer.

Denne afhandling præsenterer udviklingen af en automatisk invers parameter identifikationsramme, der kombinerer finite element modeller med gradientbaserede algoritmer og dens anvendelse til at bestemme materiale parametre for tyndvæggede metalrør. Hovedprincippet for den inverse ramme er minimering af den objektive funktion defineret som den mindst kvadratiske fejl mellem simulerede resultater og eksperimentelle observationer. Endelige elementmetoder bruges til at beskrive og analysere den eksperimentelle testproces, og gradientbaserede optimeringsteknikker justerer input materiale parametrene i modellen, indtil de beregnede resultater har en god overensstemmelse med de eksperimentelle målinger.

Gennemførligheden og ydeevnen af denne foreslåede omvendte ramme demonstreres ved at anvende den på forskellige rørhydrauliske udbulningstest med faste og tvungne endebetingelser for at identificere strømspændingsdata for tyndvæggede aluminiumsrør. Bulehøjden, den aksiale trykstyrke og poltykkelsen måles under forsøget og input til den inverse strategi. Baseret på de opnåede materialeværdier etableres finite element simulerede modeller af hydroformningsprocesser og bruges til at forudsige formegenskaberne for slutprodukter. Sammenligningen mellem simulerede forudsigelser og eksperimentelle data viser, at den udviklede inverse strategi giver en robust og effektiv metode til at bestemme materialegenskaber for tyndvæggede metalliske rør.

Endvidere er en teoretisk analyse integreret i den omvendte ramme for

at danne en hybrid strategi for at undgå lokale minimumsværdier i parameteridentifikationsprocessen. Den nye strategi er testet af de eksperimentelle data fra faste og tvungne rørhydrauliske buletests. Som et resultat af denne forskning er det muligt at konkludere, at den nye hybridstrategi ikke er stærkt afhængig af de indledende punkter og kan forbedre beregnings robustheden og identificere mere præcise konstituerende parametre for rørformede materialer.

Publications

Scientific contributions have been published or submitted to internationally acknowledged journals and conference proceedings with peer-reviewed.

Journal Papers

1. Bin Zhang, Benny Endelt, and Karl Brian Nielsen. "Characterization of mechanical properties for tubular materials based on hydraulic bulge test under axial feeding force." *Fundamental Research*. Minor revision.

2. Bin Zhang, Benny Endelt, Lihui Lang, and Karl Brian Nielsen. "Identification of constitutive parameters for thin-walled aluminium tubes using a hybrid strategy." *Materials Today Communications*. Accepted. DOI: https://doi.org/10.1016/j.mtcomm.2021.102670

3. Bin Zhang, Benny Endelt, Lihui Lang, Yang Zhao, Shu Yan, and Karl Brian Nielsen. "An inverse strategy to determine constitutive parameters of tubular materials for hydroforming processes." *Chinese Journal of Aeronautics*. Accepted. DOI: https://doi.org/10.1016/j.cja.2021.11.007

Conference Papers

1. Bin Zhang, Benny Endelt, Lihui Lang, Yang Zhao, Shu Yan and Karl Brian Nielsen. "The identification of strain-stress curve for 5049 aluminium based on tube hydraulic bulge test." In *24th International Conference on Material Forming (ESAFORM)*, Liege, Belgium, April, 2021.

2. Bin Zhang, Benny Endelt, and Karl Brian Nielsen. "Parameter automatic identification of tubular materials for metal forming processes." In *1st International Symposium on Metal Processing (ISMP)*, Shenyang, China, October, 2021.

Contents

List of Figures

Preface

This thesis is submitted to the Faculty of Engineering and Science at Aalborg University in partial fulfillment of the requirements for the degree of Doctor of Philosophy. The research work in this thesis has been carried out from November 2017 to November 2021 at Materials Processing Group of Department of Materials and Production.

This research is partially supported by China Scholarship Council, Grant No. 201706080020, which is a non-profit institution and provides the international airfare and the living stipend during the author's study at Aalborg University.

First of all I would like to express sincere gratitude to my supervisors, Associate Professor Benny Endelt and R&D Lab Scientist Karl Brian Nielsen, for their patient guidance, constant encouragement and insightful suggestions. Their comments helped me optimize the logical structure and improve the written English of published papers and this thesis.

Furthermore, I would like to thank all my colleagues I have known at Aalborg University for the created positive environment and technical support during my Ph.D. study. Also a thank to the members of my research team, Anders Noel Thomsen and Rathesan Ravendran, for valuable discussions with them on computer software and programming skills.

Last but not least, I would like to deeply thank my family and friends for their outstanding support and long-term company during the four-year study period.

Bin Zhang
Aalborg in winter

Chapter 1

Introduction

This chapter covers the project and scientific background of this thesis. Research methodology and motivation are also briefly discussed in this chapter, and finally the thesis overview is listed.

1.1 Industrial background

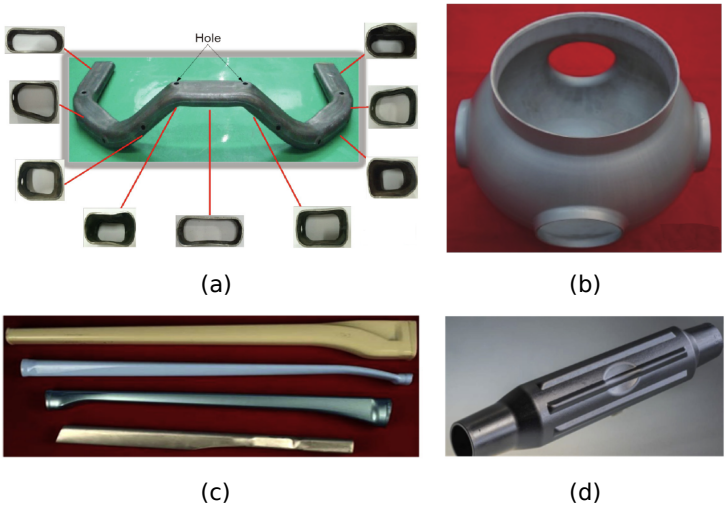

Figure. 1.1. Example of complex shaped tubular components applied in industry: (a) chassis engine cradle, (b) integrated part with five branches, (c) bicycle frame rail, and (d) exhaust system component [1, 2].

Tube hydroforming is an advanced modern manufacturing technology which can be used to form a variety of complex shaped thin-walled com-

ponents [1], as shown in Fig. 1.1. Compared with the conventional forming technique, it can not only reduce the complexity and cost of tooling sets, but also improve the dimensional tolerance and surface finish of the product [3–5]. Therefore, hydroformed tubular components are widely applied in the automotive, aerospace and aviation industries [6–9].

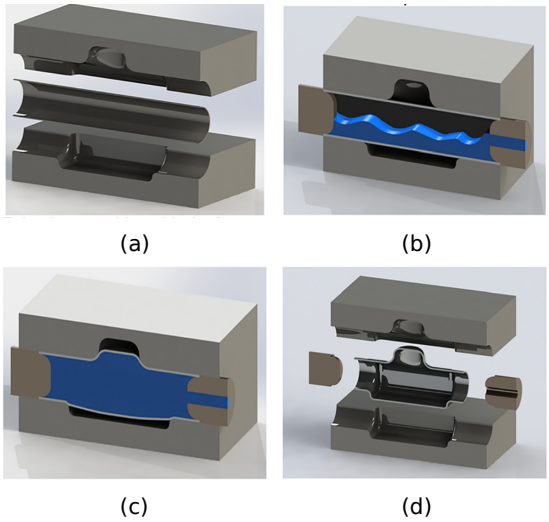

Figure. 1.2. Process sequence in tube hydroforming process: (a) installation and positioning, (b) clamping and filling medium, (c) part forming, and (d) relieve fluid pressures and obtain the final component [5].

Fig. 1.2 presents a schematic diagram of a typical tube hydroforming process. In this process, a tubular metal is formed into a die cavity of the specified shape under the internal fluid pressure with or without axial compressive forces [10]. Different types of hydroformed components, see Fig. 1.3, can be manufactured by changing the die shape and process control parameters, in which the latter one depends on loading paths, i.e., the combination of axial feeds and hydraulic internal pressures.

Axial feeds: Adjust the axial displacement and punch velocity to improve tubes' formability but excessive or rapid axial feeds may cause wrinkling or buckling of workpieces.

Internal pressures: Push the tube wall into the die cavity to avoid wrinkles but excessively high fluid pressures may lead to the bursting of tubular samples at early forming stage.

A stable hydroforming process and desired tubular finished products depends heavily on the information of the hydraulic press and its control system, raw material properties and tribological conditions. Among them, the

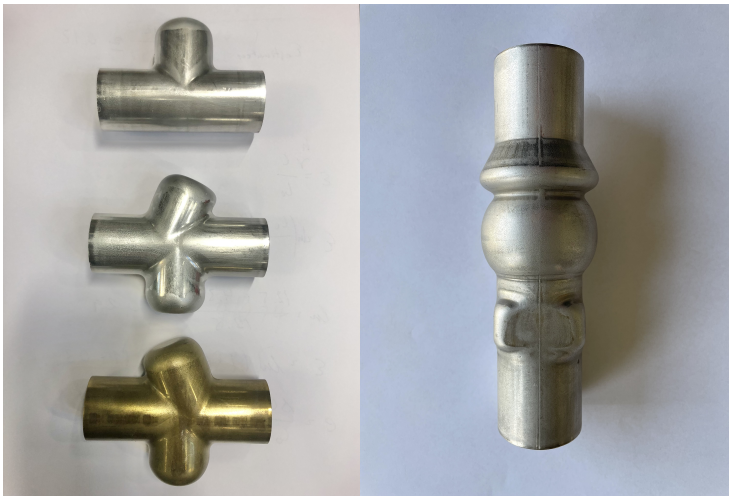

Figure. 1.3. Different hydroformed tubular components manufactured at Aalborg University.

tubular material characteristic, such as yield and tensile strength, anisotropy value, hardening exponent and so on, are the most fundamental knowledge for engineers in the actual industrial production [11–13]. It provides the basics for choosing the suitable tools under the maximum forming force of the machine and has a significant impact on final qualities of hydroformed components, so material mechanical properties must be identified before process development stage [14, 15].

On the other hand, numerical simulation technologies have presented strong superiority and potential in exploring new insights and predicting the outcome of real metal forming processes [16], especially the application of finite element(FE) methods in tube hydroforming processes. From simple axisymmetric parts to complex shaped components, from an one-step forming process to the entire production chain, from manual trial and error to intelligent optimization of simulations, a significant advance of FE modelling technique is made and it has successfully help researchers and engineers to determine the optimum process parameters and predict the material flow and final product while avoiding the wrinkling and bursting, which means that process development time and product cost can be reduced and production efficiency will be improved [17]. However, one prerequisite of the reliable prediction results from FE simulations is the more accurate input parameters of tubular material properties.

1.2 Research motivation

As mentioned above, tube hydroforming process is an advanced lightweight manufacturing technique widely used in the automotive industry, and the FE method based on computer simulations has become a necessary modelling and design tool for hydroforming processes in the scientific research and actual production. However, a successful tube hydroforming process and its corresponding reliable FE model depend heavily on the accurate input material parameters. Any errors caused by inappropriate experimental characterization tests and inaccurate post-processing procedure for experimental database can lead to undesired products and erroneous outcomes from FE simulations. Therefore, the initial problem of this research is proposed as:

1) How to characterize mechanical properties of tubular materials for hydroforming processes?
2) What is the most accurate mathematical model for post-processing experimental data?

To solve these proposed initial problems with broad scope, a detail state of the art for this topic will be summarized and analyzed. Then several research questions and hypotheses are given by the analysis of present situation. Each research hypothesis will be investigated and verified by the physical experiments and numerical simulations. Furthermore, if one of the assumptions is proved to be correct, the scientific contributions will be published in suitable journals and conferences after peer evaluations.

1.3 Thesis outline

This thesis consists of seven chapters which describe the project background, state of the art, research questions and hypotheses, experimental results and future work in detail.

Chapter 1—Introduction

This chapter presents the industrial background of tube hydroforming processes and corresponding computer simulations. The research motivation and methodology of this thesis are also described in this chapter where the includes the overview of the thesis.

Chapter 2—State of the art

This chapter discusses the state of the art of different experimental characterization tests for tubular materials and various of parameter identification strategies including the analytical model and inverse modelling technique. The advantages and drawbacks of these testing methods and post-processing procedures are summarized to propose the work objectives.

Chapter 3—Objectives of the study

This chapter lists the thesis scope and research objectives based on the analysis of the present situation for mechanical properties characterization. The research questions and corresponding hypotheses are also defined in this chapter.

Chapter 4—Paper I

This chapter describes a novel inverse strategy to determine the constitutive parameters of tubular materials using the experimental database from the hydraulic bulge test with fixed end-conditions. The performance of this proposed scheme is validated by the comparison of identified parameter from inverse models and other classical analytical models.

Chapter 5—Paper II

This chapter introduces an innovative T-shape tube hydraulic bulge test under axial feeding force to characterize the mechanical properties of thin-walled tubes at the large strain range. The developed inverse scheme in Chapter 4 is extended to post-processing the obtained experimental data from tube hydraulic bulging text with forced end-conditions.

Chapter 6—Paper III

This chapter presents a hybrid approach combining the analysis model and inverse modelling scheme to avoid local minimum pitfalls in the classical inverse parameter strategy and improve results accuracy. This method is examined by two types of hydraulic bulge test with fixed and forced end-conditions.

Chapter 7—Conclusions

This chapter contains the summary of each published journal paper and the author's contributions to the science community. It also describes the future research work of this topic.

Appendix A

Four classical gradient-based optimization algorithms for nonlinear least squares problems are built and a relatively large set of testing functions have been defined to measure their reliability and efficiency.

Appendix B

The source code of the developed automatic optimization framework using Python programming language is presented in part and the hardware basics are briefly introduced.

Appendix C

A two-stage sheet hydroforming process to form a cylindrical cup having small radii is designed, and the developed automatic optimization framework is used to determine the optimal preform geometry at the first stage.

Chapter 2

State of the art

This chapter provides the comprehensive literature review of existing experimental characterization methods and modelling of testing results for the identification of mechanical properties of tubular materials. Firstly the present research situation of four types of testing methods are reviewed and then two different parameter identification strategies to post-processing materials testing responses are described. Lastly a summary of the state of the art is given at the end of this chapter.

2.1 Review of experimental characterization method

For tubular metals, the material response in the deformation-based process shows different phenomena, such as grain growth, phase transformation, resistance to corrosion and plastic deformation, surface hardness and roughness, formability and so on, from microscopic and macroscopic perspectives [18]. It is impossible to characterize all material behavior using the experimental testing and modelling methods since it is too complicated. The resistance to plastic deformation, i.e., the flow stress of tubular materials is only considered as the most simple and important aspect because it is a necessary condition to evaluate the feasibility of the forming process [19] and describe the performance of the final product using FE simulations [20].

Several different experimental testing methods have been utilized in the characterization of mechanical properties of tubular metals, whose tests are dedicated to approaching or reproducing the deformation conditions in the real forming processes. The simplest and most commonly used method is the uniaxial tensile test, where the first category is the tension test of the full-size tube. In the experiment, both ends of the specimen are inserted into cylindrical bars to ensure stable uniaxial experimental conditions but this test is restrictive to only applied in the initial tubes with a small range of sizes [21, 22].

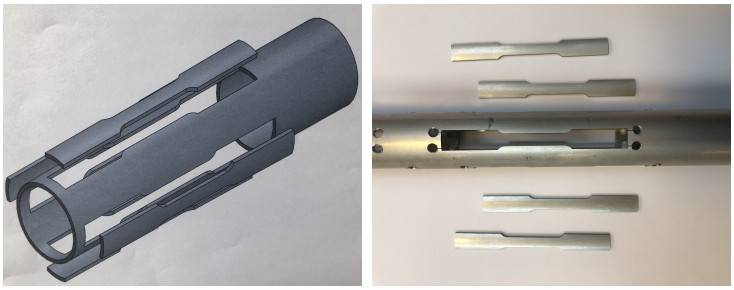

Figure. 2.1. Tensile samples taken from the initial thin-walled tubes: (a) schematic diagram and (b) real specimen.

In the second type of testing method, tensile samples are cut from the initial thin-walled tubes along the longitudinal direction at different locations of 0°, 90°, 180°, 270° circumferential positions [23, 24]. Fig. 2.1 illustrates the tensile specimens cut from the thin-walled tubes following the requirements of ASTM E8 standard [25]. From testing results, the yield and ultimate tensile strength, stress-strain curve and formability limits of tubular materials can be obtained [26]. However, the two types of uniaxial tensile tests described above only characterize the mechanical properties along the longitudinal direction [27].

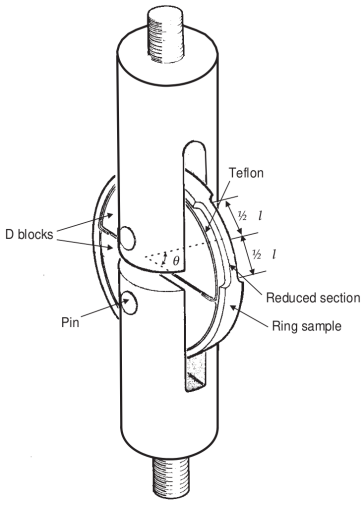

Figure. 2.2. Schematic diagram of the experimental fixture for ring hoop tensile test [28].

The flow stress curve of thin-walled metal tubes in the circumferential direction needs to be determined when the material exhibits strong anisotropy

or the main deformation occurs at the transverse position in the hydroforming process. Therefore, Wang et al. [28] develop the ring hoop tension test to determine the transverse stress-strain curve of tubular materials, in which an assembly combining the ring specimen with a pair of D-shaped blocks is stretched by a universal tensile system. Fig. 2.2 illustrates the schematic diagram of the experimental fixture for ring hoop tensile test. Later this test has been performed on a wide range of tubular materials [29–34]. Nevertheless, the friction between the ring specimen and D-shaped blocks has a effect on the measured load and change determined stress-strain curve. Some attempts have been made to address this issue, such as the lubrication [32, 35], new mechanical design [31, 36], but it does reduce the accuracy and reliability of the obtained to some extent.

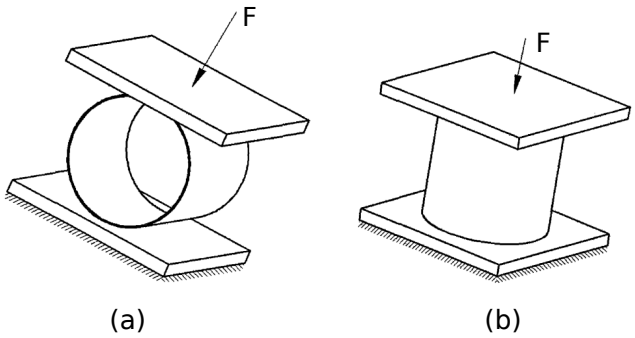

Figure. 2.3. Tube compression tests: (a) lateral direction and (b) longitudinal direction.

In addition, the true strain in real forming operations can easily reach 1.0 or greater and the strain level in the uniaxial or hoop tensile test covers a small range between 0.1 to 0.3 because of the local necking of testing samples [37]. As a result, the tension testing method can not provide the sufficient stress-strain data for the performance evaluation of final products in process simulations, and data extrapolation is required, which may lead to prediction errors with actual results. In order to address this issue, many investigations on different compression tests have been proposed. Fig. 2.3 illustrates the schematic diagram of two common distinct types of physical compression test for tubular materials.

According to some published research [19, 27], the equivalent strain value in the compression test can approach 0.7, which is significantly higher than the value in the tensile experiment. Nemat-Alla et al. [38] use the lateral compression test earlier to determine the transverse mechanical properties of tubular materials for hydroforming processes. In the experiments, a circular metal tube is placed on the base and compressed laterally by a rigid flatten punch, as shown in Fig. 2.3 (a). Then the recorded load-deflection curve will

be translated into the stress-strain data. Based on this research, later scientists extend this method to a variety of tubular materials and more complex constitutive models [39–43]. The contact interface area between the workpiece and flatted punches, on the other hand, is growing during the experiment. Friction force will have a great influence on the quality of the identified flow stress curve, which is difficult to avoid.

Another experimental characterization method to determine mechanical properties of tubular materials is the axial compression test, as presented in Fig. 2.3 (b). In this test, the identical experimental setup as the lateral compression test can be employed but the position of the workpiece is adapted from its center axis parallel to perpendicular to the flatting punch plate [44, 45]. However, axial compression tests can eliminate the influence of the significant friction force between the workpieces and dies in lateral compression tests, but the inherent buckling behavior in axial compression test can easily cause the experiment to become unstable and limit the strain value to a low level [46–48]. In summary, whether it is axial or lateral compression tests, they can evaluate the mechanical behavior of tubular materials at the larger strain scope compared with the tensile test but only along a certain direction. In this text, a more appropriate testing method needs to be developed.

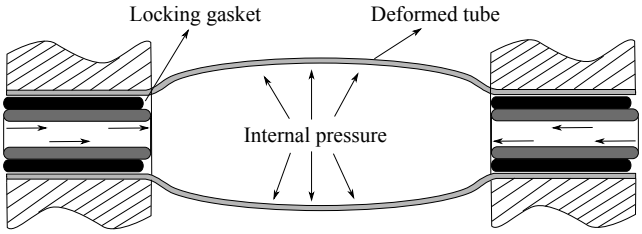

Figure. 2.4. Schematic diagram of tube hydraulic bulge test.

Tube hydraulic bulge tests combine the benefits of tensile and compression testing methods, which can be used to evaluate the comprehensive mechanical characteristics under complex loading conditions, with the advantage that is closer to actual hydroforming processes. Fig. 2.4 presents a typical schematic diagram of tube hydraulic bulge test. In this test, the tubular sample is expanded by the internal fluid pressure with or without the axial compressive force and the corresponding stress state of biaxial tension or tension-compression will appear the surface of tested specimens. Then the flow stress curve under different loading paths can be determined based on the measured experimental data.

According to different types of end-conditions of tubular specimens, the hydraulic bulge test can be categorized into free, fixed, forced bulging tests [49]. Many investigations on free and fixed hydro-bulging tests have been reported, which mainly involves the design of experimental setups and the

implementation of testing methods. To the author's knowledge, Woo and Hawkes [50–52] are the pioneers who utilize the bulging test to determine stress-strain characteristics of metal tubes. This research result indicates that small strains can be obtained when only the internal fluid pressure is used and axial feeding force can produce the stress-strain data with a larger strain scope.

A milestone progress has been made by Fuchizawa et al. [53] who design and build a special hydraulic apparatus to perform the bulging test, in which one end of tubular specimen can move freely along the axial direction, and the other end is fixed. Three position sensors are installed to measure the bulge height and the radius of meridional curvatures online. Although the precision of the experimental data collected by this apparatus is excellent, the complexity and expense of this device are increased by the use of multiple sets of sensors. Based on this machine, a similar conclusion is made that the bulging test is more suitable to characterize mechanical properties of tubular materials compared with the longitudinal uniaxial tensile test, with the advantage of larger strains and closer stress state.

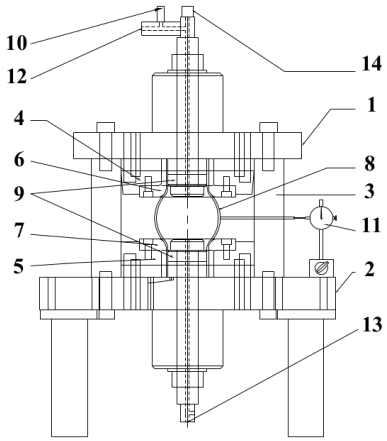

1. Upper plate	8. Tube
2. Lower plate	9. Urethane ring
3. Container	10. Pressure transducer
4. Upper fixing die	11. Dial gauge
5. Lower fixing die	12. Pressure input
6. Upper die insert	13. Pressure relief
7. Lower die insert	14. Relief valve

Figure. 2.5. Tube hydraulic testing setup developed by Hwang et al [54].

At the Engineering Research Center of Ohio State University, Altan et

al. [55–57] develop the standalone experimental setup where both ends of metal tubes can be fixed by the sealing urethane plug and tubular specimens are expanded under biaxial tension stress state. Based on the similar design concepts, a hydraulic machine, as shown in Fig. 2.5, which can implement tube bulging test with fixed end-conditions, is manufactured by Hwang et al. [54, 58–60], and the expanding diameter, internal fluid pressure and wall thickness at the tube center should be measured during the experiment. They use this recorded data to evaluate the flow stress curve, forming limit diagram of various tubular materials. But the strong friction between the tube and dies may have an influence on the formability of tubular component and lead to the failure of the sealing system, especially under high pressure bulging conditions.

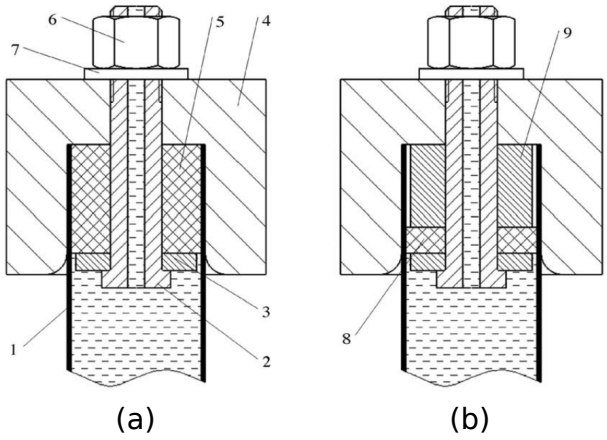

Figure. 2.6. Two type of tube hydraulic bulge test using Yang's setup: (a) fixed end and (b) free end [61].

A simple and economical testing device is built at Fllice's laboratory [62], which does not use an external hydraulic system as a pressure source and can generate high internal pressures through the axial displacement of the punch. However, different shaped dies needs to be made in order to adapt the metal tubes with various diameters. Yang et al. [61, 63] improve this setup with a more sophisticated mechanical design and this machine can realize free or fixed bulge forming test by changing the shape and material of the sealing ring, as shown in Fig. 2.6. This type of equipment has one common advantage of not relying on complicated hydraulic circuits and having cheaper tooling costs, but it consumes more expensive sealing materials.

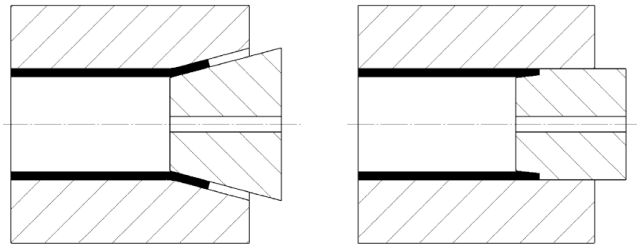

Figure. 2.7. Two different sealing principle: (a) fixed end-condition and (b) forced end-condition.

In order to address this issue, another approach to achieve hydraulic bulging test with the fixed end-condition is to employ the conical shaped punch. Fig. 2.7 (a) illustrates the structure and principle of this kind of sealing part. As shown in this Figure, the two ends of tubular specimens are deformed into a cone with a sharp angle during the forming process, which can avoid the leakage of the internal fluid and lock the workpiece. Many investigations have embraced this design concept because of its simplicity and effectiveness, as indicted by Bortot et al. [64, 65], Boudeau et al. [66–68] and later by Khalfallah et al. [69, 70] and by He et al. [71, 72]. Furthermore, Kuwabara et al. [73–75] develop a multiaxial tube bulging machine where the axial tensile force can be applied to both ends of the metal tube by two hydraulic cylinders and achieve arbitrary stress or strain path on samples. The obtained experimental data has been successfully applied to the calibration of the anisotropic yield function of tubular materials.

As previously stated, much work have been made to focus on the development of the experimental equipment and procedures for free and fixed hydraulic bulging tests where the tested tubes deform under the biaxial tension stress state. It should be noted that the tension-compression stress state dominates the loading path during actual tube hydroforming processes [76]. However, limited efforts are paid on hydraulic bulge tests with the axial compressive force which can characterize mechanical properties of tubular materials under the tension-compression stress state at a larger strain range. Korkolis et al. [77–79] investigate the yield and failure behavior of under combined internal fluid pressures and axial compressive forces using a self-designed experimental setup. Despite the fact that this study involves the properties characterization under tension-compression stress state, the ratio of the longitudinal stress component to the circumferential stress component is so small that the real tube hydroforming conditions can not be replicated.

A significant progress has recently been made by Wang et al. [80] who design and develop an advanced multiaxial compression-internal pressure bulging machine referred to Kuwabara et al. [73]. This setup applies a modified control model and the advanced digital image correlation technique

which can improve control precision for the ratio of axial compressive stress to hoop tension stress and obtain more accurate experimental results. A series of studies [81–84] on evaluating the yield function and forming limit diagrams under the large ratio of the tensile to compressive stress for several different tubular materials are performed on this machine. However, isotropic material plastic flow behaviors are not considered in these studies.

In summary, different testing methods are reviewed in this section and hydraulic bulge tests are considered as the suitable method to identify material mechanical parameters for hydroforming processes. However, most published studies focus on the fixed or free hydro-bulging tests where the effective strain is at a rather low level, thereby the first research question is proposed as following:

1) which testing method can characterize mechanical properties of tubular materials at a larger strain scope?

2.2 Review of parameter identification strategy

A parameter identification strategy must be developed to analyze the collected testing data and determine corresponding material constitutive parameters after the physical experimental characterization. According to various modelling techniques for testing processes, such as empirical, theoretical or semianalytical, numerical methods and so on, there are basically several different identification schemes which can be chosen as the post-processing procedures [85]. For hydraulic bulge tests, the widely utilized methods are the analytical approach and inverse modelling technique and a comprehensive research advancement and in-depth discussion for them will be elaborated in this section.

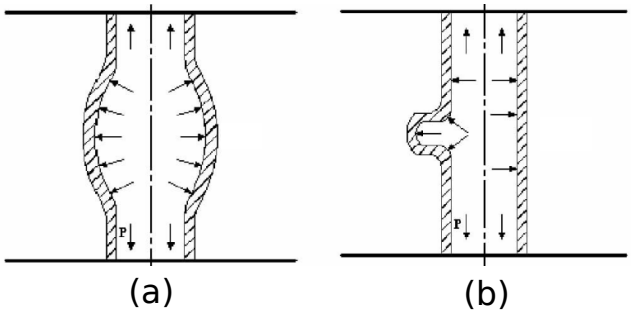

Figure. 2.8. Final shapes of tested tubes after hydraulic bulge process.

2.2.1 Analytical model

Many theoretical models have been developed to determine the flow stress curve of tubular materials based on the hydraulic bulge test [86]. Except for the end-condition at both ends of tested tubes, the type of the final shape of tested workpieces has a great impact on the model selection. Fig. 2.8 illustrates two final shapes of tested tubes after hydraulic bulge process, in which 2.8 (a) presents a rotationally symmetrical tubular component while 2.8 (b) is the bulged component with the T-branch. In the hydraulic bulge test of the former shape part, the slab method has turn out to be simple and effective technique to modelling this process [87].

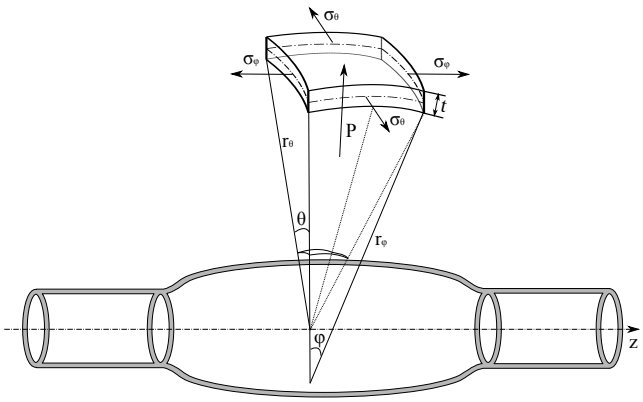

Figure. 2.9. Stress state of a small element at tube pole area.

The analysis of tube hydraulic bulging process using the slab method is based on the membrane theory where the ratio of tube wall thickness to its diameter is so small that the stress through the wall direction can be neglected [58]. The deformation of a small area at the tube center are consider as the plane stress state, as presented in Fig. 2.9. Therefore, the force equilibrium equation at the middle of the thin-walled tube can be written as:

$$\frac{\sigma_\theta}{r_\theta} + \frac{\sigma_\varphi}{r_\varphi} = \frac{P}{t} \tag{2.1}$$

$$\sigma_\varphi = \frac{P r_\theta}{2t} - \frac{F_{axial}}{2\pi r_\theta t} \tag{2.2}$$

The above equations 2.1 and 2.2 lay the foundation to calculate the circumferential and longitudinal stress components and fit the flow stress curve, which are first derived by Woo et al [50] and then used in many studies [23, 56, 66, 88–93]. Fuchizawa et al. [53] improve this stress model by taking into account the wall thickness of metal tubes, and following re-

searchers [54, 55, 58, 59, 63, 71, 72, 81, 87, 94–100] recommend this new formula because it is more in line with the actual situation.

Obviously, no matter in which formula to calculate the stress component proposed by Woo [50] or Fuchizawa [53], the internal pressure, expanding diameter, axial feeding force if necessary, meridional curve radius and pole thickness are required where the first three indicators are easy to record online in the experiment. The difficult task is to measure the meridional curve radius and pole thickness and many efforts have been made. For the pole thickness, ultrasonic sensors are placed directly above the middle of the tested metal tube to measure the wall thickness online while measured values may be affected by the internal medium and bulged profile [53, 101]. Hwang et al. [54, 58, 59] develop a self-designed dial-gauge but it can only be applied to a given length of tested tubes and has poor flexibility. He et al. [71, 72] propose a linear model which simply requires the thickness of the original and ultimate bulged tubes and can predict the pole thickness at different bulged stages. However, its application is limited to hydraulic bulging tests with fixed end-conditions. Bortot et al. [64] bulge multiple tubular sample at different pressure levels and then cut them at the middle of tubes to measure the pole thickness along four circumferential locations, which further reduces the influence of the difference in the performance of original metal tubes.

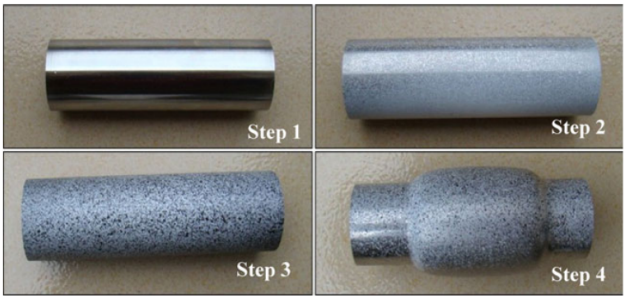

Figure. 2.10. Tested tubes using DIC technique: (1) original tube, (2)(3) tube with spray, and (4) bulged tube [92].

For the measurement of meridional curvature radii of the tube profile at the bulging area, Yang et al. [63] develop a strategy integrating mathematical methods with physical measurement techniques, where the expanding diameter at internals along the longitudinal direction is recorded during multiple bugling stages and obtained values are used to fit the spline function describing the profile shape. However, repetitive and huge amount of experimental operations are a serious challenge. In order to overcome these difficulties, they later adopt more advanced digital image correlation(DIC) system which can automatically capture coordinate points of any position on the bulged zone and obtain the profile shape online [92, 100, 102, 103], although DIC

technique requires tedious preparation for tested tubes, as shown in Fig. 2.10, and is still a highly expensive and demanding method [101].

Alternatively, another approach is the geometrical assumption method where the profile curve at the bulged region is considered to be a basic geometrical shape to prevent direct contact measurement of the axial meridional radius. For instance, Fuchizawa et al. [53] assume the deformation zone as a circular arc and three displacement transducers are used to generate data and fit the curve function. In subsequent research, this concept is continued to be adopted and more distinct types of curve hypotheses are employed, including as the elliptical curve [54, 58, 59, 71, 88, 98], cosine function [57, 97, 101], and two arcs of circumference [66, 67]. Although using this geometrical assumption may diminish the accuracy of the analytical model, it also reduces the equipment's complexity and expense.

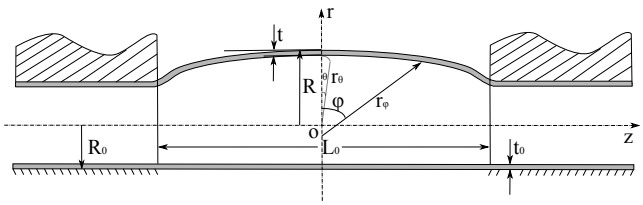

Figure. 2.11. Geometrical parameters of the meridional profile at the bulged region.

In terms of the strain calculation, several key geometric parameters of the shape profile are presented in Fig. 2.11. Therefore, corresponding strain components in the radial, circumferential and longitudinal direction can be derived, according to the definition of logarithmic strain and volume constancy law, as following [53, 54]:

$$\varepsilon_t = \ln\left(\frac{t}{t_0}\right) \tag{2.3}$$

$$\varepsilon_\theta = \ln\left(\frac{R}{R_0}\right) \tag{2.4}$$

$$\varepsilon_\varphi = -(\varepsilon_t + \varepsilon_\theta) \tag{2.5}$$

Then the flow stress curve of tested tubular materials can be determined based on the equations from 2.1 to 2.5. When an appropriate hardening model which represents a mathematical explicit function to describe the stress-strain relationship, such as the Hollomon's law or Voce's law [104], is selected, and the essential material coefficients in this model could be fitted using the obtained stress-strain data.

Until now, the theoretical analysis described above, i.e., the slab method, is widely used to model hydraulic bulge processes of rotationally symmetrical tubular samples. It is worth noting that one drawback of this methodology

is that the stress and strain are assessed separately and plastic stress-strain relationships are not introduced. In addition, the applied hypothesis in equation 2.2 in which the longitudinal stress component is approximated under the situation where the tube and dies are assumed as the integrated object is questioned [64], which may result in a significant difference between the calculated and real results. As a result, one option is to calculate the axial stress component and eliminate these controversial assumptions using the total strain theory. This proposed hypothesis will be validated in this thesis.

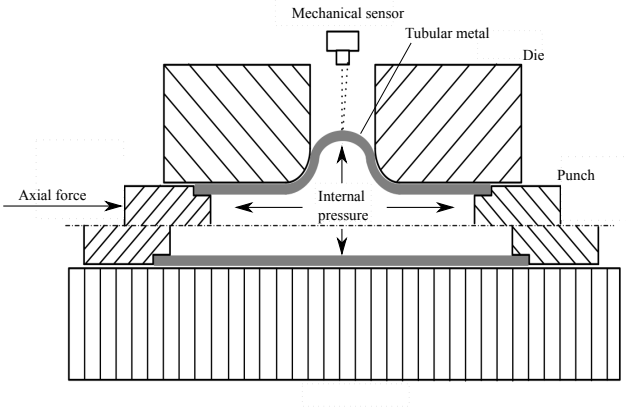

Figure. 2.12. T-shape hydraulic bulge test with forced end-conditions.

In T-shape hydraulic bulge tests with forced end-conditions, a straight tubular sample is expanded into T-shape die cavity under the internal pressure and axial compressive forces as depicted in Fig. 2.12. Because of the more complicated boundary conditions and unequal deformation, the classical slab method has great limitations in the analysis of this bulging process. The energy principle opens up novel possibilities where an optimal solution can be discovered among a wide variety of feasible alternatives instead of a rigorous closed solution [105]. Few studies are available to model and analyse hydro-bulging processes of tubular component with T-shape branches. Strano et al. [57] develop an inverse approach based on the energy balance principle to identify the flow stress data of 304 stainless steel seamless tubes, however it is only limited to fixed bulging test of axisymmetric tubular specimens.

In addition, Hartl et al. [85] give an analytical solution to estimate the axial compressive force required for T-shaped tube hydro-bulging deformation using the plastic mechanics but the used assumption where the tube wall thickness in the axial, radial and hoop direction is uniform during the process presents too much idealization. A substantial progress has been made by Moreira Filho et al. [106–110] who conduct a number of research on how

to evaluate and analyze the process parameters in T-shape tube forming applying the upper bound method in the energy theory. The predicted results using their developed model are in good agreement with the experiment but the pressure medium used in their tests is the elastomer instead of fluid. As a result, the following research question arises:

How to describe and analyse T-shape hydraulic bulge tests under axial compressive forces?

2.2.2 Inverse modelling technique

Compared with the direct approach, i.e., the analytical model described in Section 2.2.1, inverse modelling technique is a more advanced parameter identification strategy because it avoids the utilization of usual mechanical and geometrical assumptions in theoretical analysis [111–113]. This inverse scheme seamlessly integrates FE modelling with optimization algorithms and can realize automatic determination of material constitutive parameters. The fundamental principle behind it is to fit the experimental data using the numerical results from FE models. In the fitting process, the objective function which is calculated based on the gap between experimental and numerical data is minimized iteratively by adjusting the input values of material coefficients. When the best match between FE simulated predictions and experimental results is made, the final optimal solution is determined. Fig. 2.13 illustrates the flow chart of inverse modelling techniques applied on the identification of material constitutive parameters.

According to the author's expertise, Distéfano [114] is the pioneer in proposing and implementing inverse schemes for determining material behaviors of linear viscoelastic models. Later, this analogous methodology is extended to a broad variety of materials and corresponding constitutive models, including nonlinear elastic model [115], nonlinear viscoelastic model [116], orthotropic model [117], geological material [118] composite material [119], textile material [120], biological material [121], amongst others. More importantly, an early overview of the inverse scheme applied in the metal forming processes has been presented in [122] and recent progress is reported in [123–125].

In recent years, inverse modelling techniques have gradually evolved into a mature and widespreadly used post-processing procedure to identify constitutive parameters of metallic materials. Different types of physical experiments, including but not limited to the biaxial tensile test [126, 127], bulge test [128, 129], three-point bending test [130], shear test [131, 132], deep stretching test [133, 134], have been performed to provide experimental data for the inverse strategy, although the tested material focuses on the sheet metals. A small amount of research work is available to describe the inverse identification of constitutive parameters of tubular metals, especially experi-

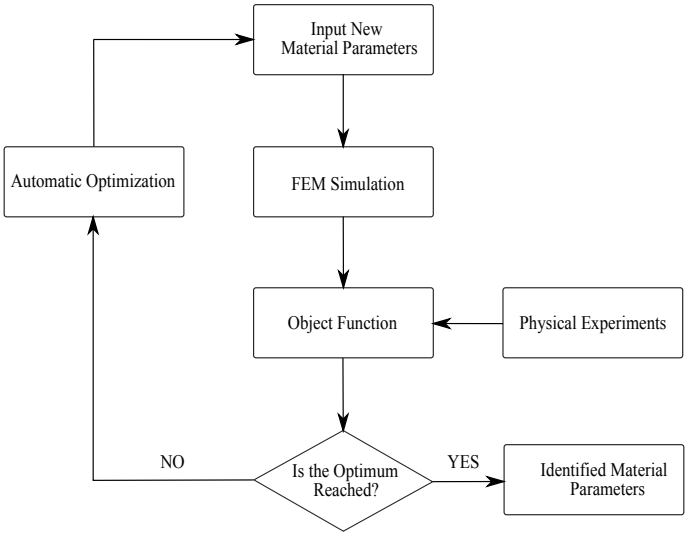

Figure. 2.13. Flow chart of inverse strategies applied in the identification of material constitutive parameters.

mental characterization methods based on hydraulic bulge tests.

Ge et al. [101] present an inverse strategy which combines gradient-based algorithms with FE codes to determine material coefficients of constitutive laws for stainless steel tubes H340 and E355. It may be due to local convergence that the final fitting quality is relatively poor, i.e., the large gap between calculated and experimental data. Khalfallah et al. [135–137] use Nelder Mead simplex method to fit the numerical output from ABAQUS FE software to experimental results. This has proven to be a success in terms of the stability of iteration processes and the accuracy of fitting results, but the optimization process requires nearly 100 iterations, see Fig. 2.14, which greatly increases the computational cost.

To address these issues, Assadi et al. [138] replace the expensive FE models of hydraulic bulging processes using a surrogate model named artificial neural networks. However, the specific calculation cost comparison between this new scheme and the method used in [135] is not given. In addition, another drawback of surrogate modelling techniques is that the approximated result may be not the real optimum and the problem of curse of dimensionality is still quite time-consuming sometimes [139]. Xu et al. [140] provide a qualitative relationship between the strength coefficient, hardening exponent and the shape of internal pressures versus bulge heights curve for screening the searching space of design variables before the optimization. However, this method is unfeasible as the number of material parameters increases.

On the other hand, some efforts have been made to avoid falling into the

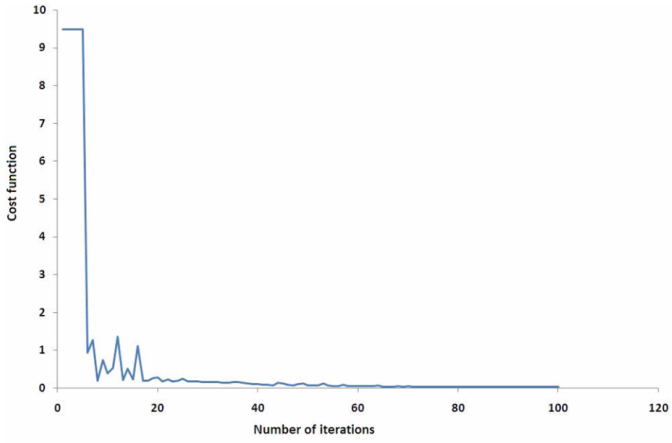

Figure. 2.14. Iteration history of the objective function using Nelder Mead simplex method [135].

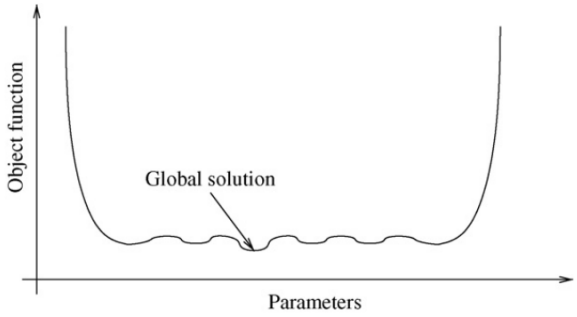

Figure. 2.15. Representation of optimal points where some local minimums are distributed around [134].

trap of a local optimum in the parameter identification process, as shown in Fig. 2.15. Bio-inspired computing methods which simulate the behavior of natural phenomena and biological system, such as simulated annealing, genetic and evolutionary algorithm, provide a promising possibility to solve this problem because they tend to converge the global optimal solution. A comprehensive summary of various bio-inspired methods applied on process optimization and parameter identification of sheet metal forming processes is reported in [141]. A similar disadvantage to the direct search approach is that a large number of function's evaluations are required at any point in the searching range of design variables [142].

As mentioned above, three different optimization algorithms, i.e., gradient-based algorithm, bio-inspired method and meta-modelling technique, are introduced into the inverse framework to complete the identification of material constitutive parameters. They have demonstrated their respective advantages and limitations in the actual application cases.

In general, gradient-based algorithms can converge quickly to the minium or maximum value if the starting point is located in the vicinity of the optimum. When initial guesses are far away from the global optimal solution, this algorithm is easy to fall into the pitfall of local optimums, especially in multi-objective optimization [143, 144]. Meta-modelling technique can replace the complicated and time-consuming FE calculation process, which can greatly save the computational cost of the entire optimization process. However, multiple approximations and experimental measurement errors may lead to the final result differing significantly from the real solution [142]. Bio-inspired approaches do not need to calculate the gradient of the cost function and tend to converge to the global optimum, but massive function's evaluations are required even in small-scale problems [145].

As a result, the hybrid and cascade strategy have received some attention since they can combine the benefits of various types of algorithms discussed above. The initial attempts are made to explore multiple possibilities for combinations of various gradient descent algorithms to improve the robustness and efficiency of the optimization process [123, 145–147]. This methodology appears hopeless because the cost function is non-convex in most cases. The next similar integration is the meta-model technique incorporating with gradient-based algorithms. It is possible to utilize a suitable gradient-based algorithm to optimize the meta-models obtained from the response surface methodology, neural networks and kriging [148–150]. Several researchers [151–153] are dedicated to merge bio-inspired methods and gradient-based algorithms, in which the initial points around the global solution are generated by a bio-inspired method in the first stage and then the gradient-based algorithm converge to the optimum quickly in the second stage. However, the function evaluation in the first stage is still time-consuming. Thus the next research question are proposed as:

How can determine the global optimal parameters of tubular materials in the parameter identification process based on hydraulic bulge tests?

2.3 Concluding remarks

This section is to summarize identified research questions based on the analysis of the state of the art presented above. To make it more clear for readers, these relevant research questions are still elaborated from three separate perspectives. The following is a list of what they are:

Experimental characterization method Hydraulic bulge tests are particular suitable for characterization the mechanical properties of thin-walled metal tubes for hydroforming processes. Most of the current research focus on hydro-bulging test with free or fixed end-conditions, in which the strain values are rather low. Thus, a research question arises:

+ How can characterize the mechanical properties of tubular materials at the larger strain scope using hydraulic bulging tests?

++ How can analyze and process the stress-strain data with the larger strain range?

Analytical model Slab methods have a wide range of applications in post-processing experimental data from rotationally symmetrical tube bulging tests, where the stress and strain are analysed in isolation without considering the plastic stress-strain relationship. Furthermore, this method has great limitations when applied to describe hydro-bulging process of tubular samples with angled branches due to the complicated boundary conditions. Therefore, some urgent research questions are proposed as following:

+ How can describe and analyze the hydraulic bulge test of axisymmetric tubular specimens when introducing the plastic stress-strain relationship?

++ How can describe and analyze T-shape hydraulic bulge test under axial compressive forces?

Inverse modelling technique Gradient-based algorithms, bio-inspired approaches and meta-modelling techniques are frequently integrated with FE models as an inverse framework to identify material parameters based on various of physical testing methods. However, for tube hydraulic bulge tests, only the research work related to direc search algorithm has been reported and this scheme requires a large number of iterations and leads to relatively expensive computational costs. Gradient-based algorithms provide the possibility to converge to the optimum quickly while it depends heavily on the starting points and easily falls into the

pitfall of local minimums. As a result, the next research question can be described as:

+ How can reduce the computational cost and improve the performance of the existing parameter identification strategy?

++ How can identify the global optimal constitutive coefficients of tubular materials in the parameter identification process?

Chapter 3

Research scope and objectives

This chapter presents the research scope and objectives of this thesis. It also lists all proposed hypotheses for defined research questions in the previous chapter.

3.1 Objectives of the study

The main objective of this proposed research is to develop an automatic parameter identification strategy to characterize the mechanical properties of tubular materials based on hydraulic bulge tests with different types of end-conditions. In particular, the overall research objective can be divided into several research questions and corresponding hypotheses to solve these problems.

3.1.1 Research questions and hypotheses

All research questions have been raised in the last section of Chapter 2 and will be further investigated and integrated based on their similarities hereby. Then, below this question, the appropriate hypothesis will be developed based on prior research summaries and experience.

Research question A In view of the current drawbacks in the analytical and inverse models for hydraulic bulge tests of axisymmetric tubular specimens, the following research questions can be considered:

+ How can describe and analyze the hydraulic bulge test of axisymmetric tubular specimen when introducing the plastic stress-strain relationship?

++ How can reduce the computational cost and improve the performance of the existing inverse parameter identification strategy?

Hypothesis A For analytical models, total strain theory in engineering plasticity can be applied to link stress-strain analysis and post-processing the obtained experimental data from hydraulic bulge tests of axisymmetric tubular samples. For inverse models, gradient-based methods, such as Levenberg-Marquardt algorithm, can integrate the FE technique and reduce the expensive computational cost instead of the existing direct search algorithm.

Research question and hypothesis A are examined in Paper I.

Research question B Aiming at the problem where the obtained strain level is rather low in hydraulic bulge tests with fixed or free end-conditions, research questions can be stated as following:

+ How can characterize the mechanical properties of tubular materials at the larger strain scope using hydraulic bulging tests?

+ How can analyze and process the stress-strain data with the larger strain range?

Hypothesis B Axial compressive forces, in addition to the internal fluid pressure, will be applied to tube ends to change the stress state of the tested specimen and increase the strain level of tubular materials in hydraulic bulging tests. Both energy methods and inverse modelling techniques can be used to investigate and process the obtained data at large strain scope.

Research question and hypothesis B are tested in Paper II.

Research question C In view of the disadvantages of the gradient-based algorithm that rely heavily on a good initial point and easily converge to the trap of the local minimum, a research question is proposed as follows:

++ How can identify the global optimal constitutive coefficients of tubular materials in the parameter identification process?

Hypothesis C A promising method to solve this problem is to develop a hybrid strategy combining a theoretical analysis and inverse model. The initial points around the vicinity of the global solution can be generated by an analytical model in the first stage, and then quickly converge to the global optimum under the optimization of gradient-based algorithms in the second stage. Fig. 3.1 illustrates the principle of this proposed hypothesis.

Research question and hypothesis C are tested in Paper III.

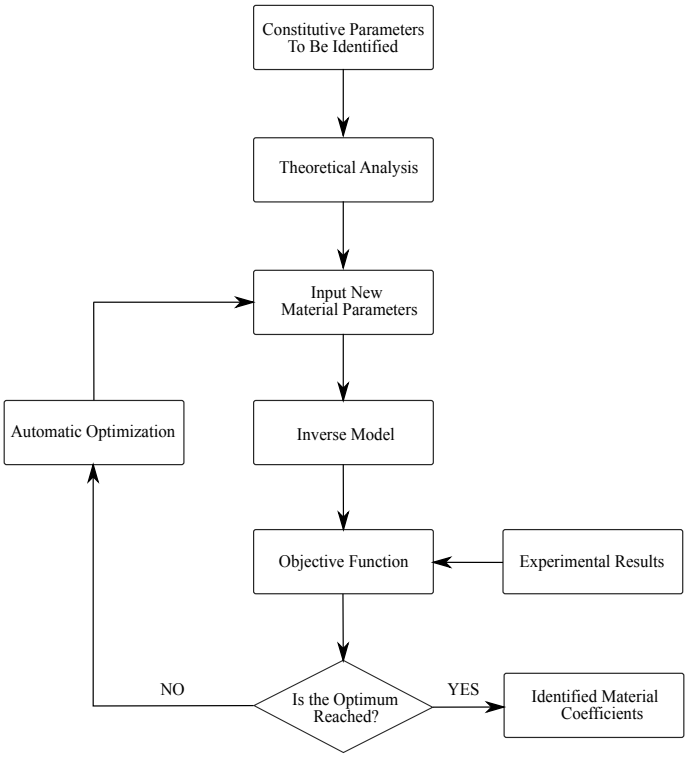

Figure. 3.1. Principle of the proposed hybrid strategy to identify material parameters.

3.2 Scope of the work

In this research, the main scope covers the design of novel tube hydraulic bulge tests with different types of end-conditions and development of an automatic, efficient and stable parameter identification strategy for thin-walled metal tubes. Tube hydraulic bulge tests provide a large number of experimental data, i.e., the bulge height, internal fluid pressure, axial compressive force and pole thickness, during the deformation. The feasibility and performance of this proposed inverse identification strategy can be demonstrated by analyzing and processing this collected experimental data. Based on the identified material constitutive parameters, FE simulations are run for hydroforming processes to validate their accuracy by the comparison with those generated by other testing methods.

Chapter 4

Paper I

An inverse strategy to determine constitutive parameters of tubular materials for hydroforming processes

Bin Zhang, Benny Endelt, Lihui Lang, Yang Zhao, Shu Yan, and Karl Brian Nielsen

The paper has been published in the
Chinese Journal of Aeronautics. DOI: https://doi.org/10.1016/j.cja.2021.11.007

Chinese Journal of Aeronautics, (2021), xxx(xx): xxx–xxx

Chinese Society of Aeronautics and Astronautics
& Beihang University

Chinese Journal of Aeronautics

cja@buaa.edu.cn
www.sciencedirect.com

An inverse strategy to determine constitutive parameters of tubular materials for hydroforming processes

Bin ZHANG [a,*], Benny ENDELT [a], Lihui LANG [b], Yang ZHAO [c], Shu YAN [c], Karl Brian NIELSEN [d]

[a] *Department of Materials and Production, Aalborg University, Aalborg 9220, Denmark*
[b] *School of Mechanical Engineering and Automation, Beihang University, Beijing 100083, China*
[c] *School of Materials Science and Engineering, Northeastern University, Shenyang 110819, China*
[d] *Department of Mechanical and Production Engineering, Aarhus University, Aarhus 8000, Denmark*

Received 6 February 2021; revised 15 November 2021; accepted 15 November 2021

KEYWORDS

Aluminum alloy;
Constitutive parameter;
Hydraulic bulging test;
Inverse modeling;
Tubular material

Abstract This paper is to determine the flow stress curve of 5049-O aluminium alloy by a tube hydraulic bulging test with fixed end-conditions. During this test, several tubular specimens are bulged under different internal pressures before their bursting, and the corresponding bulging height and wall thickness at the pole are measured. An inverse strategy is developed to determine the constitutive parameters of tubular materials based on experimental data, which combines the finite element method with gradient-based optimization techniques. In this scheme, the objective function is formulated with the sum of least squares of the error between numerical and experimental data, and finite difference approximation is used to calculate the gradient. The tubular material behavior is assumed to meet the von Mises yield criterion and Hollomon exponential hardening law. Then, constitutive parameters identification is performed by minimization of the objective function. In order to validate the performance of this framework, identified parameters are compared with those obtained by two types of theoretical models, and tensile tests are performed on specimens cut from the same tubes. The comparison shows that this inverse framework is robust and can achieve a more accurate parameter identification by eliminating mechanical and geometrical assumptions in classical theoretical analysis.

* Corresponding author.
E-mail address: zb@m-tech.aau.dk (B. ZHANG).

Peer review under responsibility of Editorial Committee of CJA.

Production and hosting by Elsevier

1. Introduction

Tube hydroforming technology has been proven to be a successful manufacturing process and can form tubular metal blanks into various complex tube components. Such a forming

https://doi.org/10.1016/j.cja.2021.11.007
1000-9361 © 2021 Production and hosting by Elsevier Ltd. on behalf of Chinese Society of Aeronautics and Astronautics.

Please cite this article in press as: ZHANG B et al. An inverse strategy to determine constitutive parameters of tubular materials for hydroforming processes, *Chin J Aeronaut* (2021), https://doi.org/10.1016/j.cja.2021.11.007

process is widely utilized in the aviation and aerospace industry[1] owing to its advantages such as weight reduction, increase of part complexity, and cost savings.[2] A robust and productive hydroforming process depends heavily on several process parameters like incoming tubular material, preforming operation, fluid pressure loading path, lubrication, equipment, and tools. Among the above factors, materials properties, i.e., the flow stress curve and the tool-workpiece friction, have drastic influences on the quality of final hydroformed parts. Besides, an accurate evaluation of incoming tube material properties is essential for the input data in the Finite Element Method (FEM).[3]

To determine tubular metal properties, a number of industrial tests have been carried out to measure material behaviors. One of the simplest methods is the tensile test which is used to test sheet metal behaviors commonly[4] When it is applied on the a tube material, specimens can be cut from the tube wall at different locations along the longitudinal and circumferential directions, and then will be flattened and tested under uniaxial tension according to the ASTM standard.[5] However, the flattening process of curved specimens before testing will change their stress–strain behaviors and formability, especially those cut from small-diameter tubes. The ring hoop tension test can avoid the unnecessary work hardening caused by flattening and measure the hoop flow stress curve of a tubular material accurately. In this test, a ring specimen with a reduced section is taken from a tube along the hoop direction and then pulled by a universal tensile apparatus. A disadvantage of this method is the friction on the interface between the specimen and a pair of blocks, which will lead to some measuring errors.[6]

Another more accurate method to measure tubular material properties is the hydraulic bulge test, because the stress state of specimens under this procedure is close to the realistic hydroforming process. A number of efforts have been made to various types of hydraulic bulge testing methods and post-processing procedures for experimental data. Fuchizwa et al.[7] ignored the stress through thickness and calculated stress components along circumferential and longitudinal directions based on the recorded internal pressure, wall thickness, and bulge height near the tube center in experiments. The use of three displacement sensors to improve the accuracy of measuring the meridian profile shape increased the complexity and cost of the hydraulic press. Hwang et al.[8] proposed a simple analytical model where the bugle profile shape was assumed as an elliptical curve to avoid measuring the longitudinal curve radius, and the flow stress curve could be obtained when only the tube center diameter and pole thickness were measured.

Other studies on theoretical analysis for the hydro bulge process are similar, in which they followed the same stress formulas as those of Hwang et al.[8] and Fuchizawa et al.[7] and only changed the shape assumption. The meridian profile shape could be assumed as two circular arcs,[9] spline functions.[10] However, to calculate the axial stress component, those researchers adopted an unreasonable hypothesis that tubular specimens and dies were regarded as a whole and isolated the analyses for stress and strain. Bortot et al.[11] introduced a plastic strain–stress relationship, i.e., strain components were proportional to the corresponding deviatoric stress to derive the longitudinal stress component while the tube thickness was ignored in the radical force equilibrium equation for a pole element. In all the above analytical approaches, the tube deformation was treated as a plane stress problem, and the tube bulge profile was assumed as a simple mathematical formula; this simplicity reduced the accuracy of results to some extent.

A substantial progress for the identification material parameters of analytical models is the application of the inverse modeling strategy which combines the optimization technique with the FEM model and obtains the optimum material coefficients by minimizing the difference between numerical simulation results and experimental data. Compared with the classical theoretical equations, it allows a more accurate determination by avoiding mechanical and geometrical assumptions.[12] A large number of publications focused on the inverse identification of sheet metal properties,[13–17] and limited work was carried out on the application of inverse modeling on the tube hydraulic bulge test. Zribi et al.[18,19] used this inverse procedure combining the FEM with Nelder Mead simplex algorithm to identify material constitutive parameters of tubular parts made of low carbon steel. The gap of the internal pressure versus the bulge curve between collected from a free hydraulic bulging experiment and FEM responses was set as the cost function. One limitation of this research was that the direct search algorithm in the strategy showed a lower efficiency and a lack of comparison with classical theoretical analysis.

In this paper, a novel and flexible hydraulic setup is designed, and several tube hydraulic tests with fixed end-conditions for annealed 5049 aluminium alloy are carried out. The bulge height, wall thickness at the pole, and applied internal pressure are measured during the process. An inverse modelling technique combing the FEM model and an improved Levenberg-Marquardt algorithm is used to determine the tubular materials of 5049-O aluminium alloy. A general objective function is created to evaluate the difference between computed and experimental data, and material constitutive parameters are identified by minimizing this function. Meanwhile, two theoretical models based on the force equilibrium and total strain theory for this process are given, and tension tests for specimens cut from the tube along the longitudinal direction are performed. In order to demonstrate the inverse strategy's feasibility and performance, a comparison of three types of methods is carried out by running FEM simulation of the tube hydraulic bulging process.

2. Hydraulic bulging test analysis

A tube hydraulic bulging test is a material characterization method which expands a tubular material into a suitable shape freely using the internal fluid pressure. In the test, some data such as the bulge height, internal pressure, and pole thickness

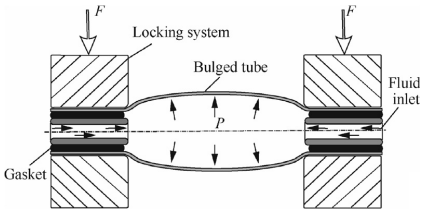

Fig. 1 Schematic for tube hydraulic bulging process.

Please cite this article in press as: ZHANG B et al. An inverse strategy to determine constitutive parameters of tubular materials for hydroforming processes, *Chin J Aeronaut* (2021), https://doi.org/10.1016/j.cja.2021.11.007

can be measured online or offline, and then these collected data can be used further to determine tubular material properties. Fig. 1 illustrates a typical tube hydraulic bulging process. In general, this test includes three types of end-conditions at tube ends: A) Free-end, B) Forced-end, and C) Fixed-end; the ends of a tubular workpiece are fixed completely in current study.

2.1. Geometrical analysis

The profile of the deformation zone on a tube is assumed as an elliptical curve.[8] The geometrical parameters for this shape are shown in Fig. 2, where R_0 is the initial external tube radius, t_0 is the initial tube wall thickness, L_0 is the length of the bulge zone, h is the bulge height. The elliptical curve can be defined as[20]

$$\frac{z^2}{a^2}+\frac{r^2}{b^2}=1 \tag{1}$$

where a and b are the half lengths of the major and minor axes of the ellipse, respectively.

In Fig. 2, it can be seen that the coordinates of the contact point between the tube and the die are ($L_0/2$, R_0), and the elliptical curve passes through this point. The pole point (0, $R_0 + h$) also meets Eq. (1), and then parameters a and b in the elliptical equation can be determined as[20]

$$a=\frac{L_0(R_0+h)}{\sqrt{4h(2R_0+h)}} \tag{2}$$

$$b=R_0+h \tag{3}$$

Based on Eqs. (1)–(3), the meridian curvature radius at the pole point can be described as[20]

$$r_\varphi=\frac{L_0^2(R_0+h)}{4h(2R_0+h)} \tag{4}$$

Then, the circumferential radius at the pole of the tube bulge zone can be written as

$$r_\theta=R_0+h \tag{5}$$

As a comparison, Hwang et al.[8] applied another elliptic shape equation to describe the profile, and r_φ can be calculated as

$$r_\varphi=\frac{a^2}{b} \tag{6}$$

It can be seen from Eq. (1)–(6) that the meridian and circumferential radii depend on the bulge height, tube thickness, and diameter, which can be measured during the hydraulic bulging test.

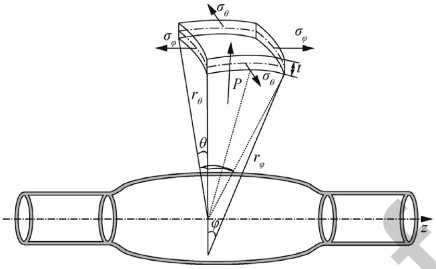

Fig. 3 Stress state of a small element at tube pole.

2.2. Stress analysis

For the thin-walled tube used in this research, the ratio of its thickness to diameter $\ll 1$, so the stress within the workpiece can be referred as the plane stress state according to assumptions in the membrane theory. It means that the stress along the thickness direction is zero, i.e.

$$\sigma_t=0 \tag{7}$$

The equivalent stress can be calculated by two stress components, σ_θ along the circumferential direction and σ_φ along the longitudinal direction. They can be determined from the force equilibrium along the thickness direction for a membrane element at the pole of the tube bulge zone, as shown in Fig. 3, which can get

$$2\sigma_\varphi(r_\theta-\frac{t}{2})t\theta\sin\frac{\varphi}{2}+2\sigma_\theta(r_\varphi-\frac{t}{2})t\varphi\sin\frac{\theta}{2} = P(r_\theta-t)\varphi(r_\varphi-t)\theta\cos\frac{\theta}{2}\sin\frac{\varphi}{2} \tag{8}$$

where r_θ and r_φ are the circumferential and meridian curve radii at a point of the tubular elliptical surface, respectively; P is the internal fluid pressure; θ and φ are the angles on the planes of hoop and meridian, respectively. When these angles are small, Eq. (8) can be rewritten as[20]

$$\frac{\sigma_\varphi}{r_\varphi-\frac{t}{2}}+\frac{\sigma_\theta}{r_\theta-\frac{t}{2}}=\frac{P(r_\theta-t)(r_\varphi-t)}{t(r_\theta-\frac{t}{2})(r_\varphi-\frac{t}{2})} \tag{9}$$

According to Fuchizawa et al.[7] and Hwang et al.,[8] the hypothesis that both ends of the tube were considered closed was applied. For a closed tube under internal pressure, from the force equilibrium equation along the longitudinal direction at the cross-section perpendicular to the tube surface, it can be expressed as[21]

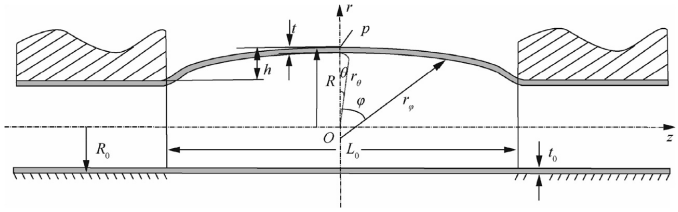

Fig. 2 Tube geometrical parameters before and after bulging test.

$$2\pi(r_\theta - \frac{t}{2})t\sigma_\varphi = P\pi(r_\theta - t)^2 \tag{10}$$

Based on hypothesis Eq. (10), the longitudinal stress at the pole can be approximately calculated as[8]

$$\sigma_\varphi = \frac{P(r_\theta - t)}{2t(r_\theta - \frac{t}{2})} \tag{11}$$

Substituting Eq. (11) into Eq. (9), the stress along the hoop direction can be written as[8]

$$\sigma_\theta = \frac{P(r_\theta - t)}{2t(r_\varphi - \frac{t}{2})}(2r_\varphi - t - r_\theta) \tag{12}$$

The other method to calculate the stress along the longitudinal direction is presented based on the total strain theory proposed by Ilyushin and Lensky.[22] During the test, the internal fluid pressure increases continuously without intermediate unloading. The Ilyushin plastic strain–stress relationship can be expressed by

$$\sigma_\varphi^{'} = \frac{2}{3}\frac{\sigma_{\text{eff}}}{\varepsilon_{\text{eff}}}\varepsilon_\varphi^{'} \tag{13}$$

$$\sigma_t^{'} = \frac{2}{3}\frac{\sigma_{\text{eff}}}{\varepsilon_{\text{eff}}}\varepsilon_t^{'} \tag{14}$$

$$\sigma_\theta^{'} = \frac{2}{3}\frac{\sigma_{\text{eff}}}{\varepsilon_{\text{eff}}}\varepsilon_\theta^{'} \tag{15}$$

where $\boldsymbol{\sigma}' = [\sigma_\varphi^{'}, \sigma_t^{'}, \sigma_\theta^{'}]$ and $\boldsymbol{\varepsilon}' = [\varepsilon_\varphi^{'}, \varepsilon_t^{'}, \varepsilon_\theta^{'}]$ are the stress and strain deviators at a certain deformation state, respectively. Considering the total stress, Eq. (16) can be derived:

$$\frac{\sigma_\varphi - \sigma_t}{\varepsilon_\varphi - \varepsilon_t} = \frac{\sigma_t - \sigma_\theta}{\varepsilon_t - \varepsilon_\theta} = \frac{\sigma_\theta - \sigma_\varphi}{\varepsilon_\theta - \varepsilon_\varphi} \tag{16}$$

where ε_φ, ε_t and ε_θ are the strains along longitudinal, thickness and circumferential directions.

Combination Eq. (16) with Eq. (9), the stress along the circumferential direction can be obtained as

$$\sigma_\theta = \frac{P(r_\varphi - t)(r_\theta - t)}{(\varepsilon_t - \varepsilon_\varphi)(r_\theta - \frac{t}{2}) + (\varepsilon_t - \varepsilon_\theta)(r_\varphi - \frac{t}{2})} \tag{17}$$

The stress along the longitudinal direction can be derived from Eq. (9) as

$$\sigma_\varphi = \frac{P(r_\theta - t)(r_\varphi - t) - \sigma_\theta t(r_\varphi - \frac{t}{2})}{t(r_\theta - \frac{t}{2})} \tag{18}$$

From the Eqs. (7)–(18), the application of the plane stress state assumption ignores the stress through the thickness and simplifies the calculation for the stress tensor at the tube pole. Classical Hwang model and total strain model are presented to calculate the other two stress components along the longitudinal and circumferential directions, respectively. Whichever method is used, it is essential to measure the bulge height and pole thickness during the test.

In this research, the tube is assumed as an isotropic material and meets von Mises yield criterion, so its effective stress can be expressed by

$$\sigma_{\text{eff}} = \frac{1}{\sqrt{2}}\sqrt{(\sigma_\theta - \sigma_t)^2 + (\sigma_t - \sigma_\varphi)^2 + (\sigma_\varphi - \sigma_\theta)^2} \tag{19}$$

where σ_t, σ_θ and σ_φ can be obtained using Eqs. (7), (17), (18).

2.3. Strain analysis

For a calculation of the strain tensor at the pole point, assume that the strain increment is continuous and the principal strain direction keeps identical during the test. Thus, the strains along the circumferential and thickness directions can be described as[7]

$$\varepsilon_\theta = \ln\frac{R_0 + h - \frac{t}{2}}{R_0 - \frac{t_0}{2}} \tag{20}$$

$$\varepsilon_t = \ln\frac{t}{t_0} \tag{21}$$

Based on the volume constancy condition, the strain component ε_φ in the longitudinal direction can be written as

$$\varepsilon_\varphi = -(\varepsilon_\theta + \varepsilon_t) \tag{22}$$

In the bulge test, the internal fluid pressure increases continuously, and no intermediate unloading occurs. Tubular metal meets von Mises yield criterion, and the associated isotropic hardening model is considered to represent the subsequent yield surface; thus, the effective strain can be derived as

$$\varepsilon_{\text{eff}} = \frac{\sqrt{2}}{3}\sqrt{(\varepsilon_\theta - \varepsilon_t)^2 + (\varepsilon_t - \varepsilon_\varphi)^2 + (\varepsilon_\varphi - \varepsilon_\theta)^2} \tag{23}$$

3. Inverse strategy

The inverse modeling technique can be used to explore the optimum process design and identify material constitutive parameters. In general, an establishment process of inverse schemes involves the following steps: A) Problem statement and FEM modelling; B) Definition of design variables, objective functions, and constraints; C) Data collection and solution for the optimization problem; D) Evaluation of potential optimum parameters. Fig. 4 illustrates the flow chart of the inverse framework applied to determine constitutive parameters of tubular materials. The key steps mentioned above will be elaborated separately.

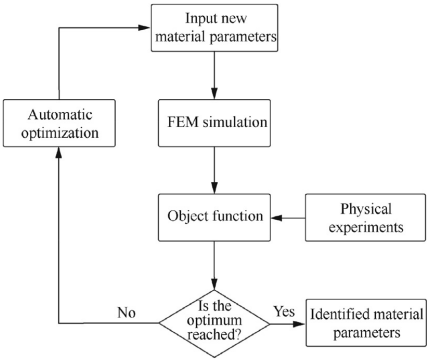

Fig. 4 Flow chart of inverse framework used for parameters identification of tubular materials.

3.1. FEM modelling of tube bulging process

The FEM model for the tube bulge process is created by general-purpose programme LS-DYNA, which is shown in Fig. 5. In this model, the tube is meshed by three-dimensional solid elements with eight-node hexahedrons, and three elements are produced through the tube wall thickness for an accurate response. Tubes used in the experiment are annealed, and the holding time lasts for 3 h, which means that the material has a strong isotropy. The von Mises yield criterion and Hollomon isotropic hardening law are used to describe the tubular materials' mechanical behaviors.

The internal fluid pressure is referred to as the compression stress and applied on the inner wall of the tube along the radial direction, and the pressure curve follows the one collected from the experiment. In order to reduce the calculation time, the mass scaling strategy is used, and a half of the tube is selected as the FEM model. Tube ends are fixed at all translational and rotational directions, because there is no sliding between tubes and the locking system by observation and measurement during the test.

3.2. Objective function and design variables

The nature of an inverse analysis is an optimization problem where design variables, i.e., material mechanical coefficients, are identified by minimizing the objective function under specified constraints. The material response under plastic deformation can be described by variety of constitutive equations with mathematical coefficients which will also be imported into FEM models easily. Therefore, the objective of the inverse analysis is to find the material parameters in the constitutive models, and the design variables can be defined as

$$\boldsymbol{x} = [x_1, x_2, ..., x_n]^{\mathrm{T}} \tag{24}$$

where n is the number of coefficients in the material model, and x_j is the j th element in this vector. To characterize tubular material mechanical properties with unknown design variables, a common elastic–plastic model with power law isotropic hardening is used to describe its behavior where the flow stress equation can be expressed as

$$\sigma = K\varepsilon^e \tag{25}$$

where K is the strength coefficient; e is the hardening exponent, and these two material parameters can be selected as design variables.

The objective function is a pointer to evaluate the error between experimental and simulated data, which should have the following properties:[23]

(1) All collected experimental data using different methods and equipment should be involved in the iteration process.
(2) The final optimization results should not be sensitive to the unit of the data.
(3) Weighting factors need to be allocated to different experimental points according to their physical characteristics.

In the tube hydraulic bulge test, the filling height and pole thickness under different internal pressures are collected, so the cost function should consist of the above two terms. Meanwhile, an error definition with a least square structure is introduced to increase the sensitivity of the cost function to the design variables and reduce the influences of the two measure indicators' magnitudes.[24] Therefore, the objective function can be defined as

$$f = \alpha f_1 + (1-\alpha) f_2 \tag{26}$$

$$f_1 = \sum_{i_1=1}^{n_1} \left[\omega_{i_1}\left(h_{i_1}^{\exp} - h_{i_1}^{\mathrm{sim}}\right)\right]^2 \tag{27}$$

$$f_2 = \sum_{i_2=1}^{n_2} \left[\omega_{i_2}\left(t_{i_2}^{\exp} - t_{i_2}^{\mathrm{sim}}\right)\right]^2 \tag{28}$$

where f_1 is the first part in the cost function for representing the residual of the bulge height h under different pressures; f_2 is the second residual of the pole thickness t obtained by simulations and experiments; α is a weighted factor ranging from 0 to 1 to represent the importance of the two sub-objectives of the cost function; the subscript i_1 and i_2 represent the i_1 th data point of the bulge height and the i_2 th data point of the pole thickness, respectively; the superscript exp and sim represent the data point of experiment and simulation; n_1 and n_2 are the total experimental point numbers for the pole thickness and bulge height, respectively; ω is an automatic scaling factor to increase the sensitivity of experimental points especially in the area of large plastic deformation for the two sub-objective functions, and can be expressed as[24]

$$\omega_{i_1} = \frac{2(n_1+n_2)h_{i_1}^{\exp}}{\sum_{i_1=1}^{n_1}\sum_{i_2=1}^{n_2}\left(h_{i_1}^{\exp} + t_{i_2}^{\exp}\right)} \tag{29}$$

The scaling factor ω_{i_1} calculated by this equation can be distributed to the corresponding residuals in the first sub-objective function. ω_{i_2} can be obtained by a similar formula to Eq. (29) and is used for the second sub-objective function.

3.3. Optimization algorithm

The inverse parameter identification can be seen as an optimization problem, so an efficient and robust optimization method is necessary to minimize the defined cost function in Eq. (26). In the present research, a classical and robust gradient-based optimization method, i.e., an improved Levenberg-Marquardt algorithm is used to identify the tubular mechanical parameters.

As can be seen from Eqs. (26)–(29), the objective function consists of the sum of the squares of the true errors between experimental and simulated responses and can be regarded as a nonlinear least square problem. The Gauss-Newton

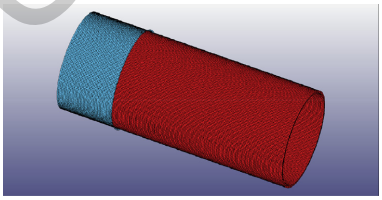

Fig. 5 FEM model for hydraulic bulging process.

method with line search performs very poorly and leads to numerical convergence difficulties, because the true error, i.e., the residual function $\boldsymbol{r}(\boldsymbol{x})$ including the FEM model, exhibits severe nonlinearity. In order to overcome these difficulties, an improved Levenberg-Marquardt algorithm with the trust region strategy is considered where the objective function can be approximated as a quadratic model in the neighborhood of a given starting point $\boldsymbol{x}_k$ as

$$\boldsymbol{f}(\boldsymbol{x}_k+\boldsymbol{s}_k)-\bar{\boldsymbol{f}}(\boldsymbol{s}_k)=\boldsymbol{f}(\boldsymbol{x}_k)+\boldsymbol{g}^{\mathrm{T}}(\boldsymbol{x}_k)\boldsymbol{s}_k+\frac{1}{2}\boldsymbol{s}_k^{\mathrm{T}}\boldsymbol{G}(\boldsymbol{x}_k)\boldsymbol{s}_k \tag{30}$$

where $\boldsymbol{x}_k$ is design variable at k th iteration; $\boldsymbol{s}_k$ is step size; $\boldsymbol{g}^{\mathrm{T}}(\boldsymbol{x}_k)$ and $\boldsymbol{G}(\boldsymbol{x}_k)$ are the gradient and Hessian matrix of the cost function, respectively, which can then be expressed as

$$\boldsymbol{g}(\boldsymbol{x}_k)=\boldsymbol{J}^{\mathrm{T}}(\boldsymbol{x}_k)\boldsymbol{r}(\boldsymbol{x}_k) \tag{31}$$

$$\boldsymbol{G}(\boldsymbol{x}_k)=\boldsymbol{J}^{\mathrm{T}}(\boldsymbol{x}_k)\boldsymbol{J}(\boldsymbol{x}_k)+\boldsymbol{S}(\boldsymbol{x}_k) \tag{32}$$

where $\boldsymbol{S}(\boldsymbol{x}_k)$ is second term in the Hessian matrix; $\boldsymbol{J}(\boldsymbol{x}_k)$ is Jacobian matrix of the cost function.

The Jacobian matrix $\boldsymbol{J}(\boldsymbol{x}_k)$ is the first partial derivatives of the residual function $\boldsymbol{r}(\boldsymbol{x})$. It is impossible to give an analytical formula for Jacobian $\boldsymbol{J}(\boldsymbol{x}_k)$, because $\boldsymbol{f}(\boldsymbol{x})$ is a nonlinear implicit function and given in a black box. Therefore, the finite difference strategy is introduced to calculate the $(i,\,j)^{\mathrm{th}}$ element in Jacobian matrix $\boldsymbol{J}(\boldsymbol{x}_k)$ by

$$\frac{\partial \boldsymbol{r}_i}{\partial \boldsymbol{x}_j}=\frac{\boldsymbol{r}_i(\boldsymbol{x}_k+\delta\boldsymbol{e}_j)-\boldsymbol{r}_i(\boldsymbol{x}_k)}{\delta} \tag{33}$$

where $\boldsymbol{r}_i$ is the i th component of objective function; δ is chosen appropriately small; $\boldsymbol{e}_j$ is the unit vector. Then the step size $\boldsymbol{s}_k$ can be defined by the solution of Eqs. (30)–(33) using the trust region technique as

$$\boldsymbol{x}_{k+1}=\boldsymbol{x}_k-(\boldsymbol{J}^{\mathrm{T}}(\boldsymbol{x}_k)\boldsymbol{J}(\boldsymbol{x}_k)+\boldsymbol{S}(\boldsymbol{x}_k))\boldsymbol{g}(\boldsymbol{x}_k) \tag{34}$$

$$\boldsymbol{S}(\boldsymbol{x}_k)=\mu_k\boldsymbol{D}_k^{\mathrm{T}}\boldsymbol{D}_k \tag{35}$$

where μ_k is damping factor.

The damping factor μ_k can be used to control the searching direction and step size in the current iteration. A new update strategy for the value of μ_k is recommended and numerical experiments demonstrate its good robustness and smoothness.[25] The change of μ_k depends on the gain ratio ρ which indicates the agreement of the approximated function to the actual objective function and can be written as

$$\rho=\frac{\|\boldsymbol{r}(\boldsymbol{x}_k)\|^2-\|\boldsymbol{r}(\boldsymbol{x}_k+\boldsymbol{s}_k)\|^2}{\|\boldsymbol{r}(\boldsymbol{x}_k)\|^2-\|\boldsymbol{r}(\boldsymbol{x}_k)+\boldsymbol{J}(\boldsymbol{x}_k)\boldsymbol{s}_k\|^2} \tag{36}$$

A wide variation of values between the strength coefficient and the hardening exponent could be of order 10^4. The ellipsoidal trust region[26] is used to reduce the effects of poor scaling in inverse problems, where a diagonal and positive definite matrix $\boldsymbol{D}_k$ is introduced into this formula, of which diagonal entries can be updated from iteration to iteration by

$$\boldsymbol{D}_k=\mathrm{diag}(d_1^k,d_2^k,\cdots,d_{n_1+n_2}^k) \tag{37}$$

$$d_i^0=\|\frac{\partial \boldsymbol{r}_i(\boldsymbol{x}_0)}{\partial \boldsymbol{x}_0}\| \tag{38}$$

$$d_i^k=\max\left(d_i^{k-1},\|\frac{\partial \boldsymbol{r}_i(\boldsymbol{x}_k)}{\partial \boldsymbol{x}_k}\|\right)\quad k\geq 1 \tag{39}$$

The new point $\boldsymbol{x}_{k+1}$ can be updated iteration by iteration using the solution of Eq. (34). Then, the optimum point will be obtained when the optimization process meets the convergence conditions. Therefore, the following two stopping criteria are used in this algorithm:

$$\|\boldsymbol{g}(\boldsymbol{x}_k)\|\leq\delta_1 \tag{40}$$

$$\|\boldsymbol{x}_{k+1}-\boldsymbol{x}_k\|\leq\delta_2(\|\boldsymbol{x}_k\|+\delta_2) \tag{41}$$

where δ_1 and δ_2 are two small and positive real numbers given by a user. When these two criteria are satisfied, the iteration process will be terminated.

4. Experimental tooling and method

4.1. Tensile test

A standard uni-axial tensile test has been conducted to characterize the flow stress curve of used tubular aluminium tubes. Tension specimens are cut directly from the tubes along the longitudinal direction as shown in Fig. 6, and their geometric dimensions follow the ASTM E8/E8M-21 standard.[5] However, the subsize specimen type is used for the tensile test, because the diameter of the tubes is so small that standard tension specimens are difficult to be machined. The tensile test is performed at room temperature and under a strain rate of 1.4 mm/min using a CMT electrical universal testing machine.

4.2. Hydraulic bulge test

A flexible tube hydraulic bulging device has been designed and manufactured to determine the tubular material flow stress–strain behavior under the bi-axial stress state, as shown in Fig. 7. It can be seen that this setup is mainly comprised of a hydraulic power system, a control system, and basic die sets. The two outermost hydraulic cylinders can not only move on the basement horizontally and achieve more flexibility for testing tubes with different lengths, but also apply an axial force or even a stretch force on tube ends and produce different stress states for specimens during a test.

Tube ends could be locked by two hydraulic clamping devices in the middle to guarantee no sliding along the axial direction of specimens and fluid leakage. By changing the mandrels and gaskets in the locking system, tubes with different

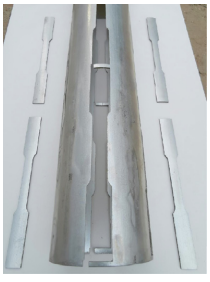

Fig. 6 Specimens for tensile test cut from tube along longitudinal direction.

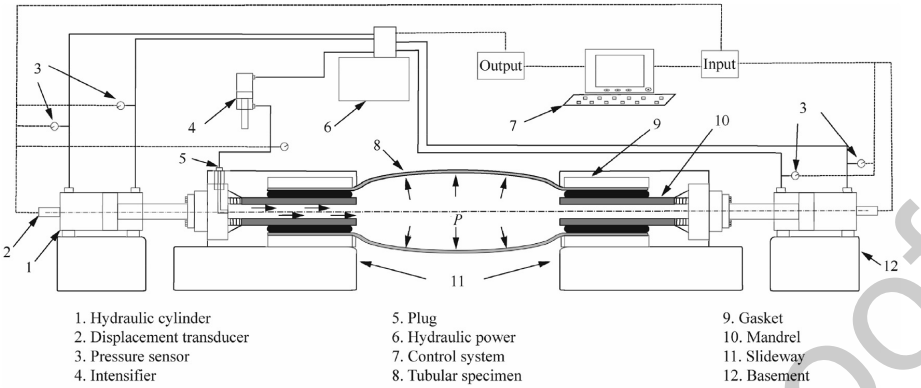

Fig. 7 Schematic diagram for hydraulic bulging setup.

diameters and wall thicknesses can be tested. Fig. 8 illustrates the schematic diagram of this flexible locking setup.

Bulging tests of annealed aluminium alloy tubes are performed on this hydraulic machine. The maximum bulging pressure is determined firstly by a general tube bulge until its bursting, and this procedure is repeated at least three times to get an accurate average bursting value. Then several tubular specimens are formed under different pressure levels lower than the maximum bursting pressure. After the bulging pressure reaches to a specified value, the tube is taken off from the machine. The bulge height and pole thickness can be measured by a micrometer, and the corresponding internal pressure is recorded by a transducer on the machine.

5. Results and discussion

Fully-annealed 5049 aluminium seamless tubes are used and investigated, of which chemical compositions are displayed in Table 1. The initial diameter and wall thickness of tested samples are 50.00 mm and 1.086 mm, respectively. The total length of every tubular specimen in the hydraulic bulge test is 300.00 mm, and the bulge zone is about 243.00 mm long.

The maximum bulging pressure is 7.8 MPa determined by the observation of the first tubular specimen bursting. Below this pressure value, more tube hydraulic bulging tests are performed under different pressure levels. To obtain more equivalent strain–stress points, 16 pressure levels with distinct intervals are inserted into the reasonable range. After the bulging, the corresponding bulge height and wall thickness at the tube pole are measured every 90° along the tube circumferential direction in the middle cross-section of the bulged tube, and several recorded typical values are displayed in Table 2. It is obvious that with an increase of the internal pressure, the bulge height of the tube is increased, and the wall thickness becomes thinner.

Fig. 9 shows the profile shape of all tubular specimens at the end of the bulging test. It can be seen that the total length of tubes before and after bulging tests has almost no change by observation. This phenomenon is verified by actual measurements for all tubular specimens after deformation, which means that the tube ends are fixed by the locking system on the machine, so there is no slippage between specimens and die sets during the deformation. Therefore, clear boundary conditions that tubes are bulged under a bi-axial stress state

Table 1 Chemical compositions of tested 5049-O aluminum alloy tubes.

Element	Content (wt%)
Fe	0.154
Si	0.071
Cu	0.004
Mg	1.87
Mn	0.72
Zn	0.015
Ti	0.007
Cr	0.009

Fig. 8 Locking system for ends of tubular specimens on machine.

Table 2 Selected experimental results from tube hydraulic bulge test.

Specimen No.	Pressure (MPa)	Diameter (mm)	Pole thickness (mm)
1	2.0	50.09	1.085
2	4.0	50.28	1.078
3	6.0	51.05	1.063
4	6.6	51.78	1.055
5	7.0	52.35	1.041
6	7.4	52.87	1.024

Fig. 9 Tubular specimens before and after hydraulic test.

can be achieved, and the interface friction between tools and parts can be neglected in analytical or numerical models.

Based on this bulge test data, the inverse identification of tubular material parameters is performed using the optimization technique developed in Section 3.3. Several different sets of starting points in a feasible region are tested in this inverse analysis. The determined optimum parameters, the corresponding gradient of the cost function to design variables, and the error between experimental and computed data at optimum points are presented in Table 3. As can be seen from Table 3, although the guessed initial values cover a large range sometimes even far from the optimum point where the hardening strength ranges from 300.00 to 500.00, e-value from 0.20 to 0.40, the final identified material coefficients converge to the same solution. Besides, values of the objective function and their gradients in all cases are reduced to the same level approximately and satisfy the optimality conditions, which illustrates the stability and robustness of the inverse framework.

An iteration process of the objective function and its corresponding gradient for the 5th initial value is plotted and presented in Fig. 10. From Fig. 10, it is possible to conclude that the least square error is reduced to a small value close to zero after 5 iterations, which leads to a satisfied fitting quality between experimental and computed data. At the same time, the gradient of the cost function reaches a lower value than the one defined in the stopping criteria and terminates the optimization process. Fig. 11 illustrates the evolution process of material constitutive parameters during the optimization. For design variables, the hardening exponent sharply increases from the initial 0.200 to 0.302 after 1 iteration while remaining the same value at the 2nd iteration and then increasing and reaching the optimum value in next iterations. The

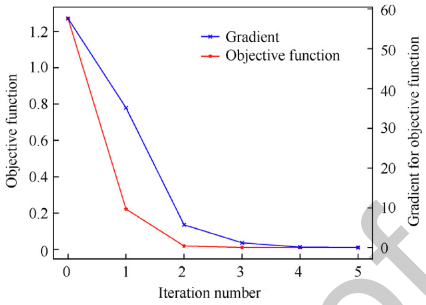

Fig. 10 Iteration process of objective function and its gradient during optimization.

strength coefficient has a gradual rise from the initial 300.00 to 379.01 as the number of iterations increases. Only 5 iterations are needed to perform in this framework, and the small number of iterations shows the efficiency of the developed optimization technique to solve the inverse problem.

The experimental data obtained from the tube bulge test is imported into the total strain model and Hwang model, and several pairs of points in the strain–stress curve are determined. Fitting these points to the material hardening model defined in Eq. (25) using a least square method, the material strength coefficient and hardening exponent are obtained. As a comparison, material parameters identified by the inverse strategy and two different analytical models are shown in Table 4, and the corresponding flow stress curve can be obtained as shown in Fig. 12.

The strain–stress relationship determined by the universal tensile test is plotted and displayed in Fig. 12. It can be seen from the comparison that there are some differences between the flow stress curve determined by tension tests and that by hydro bulge tests. The effective stress obtained by bulge tests is lower than that determined by tension tests, especially at large plastic effective strains. Moreover, a tensile test under a uni-axial stress state overestimates the material deformation limit under a bi-axial tension stress state when compared with a bulge test. For fitted stress–strain curves based on bulging tests, three models give identical results of tension tests in

Table 3 Identified optimal values for several sets of different initial points.

Set	Initial point x_0				Optimum solution x^*			
	K	e	$f(x_0)$	$f'(x_0)$	K	e	$f(x^*)$	$f'(x^*)$
1	500.00	0.40	6.43×10^{-2}	1.89	380.88	0.312	9.99×10^{-3}	6.00×10^{-2}
2	450.00	0.35	1.91×10^{-1}	1.66×10^{1}	378.88	0.310	9.95×10^{-3}	5.22×10^{-2}
3	400.00	0.30	5.08×10^{-1}	3.01×10^{1}	379.07	0.310	9.96×10^{-3}	9.64×10^{-2}
4	350.00	0.25	9.16×10^{-1}	4.30×10^{1}	379.15	0.310	9.96×10^{-3}	8.83×10^{-2}
5	300.00	0.20	1.27	5.76×10^{1}	379.01	0.310	9.96×10^{-3}	6.61×10^{-2}
6	300.00	0.40	5.23×10^{3}	1.30×10^{5}	379.04	0.310	9.95×10^{-3}	7.32×10^{-2}
7	350.00	0.35	1.55×10^{1}	7.58×10^{2}	378.73	0.310	9.96×10^{-3}	1.04×10^{-1}
8	450.00	0.30	1.63	3.50×10^{1}	379.89	0.311	9.97×10^{-3}	5.77×10^{-2}
9	500.00	0.25	3.38	2.62×10^{1}	379.30	0.310	9.96×10^{-3}	8.21×10^{-2}
Mean value					379.33	0.310		

Please cite this article in press as: ZHANG B et al. An inverse strategy to determine constitutive parameters of tubular materials for hydroforming processes, *Chin J Aeronaut* (2021), https://doi.org/10.1016/j.cja.2021.11.007

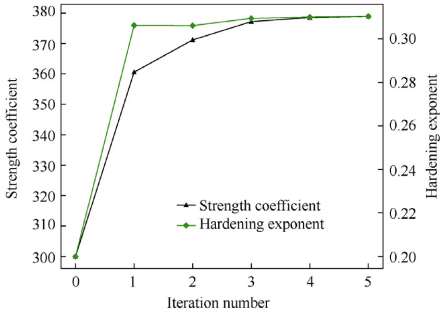

Fig. 11 Iteration process of design variables during optimization.

Table 4 Identified flow stress models using different methods.

Testing method	Model	Stress–strain relation
Tensile test		$\sigma = 396.75\varepsilon^{0.297}$
Bulge test	Inverse	$\sigma = 379.33\varepsilon^{0.310}$
	Hwang	$\sigma = 418.08\varepsilon^{0.366}$
	Total strain	$\sigma = 433.16\varepsilon^{0.362}$

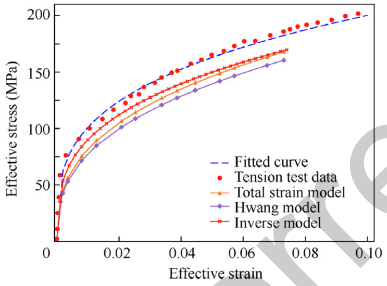

Fig. 12 Comparison of effective strain–stress curves obtained by tensile test and bulge test.

the small strain region, and the stress difference raises with an increase of the strain. The effective stress predicted by Hwang model is always lower than those by the other two models. Then the flow stress curve determined by the inverse model is very close to that by the total strain model in a large strain range, while the difference between the results of the inverse model and the tensile test is smaller compared with those of the other two analytical models.

In order to evaluate the performance of different tests and models, FEM simulations for the tube hydraulic bulging process are performed by LS-DYNA program with identified flow stress curves. Other input data like the pressure loading curve and simulation speed are identical in numerical models. The calculated pole thickness, bulge height, and profile shape in the deformation zone are analyzed and compared with those from the physical experiment.

Fig. 13 shows the comparison of the internal pressure versus the bulge height curve between experimental values and numerical outputs of FEM models using material parameters given in Table 4. It can be seen that the calculated bulge height with a flow curve identified by the inverse model has a good agreement with the experimental data when compared with the other three methods. Furthermore, a detailed quantitative deviation is displayed in Table 5 and Fig. 14. It is demonstrated that the relative errors between simulation results of all methods and experimental measurements are higher at lower bulging pressures, while these differences are reduced as the pressure increases. Furthermore, the smallest mean value of the relative deviation also validates that material parameters obtained by the inverse model are more accurate than those by Hwang and total strain models.

Fig. 15 shows the comparison of the internal pressure versus the pole thickness curve between experimental data and the corresponding FEM results using various flow stress curves. Fig. 16 and Table 5 illustrate a quantitative error comparison and analysis. As can be seen from these results, material parameters determined by inverse model lead to satisfactory fitting agreement and the smallest mean deviation between experimental and numerical data. A higher relative error is observed at high bulging pressure levels for Hwang model and tension tests. For the total strain and inverse models, the small deviation is still kept throughout the deformation process, especially for the inverse model which performs better than other models at a large-deformation state.

The calculated bulge profile using constitutive parameters determined by different models can be observed in Fig. 17, in which the measured tube radii along longitudinal positions in experiments are presented. It is obvious that the predicted bulge profile based on the tube bulge test matches better to experimental measures compared with that of the tensile test. The quantitative gap between experimental data and FEM outputs by three models can be observed in Fig. 18 and Table 5, and it can be seen that the bulge profile calculated by the inverse model leads to the smallest deviation and is very close to experimental results compared with those of Hwang and total strain models.

From these comparisons, it can be concluded that the three models, i.e., the inverse model, the total strain model, and Hwang model, can be used to translate the collected experimental data into a flow stress curve, while the inverse model presents more satisfying results to experimental measures com-

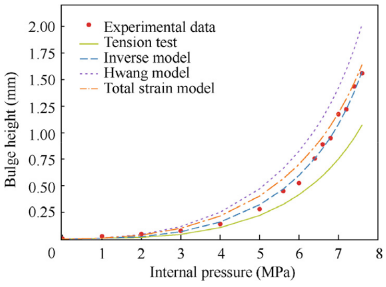

Fig. 13 Comparison of internal pressure versus bulge height curves obtained by different methods.

Table 5 Relative errors between simulation data and experimental measured results.

Data type	Test method and model	Relative error (%)		
		Min	Mean	Max
Bulge height	Inverse model	5.74×10^{-4}	1.44×10^{-1}	7.18×10^{-1}
	Hwang model	9.66×10^{-2}	4.21×10^{-1}	7.89×10^{-1}
	Total strain model	8.63×10^{-3}	2.39×10^{-1}	7.17×10^{-1}
	Tensile test	2.09×10^{-1}	3.60×10^{-1}	7.20×10^{-1}
Pole thickness	Inverse model	1.73×10^{-4}	1.48×10^{-3}	4.41×10^{-3}
	Hwang model	1.66×10^{-4}	8.48×10^{-3}	1.58×10^{-2}
	Total strain model	8.30×10^{-5}	3.15×10^{-3}	8.35×10^{-3}
	Tensile test	2.30×10^{-4}	7.81×10^{-3}	2.18×10^{-2}
Bulge profile	Inverse model	3.79×10^{-4}	1.58×10^{-3}	3.04×10^{-3}
	Hwang model	7.33×10^{-3}	1.26×10^{-2}	1.80×10^{-2}
	Total strain model	3.18×10^{-3}	3.52×10^{-3}	5.01×10^{-3}
	Tensile test	6.12×10^{-3}	1.20×10^{-2}	1.76×10^{-2}

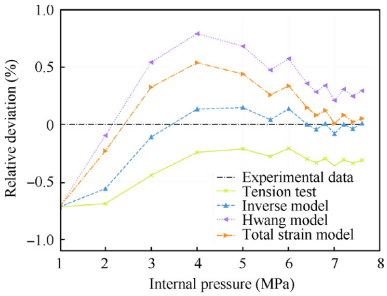

Fig. 14 Deviation analysis of internal pressure versus bulge height curves obtained by different methods.

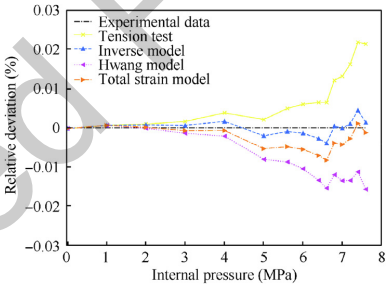

Fig. 16 Deviation analysis of internal pressure versus pole thickness curves obtained by different methods.

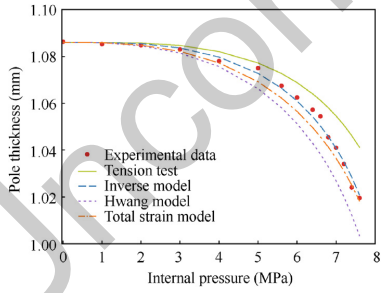

Fig. 15 Comparison of internal pressure versus pole thickness curves obtained by different methods.

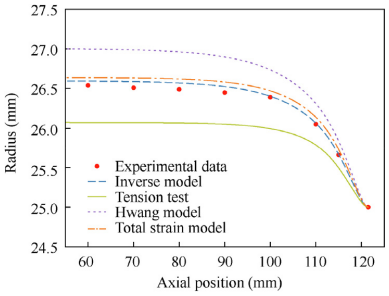

Fig. 17 Comparison of axial position versus bulge profile obtained by different methods.

pared with those of the other two models. One reason for that is the inverse model removes the geometrical and mechanical assumptions in analytical models, and the isolated analysis of the stress and strain in Hwang model and assumptions in the total strain model lead to a big difference between simulated and experimental data.

6. Conclusions

(1) Tube bulging tests with fixed-end conditions for 5049-O aluminium alloy are performed on a flexible hydraulic forming press. The bulge height, pole thickness, and bulge profile under different fluid pressure levels are measured during experiments.

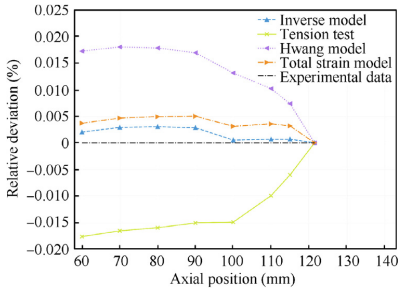

Fig. 18 Deviation analysis of axial position versus bulge profile obtained by different methods.

(2) An inverse framework combining the incremental strain theory with an improved Levenberg-Marquardt algorithm is developed to identify tubular metal properties by a minimization of the least square error between calculated and experimental data. Several sets of initial guesses are tested for this inverse strategy, and the convergence to an identical optimum solution shows that this framework is robust and efficient for characterization of tubular materials.

(3) Two analytical models based on membrane mechanics and the total strain theory are proposed to model the hydro bulging process and determine the strain–stress relationship of 5049-0 aluminium alloy. Obtained flow stress curves are compared with that from a tensile test, which demonstrates that a bulge test is more suited to characterize the tubular material behavior because its stress state is closer to the actual hydroforming process.

(4) FEM simulations for a free bulge test are conducted using identified flow stress curves from different tests and models. Predicted bulge height, bulge profile shape, and pole thickness from FEM models are compared with measured values, and results from the inverse model show a good agreement with experimental data. It can be concluded that the inverse model is more accurate than Hwang and total strain models for characterization of tubular material properties.

Acknowledgements

The first author acknowledges the financial support from China Scholarship Council (CSC)_(No. 201706080020) for his study at Aalborg University in Denmark.

Data availability statement

The raw data required to reproduce these findings are available from the corresponding author upon reasonable request.

References

1. Wang Y, Lang L, Sherkatghanad E, et al. Design of an innovative multi-stage forming process for a complex aeronautical thin-walled part with very small radii. *Chin J Aeronaut* 2018;**31**(11):2165–75.
2. Zhan M, Guo K, Yang H. Advances and trends in plastic forming technologies for welded tubes. *Chin J Aeronaut* 2016;**29**(2):305–15.
3. Alaswad A, Benyounis KY, Olabi AG. Tube hydroforming process: A reference guide. *Mater Des* 2012;**33**:328–39.
4. Bruschi S, Altan T, Banabic D, et al. Testing and modelling of material behaviour and formability in sheet metal forming. *CIRP Ann* 2014;**63**(2):727–49.
5. ASTM E8/E8M-21. *Standard test methods for tension testing of metallic materials*. West Conshohocken: ASTM International; 2021.
6. Wang H, Martin P. Tube formability assessment for tube hydroforming. *SAE Int J Mater Manuf* 2002;**111**(5):880–9.
7. Fuchizawa S, Narazaki, Yuki H. Bulge test for determining stress-strain characteristics of thin tubes. In: Wang ZR, He YX, editors. *Advanced technology of plasticity. Proceedings of the 4th International Conference on Technology of Plasticity; 1993 Sep 5–9; Beijing, China*. Beijing: International Academic Publishers; 1993. p. 488–93.
8. Hwang YM, Lin YK, Altan T. Evaluation of tubular materials by a hydraulic bulge test. *Int J Mach Tools Manuf* 2007;**47**(2):343–51.
9. Velasco R, Boudeau N. Tube bulging test: Theoretical analysis and numerical validation. *J Mater Process Technol* 2008;**205**(1-3):51–9.
10. Ynag LF, Guo C. Determination of stress-strain relationship of tubular material with hydraulic bulge test. *Thin Walled Struct* 2008;**46**(2):147–54.
11. Bortot P, Ceretti E, Giardini C. The determination of flow stress of tubular material for hydroforming applications. *J Mater Process Technol* 2008;**203**(1–3):381–8.
12. Ponthot JP, Kleinermann JP. A cascade optimization methodology for automatic parameter identification and shape/process optimization in metal forming simulation. *Comput Methods Appl Mech Eng* 2006;**195**(41–43):5472–508.
13. Cho H, Altan T. Determination of flow stress and interface friction at elevated temperatures by inverse analysis technique. *J Mater Process Technol* 2005;**170**(1-2):64–70.
14. Andrade-Campos A, Thuillier S, Pilvin P, et al. On the determination of material parameters for internal variable thermoelastic-viscoplastic constitutive models. *Int J Plast* 2007;**23**(8):1349–79.
15. de-Carvalho R, Valente RAF, Andrade-Campos A. Optimization strategies for non-linear material parameters identification in metal forming problems. *Comput Struct* 2011;**89**(1-2):246–55.
16. Shrot A, Bäker M. A study of non-uniqueness during the inverse identification of material parameters. In: Wegener K, editor. *CIRP: Proceedings of 5th CIRP Conference on High Performance Cutting; 2012 Jun 4–7; Zürich, Switzerland*. New York: Curran; 2012. p. 72–7.
17. Rauchs G, Bardon J. Identification of elasto-viscoplastic material parameters by indentation testing and combined finite element modelling and numerical optimization. *Finite Elem Anal Des* 2011;**47**(7):653–67.
18. Zribi T, Khalfallah A, BelHadjSalah H. Experimental characterization and inverse constitutive parameters identification of tubular materials for tube hydroforming process. *Mater Des* 2013;**49**:866–77.
19. Khalfallah A, Oliveira MC, Alves JL, et al. Mechanical characterization and constitutive parameter identification of anisotropic tubular materials for hydroforming applications. *Int J Mech Sci* 2015;**104**:91–103.
20. He ZB, Yuan SJ, Lin YL, et al. Analytical model for tube hydro-bulging test, Part I: Models for stress components and bulging zone profile. *Int J Mech Sci* 2014;**87**:297–306.
21. Song WJ, Kim J, Kang BS. Experimental and analytical evaluation on flow stress of tubular material for tube hydroforming simulation. *J Mater Process Technol* 2007;**191**(1-3):368–71.
22. Ilyushin AA, Lensky VS. *Strength of materials*. Oxford: Pergamon Press; 1967. p. 199–207.

23. Andrade-Campos A, de-Carvalho R, Valente RAF. Novel criteria for determination of material model parameters. *Int J Mech Sci* 2012;**54**(1):294–305.
24. Cao J, Lin J. A study on formulation of objective functions for determining material models. *Int J Mech Sci* 2008;**50**(2):193–204.
25. Nielsen HB. Damping parameter in Marquardt's method. Lyngby: Technical University of Denmark; 1999. Report No.: IMM-REP-1999-05.
26. Moré JJ. The Levenberg-Marquardt algorithm: Implementation and theory. In: Watson GA, editor. *Numerical analysis. Proceedings of the Biennial Conference; 1977 Jun 28–Jul 1; Dundee, Scotland*. Berlin: Springer; 1978. p. 5–16.

Please cite this article in press as: ZHANG B et al. An inverse strategy to determine constitutive parameters of tubular materials for hydroforming processes, *Chin J Aeronaut* (2021), https://doi.org/10.1016/j.cja.2021.11.007

Chapter 5

Paper II

Characterization of mechanical properties for tubular materials based on hydraulic bulge test under axial feeding force

Bin Zhang, Benny Endelt, and Karl Brian Nielsen

The paper has been submitted to the
Fundamental Research.

Characterization of mechanical properties for tubular materials based on hydraulic bulge test under axial feeding force

Bin Zhang[a,*], Benny Endelt[a], Karl Brian Nielsen[b]

[a] *Department of Materials and Production, Aalborg University, Aalborg 9220, Denmark*
[b] *Department of Mechanical and Production Engineering, Aarhus University, Aarhus 8000, Denmark*

Abstract

A T-shape tube hydraulic bulge test under axial feeding force is carried out to characterize the mechanical properties of EN AW 5049-O and 6060-O aluminium alloys. The punch displacement, T-branch height and axial compressive force are recorded online during the experiment. An intelligent inverse identification framework combining the finite element method and numerical optimization algorithm is developed to determine material parameters by fitting simulated results to the experimental data iteratively. The identified constitutive parameters using the inverse modelling technique are compared with those determined by the theoretical analysis and uniaxial tensile test. The comparison shows that the predicted bulge height and punch force based on the material parameters obtained by the three methods are different and the inverse strategy produces the smallest gap between numerical and experimental values. It is possible to conclude that the hydraulic bulge test can be applied to characterize the stress-strain curve of tubular materials at the large strain scope, and the automatic inverse framework is a more accurate post-processing procedure to identify material constitutive parameters compared with the classical analytical model.

Keywords: Intelligent optimization, Tubular material, Parameter

*Corresponding Author.
E-mail: zhangbin20100@outlook.com.
Address: Department of Materials and Production, Aalborg University, Fibigerstræde 16, Aalborg DK-9220, Denmark.

identification, Hydraulic bulge test, Constitutive model

1. Introduction

Tube hydroforming technologies are playing an increasingly important role in modern advanced manufacturing processes, which provide more possibilities for lightweight design and precision production of complex tubular components used in the automotive and aerospace industries[1,2]. The stable quality and excellent performance of tubular products in the metal forming processes require essential information such as the hardening and fracture of the incoming metallic tube[3,4]. Further, an accurate output from the finite element (FE) method also depends heavily on the reliable mechanical property characterization[5–7].

Scientists and engineers have proposed many different experimental methods to characterize the mechanical properties of thin-walled tubes. Tensile tests are carried out for the specimens cut from tubes along the longitudinal direction, but this operation is difficult to achieve on tubes with small diameters[8,9]. Ring samples can be cut from small thin-walled tubes along the circumferential direction[10,11]. However, the stress and strain state of these samples in the longitudinal or circumferential tension test is quite different from that in the actual tube forming process where the equivalent plastic strain is in the range of 1 - 1.5 and dominated by compression whereas the uniaxial data is in the range of 0.15 to 0.4 depending on the material[9]. Thus, FE models depend heavily on extrapolation of the hardening behavior and such an extrapolation can reduce the prediction accuracy from FE outputs[12].

Axial and lateral compression tests of the whole tube can be performed to determine the flow stress curve of the tubular material under compressive stress state and without machining specified shaped samples, which are described in these works[13–15]. One drawback of these test methods is that the sudden buckling of tubular specimens causes unstable and incomplete data collection during the experiment, and this test is only limited to determining material behaviour in one direction, which may lead to large errors for FE simulations in some cases[16]. Compared with the above experimental methods, tube hydraulic bulge test is a more advanced characterization technique that can comprehensively represent the mechanical properties of tubular materials with flexible end-conditions[17].

Many researchers have investigated different types of hydraulic bulge tests but most of them focus on tube hydro bulging processes with free or fixed

end-conditions[18–24]. Various experimental setups have been designed and manufactured to carry out the above experiments. For instance, Fuchizawa et al.[19] have designed a bulging device where tube ends are locked on the end supports to seal the internal liquid, and one of the supports can move freely to reduce the longitudinal stretching of specimens. Koc et al.[20,25,26] use a stand alone press to bulge tubular materials, in which both ends of the tube are completely fixed by the friction between dies and urethane expansion plugs. Zhang et al.[27] apply a more flexible locking system to restrain the axial movements of samples, and tubes with different diameters and wall thicknesses can be tested by replacing gaskets. Another design mechanism has been proposed[22] to achieve a fixed end-condition, where conical punches with an angel are used to form tube ends with the wedge expansion shape to avoid the axial sliding of tubular samples. However, free or fixed bulge tests without axial feeding force will reduce the bulge height and the equivalent strain in a small range can be obtained.

On the other hand, a number of efforts have been made in the modelling of tube hydraulic bulging processes with fixed and free end-conditions to determine the flow stress curve of tested tubular materials. These developed theoretical models are based on membrane theory where a force equilibrium equation is constructed on the thin element at the center of the bulge deformation zone using the plane stress hypothesis[28]. Strain components are calculated based on the volume constancy law and different geometrical assumptions for the bulge profile shape such as a circular arc[19], two circumference arcs[23,29], an eplliptical curve[30,31] and a spline function[21]. A detailed comparison of advantages and drawbacks for the above models is presented in these works[32–34], and isolated stress-strain solutions and excessive assumptions can reduce the accuracy of identified results using the above methods. It should be pointed out that the inverse strategy has made substantial progress in accuracy improvement of determined parameters for tubular materials[27,35]. However, the application cases of the inverse scheme focus on the free and fixed hydro bulging processes[24,27,36–39], and fewer papers have reported on the inverse strategy applied to the tube hydraulic bulge test under axial compressive force.

In this study, T-shape hydraulic bulge tests under axial feeding force for two types of thin-walled metal tubes have been performed on a multifunctional hydraulic machine. An inverse framework combining the FE method with the Levenberg-Marquardt algorithm is used to identify material parameters based on the experimental data collected from bulge tests. The paper

structure is as follows: Section 2 presents all the experimental work including tested tubular materials and experimental tools. The inverse strategy and theoretical analysis to determine the parameters of tubular materials are introduced in Section 3. In Section 4, the experimental data and results comparison of identified material parameters obtained by different methods are discussed. The main conclusions are drawn in Section 5.

2. Experimental work

2.1. Tested material

Hydraulic bulge tests were carried out for the thin-walled seamless tubes made of EN AW 5409-O and EN AW 6060-O aluminium alloys. 5049-O aluminium is widely applied to the air cooling and heat exchanger system of an automotive because of its excellent formability and corrosion resistance[40]. The latter material is a common commercial aluminium alloy used in civil and architecture engineering[41]. In the current study, the used tubular samples were fully annealed before actual experiments and their initial nominal wall thickness and external diameter are $1.50mm$ and $32.00mm$, respectively. Tested specimens are cut into $150.00mm$ length from the same tube batch to reduce unpredictable errors.

Figure 1: Experimental setup for tube hydraulic bulge test

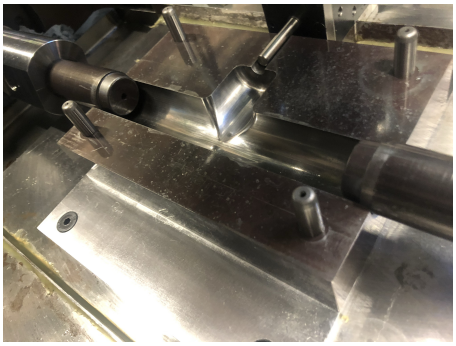

Figure 2: Dies and axial punches in experimental tools

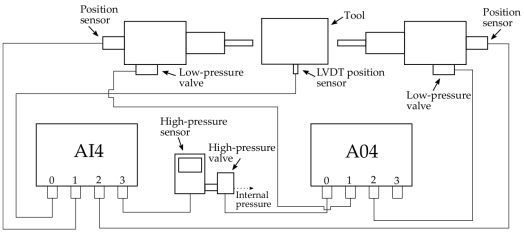

Figure 3: Flow chart of the overall electrical system for hydraulic press

2.2. Experimental setup

A special hydraulic press is developed to perform the tube hydraulic bulge test under axial feeding force for the above two materials. Fig. 1 presents an overall view of this designed experimental equipment. The hydroforming machine consists of the pressure system, clamping devices, tools and the control system, in which a short-stroke vertical hydraulic cylinder is used to provide enough closing force to lock the T-shape die during the forming process. The longitudinal feeding force is provided by two axial hydraulic cylinders that control the positions of the two punches at the same time. Two punches can be easily replaced with various of sizes and dimensions to achieve a more flexible test. The shape of the axial punch ends is a tapered curve to avoid fluid leakages and pressure losses, which is shown in Fig. 2. The combined utilization of a low-pressure pump and intensifier can deliver

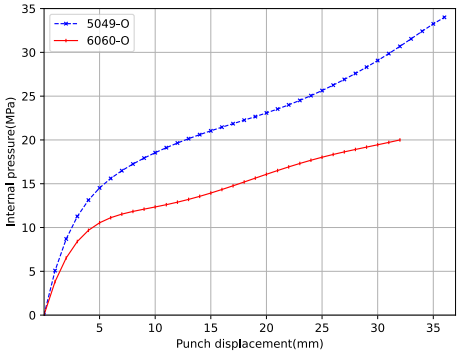

Figure 4: Approximate loading path for 5049-O and 6060-O aluminium alloys in hydraulic bulge test

sufficient internal pressure, up to $80MPa$ in the current research.

To measure the axial displacement precisely, a digital position transducer is installed on the punch end, which can record the accurate coordinate of the axial punch during the forming process. At the same position, a force transducer is integrated into it to acquire the punch force at different stages. The sensor connected to a high pressure valve can measure the internal pressure in the tube and the application of the closed-loop control system enables the actual fluid pressure to reach the predefined value. A linear variable differential transformer position sensor is used to collect the filling height of the tube branches online. Fig. 3 shows a flow chart of the electrical system for this hydraulic press. All operations including data acquisition and process control will be completed on an industrial computer running the GNU/Linux operating system.

2.3. Tube hydraulic bulge test

The T-shape tube hydraulic bulge test for aluminium alloys 5049-O and 6060-O is conducted on the machine shown in Fig. 1. A complete experimental process can be divided into two stages. In the first step, the objective is to generate a reasonable loading path, i.e., axial displacement versus internal pressure for the hydraulic bulge test. Several potential loading paths obtained by an automatic optimization program are tested on the actual

Table 1: Material constitutive parameters identified by tensile test for 5049-O aluminium alloy

Circumferential position	Yield strength(MPa)	Ultimate tensile strength(MPa)	Elongation(%)	Strength coefficient(MPa)	Hardening exponent
0°	73.36	226.47	12.94	431.52	0.323
90°	73.69	227.70	13.04	433.21	0.324
180°	69.22	224.61	13.37	431.38	0.325
270°	70.50	223.20	13.10	432.36	0.321
Mean value	71.69	225.50	13.11	432.12	0.323

press until a perfect tubular component that has no wrinkles and fractures is produced. Furthermore, three tubular samples are repeatedly tested using the selected loading path to ensure its effectiveness and robustness. Fig. 4 presents the optimized loading path for two aluminium alloys.

In the second stage, thin-walled aluminium alloy tubes are bulged under internal fluid pressure and axial compressive force. The loading path follows the one obtained in the first stage, and the feedback control system can guarantee that the actual loading path is consistent with the definition. The experimental data, i.e., filling height, axial feeding force and punch axial displacement, is recorded online by the data acquisition system while the pole thickness at the tube center is manually measured after the deformation.

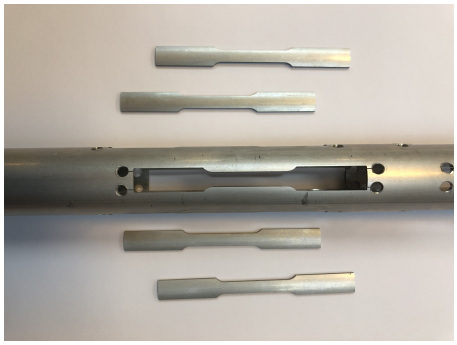

Figure 5: Illustration of how tensile specimens are cut from the tested tube at different circumferential positions

2.4. Tensile test

The universal tensile test is conducted to determine the mechanical property and flow stress curve of used tubular materials. Tension specimens are

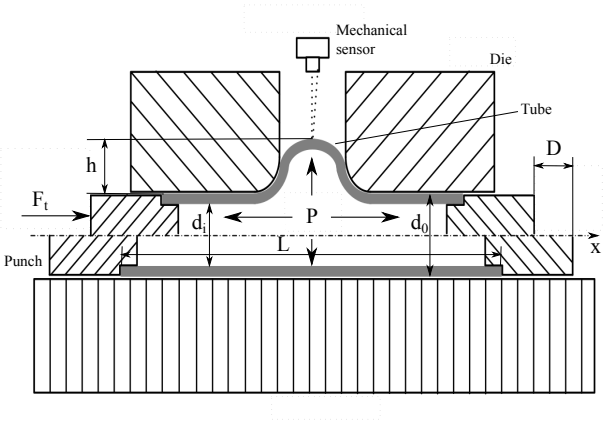

Figure 6: Schematic diagram of T-shape tube hydraulic bulge test

Table 2: Material constitutive parameters identified by tensile test for 6060-O aluminium alloy

Circumferential position	Yield strength(MPa)	Ultimate tensile strength(MPa)	Elongation(%)	Strength coefficient(MPa)	Hardening exponent
0°	54.88	115.40	9.68	201.94	0.221
90°	54.58	114.01	8.95	202.99	0.223
180°	53.73	114.00	9.78	199.48	0.222
270°	54.72	113.90	9.16	202.65	0.222
Mean value	54.48	114.33	9.39	201.77	0.222

cut at four different positions, i.e., $0°, 90°, 180°$ and $270°$, along the circumferential direction on the used tubes. Their sizes and dimensions follow the ASTM E8 standard[42]. Fig. 5 illustrates how tension specimens are cut from the tubular materials in the longitudinal direction. All tests are performed on an electrical universal testing machine from Instron corporation, and the punch velocity is $4mm/min$ at room temperature. A mechanical extensometer is used to measure the deformation data like the displacement and load of tension samples during the test. All collected experimental data will be used to determine the parameters of tubular materials.

3. Parameter identification method

The T-shape hydraulic bulge test is an experimental characterization method to describe mechanical properties of tubular materials, which can reproduce the actual process condition in a tube hydroforming operation

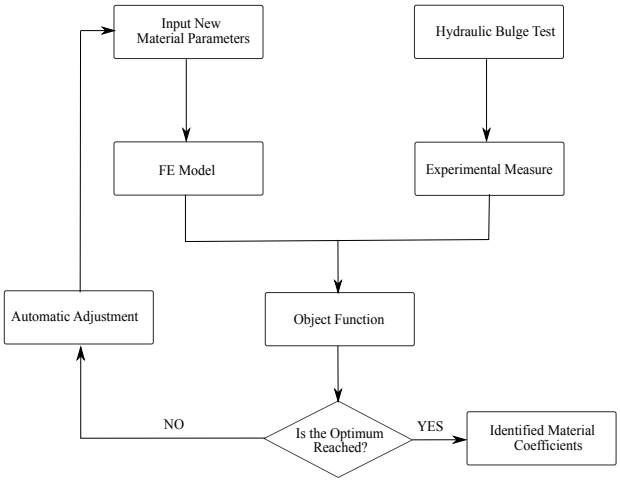

Figure 7: Illustration of the flow chart of inverse strategy utilized in parameter identification based on hydraulic bulge test

and generate the basic database for the identification of material constitutive parameters. Fig. 6 illustrates the schematic diagram for the T-shape tube hydraulic bulge test. Various analytical and numerical models are developed for the bulging process and their advantages and limitations are presented[32,34]. In the following sections, two types of models are used as post-processing procedures to identify material constitutive parameters. One is an analytical model based on energy theory, and the other is an inverse model combining FE simulations with gradient-based algorithms.

3.1. Analytical model

The classical slab method is widely used for the modelling of hydraulic bulge tests of axisymmetrical tubular components, which can determine the stress-strain curve analytically by solving a force equilibrium equation defined on a small element of hydroformed parts[26]. However, this theoretical approach can not analyze and describe the T-shape tube hydraulic bulge process because the final hydroformed parts are not axisymmetrical and angled branches increase the complexity of boundary conditions. The energy theory provides a possibility to analyze the T-shape tube hydraulic bulging process

without considering force balance equations and boundary conditions.

As shown in Fig. 6, the T-shape tube hydraulic bulging process can be considered as a plane strain case where the strain component in the longitudinal direction can be neglected, i.e., $\varepsilon_x = 0$. From the condition of volume constancy, the radial and circumferential strain on the branch center can be calculated as:

$$\varepsilon_t = \ln \frac{t}{t_0} \tag{1}$$

$$\varepsilon_\theta = -(\varepsilon_t + \varepsilon_x) \tag{2}$$

where t_0 and t are the initial and final tube wall thickness. Mises yield criterion and the associated isotropic hardening model are used in the current study; the effective strain ε_e can be derived as:

$$\bar{\varepsilon}_e = \frac{\sqrt{2}}{3}\sqrt{(\varepsilon_t - \varepsilon_\theta)^2 + (\varepsilon_\theta - \varepsilon_x)^2 + (\varepsilon_x - \varepsilon_t)^2} \tag{3}$$

Based on the principle of energy balance, the external total power J^* required in the hydro bulging process consists of the following terms, which can be expressed by the formula:

$$J^* = \dot{W}_i + \dot{W}_f + \dot{W}_b \tag{4}$$

in which $\dot{W}_i, \dot{W}_f$ and $\dot{W}_b$ represent internal deformation power, contact surface friction power and additional power, respectively. On a kinematically admissible velocity field with discontinuous lines S with sliding $\dot{U}$, they can be defined as[43]:

$$J^* = 2F_t\dot{U} \tag{5}$$

$$\dot{W}_i = \frac{\bar{\sigma}_t\pi(d_0^2 - d_i^2)}{2\sqrt{3}}\dot{U} \tag{6}$$

$$\dot{W}_f = \frac{\bar{\sigma}_t\pi c d_0(L - D + h)}{\sqrt{3}}\dot{U} \tag{7}$$

$$\dot{W}_b = \frac{P\pi d_i^2 D}{2L}\dot{U} \tag{8}$$

Substituting equations (5), (6), (7), (8) into (4), an approximate formula to calculate the flow stress obtained by the hydraulic bulge test can be derived

as:

$$\bar{\sigma_t} = \frac{\sqrt{3}(4F_tL - P\pi d_i^2 D)}{\pi L[d_0^2 - d_i^2 + 2cd_0(L - D + h)]} \tag{9}$$

in which F_t is the total forming load and P is the internal fluid pressure. d_0 and d_i are the initial outer and inner diameter of tested tubes. L is the original tube length and c is the shear friction coefficient. D is the axial punch displacement and h is the filling height.

It is evident that the flow stress and corresponding strain can be identified using the above equations based on the recorded experimental data such as axial feeding force, bulge height and so on. Hollomon isotropic hardening law is used to describe the strain-stress relationship of thin-walled aluminium alloy tubes, which can be written as:

$$\bar{\sigma} = K\bar{\varepsilon}^m \tag{10}$$

where K is the strength coefficient and m is the hardening exponent.

3.2. Inverse strategy

Inverse modelling techniques are widely used in the identification of material constitutive parameters for metal forming processes. They integrates FE simulations, optimization algorithms and actual physical experiments and can determine more accurate results by eliminating the mechanical and geometrical assumptions of classical analytical models. In this study, an automatic inverse framework has been developed to identify the material hardening parameters of aluminium alloy tubes.

The main principle behind the inverse analysis is to match experimental data from T-shape tube hydraulic bulge tests with FE simulation outputs. This fitting process is performed iteratively by adjusting design variables using Levenberg-Marquardt algorithm. When the cost function based on the difference between experimental and simulated data is minimized, the iterative process will be terminated and the optimum solution is identified. Fig. 7 illustrates the flow chart of the inverse scheme utilized in parameter identification based on the T-shape tube hydraulic bulge test.

Objective functions are defined to evaluate the fitting quality between numerical results and experimental observations. Furthermore, a suitable cost function can determine more accurate material parameters and enable the optimization process to be more robust. The T-branch height, internal

pressure, punch displacement and axial feeding force in the T-shape tube hydraulic bulge test are recorded as experimental data. The corresponding simulated results can be calculated by FE models. To correlate these two databases, the definition of the objective function follows the sum of least square errors, which can be written as:

$$f_1 = \beta_1 f_{11} + \beta_2 f_{12} + \beta_3 f_{13} \tag{11}$$

$$f_{11} = \sum_{p=1}^{n_1} [\omega_p (h_p^{exp} - h_p^{sim})]^2 \tag{12}$$

$$f_{12} = \sum_{q=1}^{n_2} [\omega_q (t_q^{exp} - t_q^{sim})]^2 \tag{13}$$

$$f_{13} = \sum_{r=1}^{n_3} [\omega_r (F_r^{exp} - F_r^{sim})]^2 \tag{14}$$

in which $\beta_1, \beta_2, \beta_3$ are the scaling factors for different parts in the objective function, which satisfy $\beta_1 + \beta_2 + \beta_3 = 1$. F, h and t represent the axial feeding force, T-branch height and pole thickness, respectively. n_1, n_2, n_3 are the number of collected different types of experimental data. ω is the weighting coefficient for the pth point in the sub-objective function, which can be expressed as:

$$\omega_p = M \frac{h_p^{exp}}{\sum_{p=1}^{n_1} \sum_{q=1}^{n_2} \sum_{r=1}^{n_3} (h_p^{exp} + t_q^{exp} + F_r^{exp})} \tag{15}$$

in which M is the total number of various experimental indicators, i.e., $M = n_1 + n_2 + n_3$. The other two weighting coefficients in the objective function can be expressed by similar formulas.

Hollomon's power hardening model is used to describe the stress-strain behaviour of tubular materials in work hardening. The strength coefficient K and hardening exponent m in this equation are considered as the design variables, i.e., $\mathbf{x} = [K, m]$. There are no special constraints on these two design parameters except that they must be greater than zero because the material behaviour should conform to the real physical world. This trust region scheme will be activated and ensure that all design variables are within a reasonable range once the new parameter to be solved exceeds the predetermined search space.

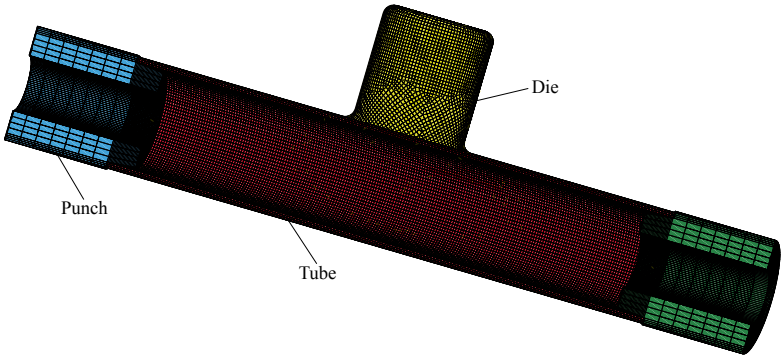

Figure 8: FE model for the T-shape tube hydraulic bulge process

Fig. 8 presents the FE model of the T-shape tube hydraulic bulge process. The tube, punches and dies constitute the entire model where 3D brick elements with eight nodes are assigned to the first two parts, and the latter part is set as a rigid body with four nodes 2D shell elements. The type and size of tubular materials used in the model are consistent with the actual test and these details are shown in Section 2.1. Mises yield criterion and isotropic power hardening law denote the material stress-strain behaviour. In the simulation, the movement of two punches and internal fluid pressure curves follow the loading path recorded in the actual experiment, as shown in Fig. 4. The friction between the workpiece and dies is described by Coulomb law with 0.1 of the friction coefficient. To reduce the computation time, the mass scaling factor is introduced into the FE model. Moreover, due to the symmetry of the geometry, material properties and loads, a half of FE model for the whole assembly is constructed to improve calculation efficiency as well.

The inverse problem can be considered as an optimization problem to be solved, and an improved Levenberg-Marquardt algorithm[44] is constructed to minimize the objective function defined in equation (11) with respect to the design variable $\mathbf{x} = [K, m]$ subject to specific constraints. The ellipsoidal trust region scheme is introduced into the Levenberg-Marquardt algorithm to solve the approximated model and can remove the influence of poor scaling problems in the numerical optimization, where the magnitude of design variables, i.e., the strength coefficient and hardening exponent, has different

Table 3: Typical experimental data obtained by T-shape tube hydraulic bulge test for 5049-O aluminium alloy

Stage No.	Punch displacement(mm)	Internal pressure(MPa)	Filling height(mm)	Axial feeding force(kN)
1	1.04	0.39	0.17	28.33
2	5.15	15.94	4.70	50.23
3	9.27	18.60	8.17	59.04
4	13.40	20.65	10.79	68.03
5	17.51	22.52	13.44	76.83
6	21.64	24.20	16.28	84.92
7	25.75	26.63	19.36	93.99
8	29.85	29.34	22.66	103.28
9	36.02	34.23	28.94	119.21

orders.

Identified material parameters from the tensile test are chosen as the starting point for the inverse model, then a new point can be defined as:

$$\mathbf{x}_{new} = \mathbf{x} + [J(\mathbf{x})^T J(\mathbf{x}) + \mu D(\mathbf{x})^T D(\mathbf{x})] J(\mathbf{x})^T f(\mathbf{x}) \tag{16}$$

where $J(\mathbf{x})$ is the Jocabian matrix of the objective function at the current point and can be obtained using the finite difference method. $D(\mathbf{x})$ is a diagonal matrix that enables the algorithm invariant and is calculated based on the information from the first derivative of the objective function. The damping parameter μ can control the searching direction and step size for the next iteration.

During the optimization, material parameters are updated by the equation (16) step by step. When the gradient of the objective function or the change of $\mathbf{x}$ is less than a small positive constant ϵ given by users, the iteration process will be terminated. Moreover, a maximum iteration number k_{max} is defined as a safeguard to avoid an infinite loop and the stopping criteria can be expressed as:

$$\|\mathbf{x}_{new} - \mathbf{x}\| \leq \epsilon_1(\|\mathbf{x}\| + \epsilon_1) \tag{17}$$

$$\|J(\mathbf{x}_{new})^T f(\mathbf{x}_{new})\| \leq \epsilon_2 \tag{18}$$

4. Results and discussion

In this section, the obtained experimental results and their comparisons will be discussed. The recorded tensile data is translated into the true strain-stress curves and corresponding material parameters can be determined using

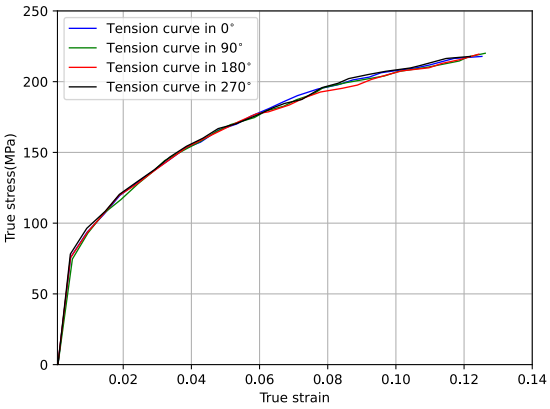

Figure 9: True stress-strain curve determined by tensile test for 5049-O aluminium alloy

the least square fitting method. Figs. 9 and 10 present the true stress-strain curves identified by tensile tests for 5049-O and 6060-O aluminium alloys. The difference among stress-strain curves at different circumferential positions is so small that it can be ignored. It can be concluded that the two types of materials show strong isotropic features after the fully annealing heat treatment process, and the isotropic power hardening law can be used to describe the deformation behaviour in the forming process. Tables 1 and 2 present the material property such as yield stress, ultimate strength and fitted constitutive coefficients for aluminium alloys 5049-O and 6060-O, which

Table 4: Typical experimental data obtained by T-shape tube hydraulic bulge test for 6060-O aluminium alloy

Stage No.	Punch displacement(mm)	Internal pressure(MPa)	Filling height(mm)	Axial feeding force(kN)
1	1.06	6.70	0.32	32.39
2	4.13	10.91	3.90	43.42
3	7.24	11.71	6.39	49.52
4	10.34	12.63	8.01	54.72
5	13.43	13.56	9.81	58.68
6	19.64	15.98	13.52	68.76
7	25.86	18.48	18.17	76.23
8	32.01	20.07	23.39	84.53

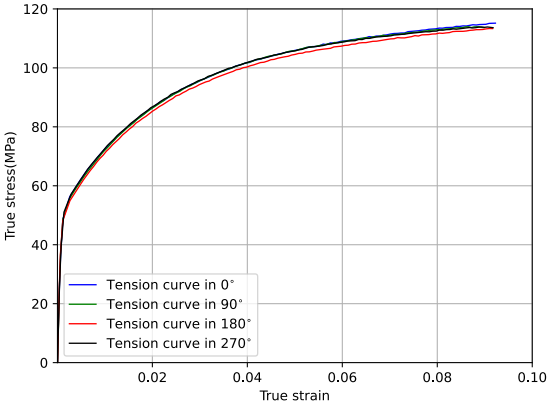

Figure 10: True stress-strain curve determined by tensile test for 6060-O aluminium alloy

Table 5: Comparison of identified constitutive parameters based on bulge test and tensile tests

Experimental type	6060-O aluminium alloy		5049-O aluminium alloy	
	Strength coefficient(MPa)	Hardening exponenet	Strength coefficient(MPa)	Hardening exponent
Bulge test				
Inverse scheme	270.63	0.201	374.60	0.320
Analytical method	212.47	0.350	403.06	0.460
Tensile test	201.77	0.222	432.12	0.323

show consistent results with the above Figs. 9 and 10 as well.

Fig. 11 presents the original and bulged tubular components for aluminium alloys 5049-O and 6060-O. It can be observed that these deformed samples have no fracture and wrinkling, which means the defined loading path can produce perfect components and generate the reasonable experimental databases for the parameter identification process. Tables 3 and 4 show the part of the measured data at different bulging stages for aluminium alloys 5049-O and 6060-O. The developed inverse strategy is used to determine the strength coefficient and hardening exponent by reducing the difference between the experimental data and simulated predictions.

The iteration history of two design variables is shown in Fig. 12, where the identified parameters from the tensile test are chosen as the initial points. Fig. 13 illustrates the changing process of the objective function and its

Figure 11: Hydro bulged specimens before and after test for aluminium alloys 5049-O and 6060-O

gradient during the automatic identification. As the results indicate, the strength coefficient K and hardening exponent m gradually converge to the optimal value while the objective function and its gradient are reduced to the lower level close to zero after fewer iterations, which proves that the inverse modelling strategy can be applied to identify material parameters for the T-shape tube hydraulic bulge process with axial feeding force and it shows a good performance in terms of the robustness and efficiency.

The other analytical model described in Section 3.1 is also selected as a post-processing procedure to fit the experimental data using the power hardening law. The material parameters identified by the theoretical model and other methods are presented in Table 5. It can be observed that the values of strength coefficient and hardening exponent of 5049-O and 6060-O aluminium tubes determined by the bulge test and tensile test have a large discrepancy because the strain range in the uniaxial tensile test is $10\% - 20\%$, but it can be higher than 100% in the hydraulic bulge test. Moreover, material parameters calculated by the inverse strategy and analytical model based on the bulge test are quite different, and one reason for this is that the inverse scheme combines the incremental theory with the gradient-based optimization algorithm while the theoretical model is based on membrane theory with geometrical and mechanical assumptions.

To evaluate the accuracy of the obtained results, T-shape tube hydroforming processes under different loading paths are performed for 5049-O and 6060-O thin-walled aluminium alloys, and corresponding FE simulations are conducted using material parameters obtained by above three methods. The predicted T-branch height and axial feeding force are used to compare with that recorded during the experiments. Figs. 14 and 15 present the comparison of punch displacement versus T-branch height between FE sim-

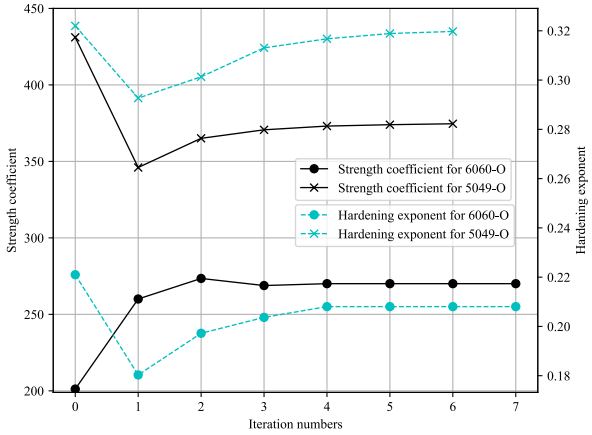

Figure 12: Iteration history of two design variables

Table 6: Quantitative comparisons between FE predictions and experimental values for 5049-O and 6060-O aluminium alloys

Data type	Reference	Model	5049-O aluminium			6060-O aluminium		
			Max(%)	Mean(%)	Min(%)	Max(%)	Mean(%)	Min(%)
Bulge height	Experiment	Tensile test	12.46	7.24	4.68	17.68	15.37	8.98
		Inverse model	6.31	1.31	0.12	8.25	2.11	0.003
		Theoretical model	2.99	2.06	0.28	28.13	26.40	21.85
Punch force	Experiment	Tensile test	12.52	8.74	6.11	22.29	20.74	19.88
		Inverse model	3.49	2.06	0.19	2.13	1.15	0.30
		Theoretical model	10.30	5.40	0.32	30.57	27.33	23.74

ulated outputs and experimental measured values for 5060-O and 6060-O aluminium.

It can be observed that the predicted bulge height using material parameters obtained from the tensile test differs greatly with the experimental values. Further, FE outputs with the inverse model based on the bulge test have the best agreement with the experiment data among them while the analytical model leads to a slight increase of the fitting error. The comparison of punch displacement versus axial feeding force between FE predictions and experimental measurements for two materials is shown in Figs. 16 and 17. The inverse strategy based on bulge tests shows a better fitting quality compared with the analytical model and tensile test. A similar phenomenon is

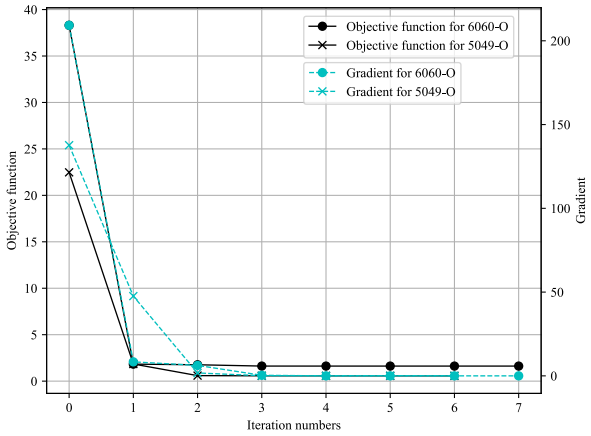

Figure 13: Iteration history of the objective function and its gradient

due to the maximum effective strain before necking in the tensile test being lower than that in the bulge test and the biaxial stress state in the bulge test being closer to the one in the actual hydroforming process.

For more in-depth comparisons, the resulting error between FE predictions and experimental measurements is quantified using the maximum, mean and minimum of variation values, where the average value of the relative deviation can be expressed as: $\Psi = {}^{1}/_{N} \sum_{i=1}^{N} \left({}^{(D^i_{exp} - D^i_{sim})}/_{D^i_{exp}} \right)$. N is the total number of experimental points. D^i_{exp} and D^i_{sim} represent the experimental and simulated results, respectively. Table 6 summarises the quantitative comparisons of all types of experimental data for 5049-O and 6060-O aluminium alloys. Figs. 18 and 19 graphically show the most representative mean relative error obtained by different methods.

From the results presented, it is evident that the mean deviations of 7.24% of the T-branch height and 8.74% of the punch force predicted by the tensile test are higher than corresponding values of 2.06% and 5.40% obtained by the analytical model for the 5049-O aluminium alloy. For the 6060-O aluminium alloy, the theoretical model presents a larger relative error to the experimental data compared with the tensile test with respect to the bulge height and compressive force. It is worth pointing out that the inverse model produces

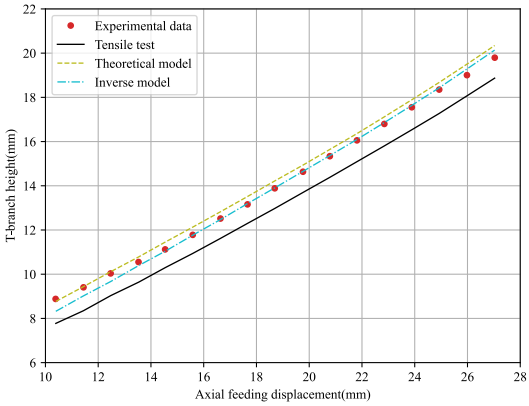

Figure 14: Comparison of FE outputs and experimental data of punch displacement versus T-branch height for 5049-O aluminium

the smallest fitting gap to the measured bulge height and punch force for two types of tubular materials. One possible reason is that the hydraulic bulge test reproduces similar loading conditions to the tube forming process, and the inverse model based on the incremental theory eliminates excessive assumptions in the classical theoretical model.

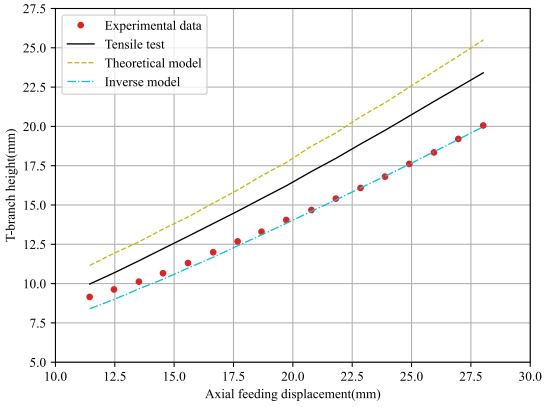

Figure 15: Comparison of FE outputs and experimental data of punch displacement versus T-branch height for 6060-O aluminium

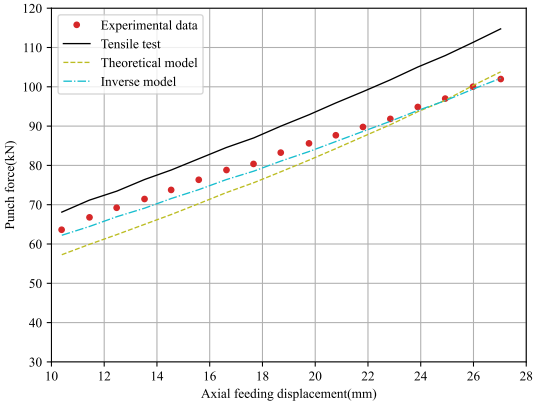

Figure 16: Comparison of FE outputs and experimental data of punch displacement versus axial feeding force for 5049-O aluminium

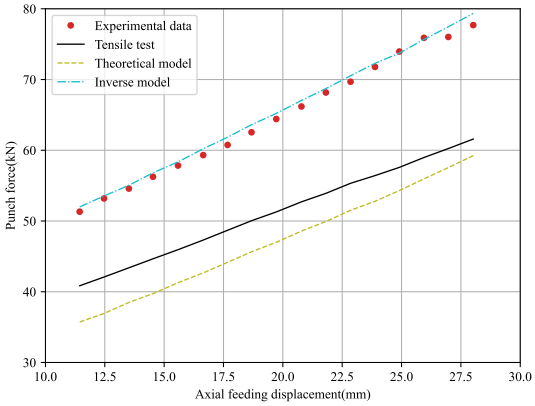

Figure 17: Comparison of FE outputs and experimental data of punch displacement versus axial feeding force for 6060-O aluminium

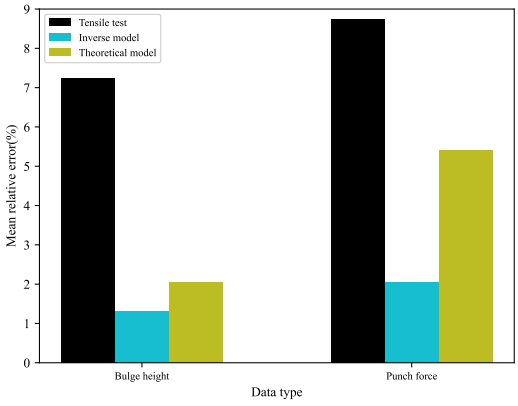

Figure 18: Different mean errors obtained by three methods for 5049-O aluminium

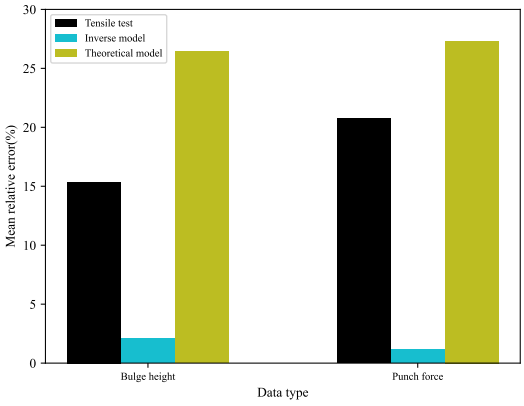

Figure 19: Different mean errors obtained by three methods for 6060-O aluminium

5. Conclusions

To evaluate stress-strain characteristics of tubular materials at the large strain range, hydraulic bulging tests under axial compressive force have been performed. An intelligent inverse strategy integrating FE simulations with gradient-based optimization algorithms is proposed to process and analyze the collected T-branch height, punch displacement and axial feeding force during the experiment. The determined material parameters using the inverse scheme based on the novel bulge test are compared with that obtained by the tensile test and a theoretical analysis. The main conclusions can be drawn as follows:

(1) The values of the strength coefficient and hardening exponent of EN AW 5049-O and 6060-O aluminium tubes calculated by the above three methods are different, and the hydraulic bulge test can characterize the mechanical properties of tubular materials in the range of larger strains and reduce the extrapolation of stress-strain data in FE simulations compared with the uniaxial tensile test.

(2) The proposed automatic inverse identification framework can be extended to the tube hydraulic bulge test under axial compressive force, and its capabilities for post-processing experimental resources have been verified by characterizing two different types of thin-walled tubes. The analytical model is a simple method to determine the stress-strain data from the bulge test compared with the complex inverse strategy and can sometimes improve the results accuracy compared with that from the uniaxial tensile test.

(3) Predicted bulge height and axial feeding force from FE simulations using material parameters identified by the inverse modelling technique, analytical model based on the bulge test and uniaxial tensile test are used for comparison with the experimental data. The results show that the inverse model leads to the smallest fitting error between numerical and experimental values, which means the intelligent inverse identification framework is the most accurate post-processing procedure to characterize mechanical properties of tubular materials.

Acknowledgements

The first author was supported by China Scholarship Council (CSC) (No. 201706080020) from the Ministry of Education of P.R. China and expresses his appreciation to CSC for their financial support.

Data availability statement

The raw data required to reproduce these findings can be available from the corresponding author upon reasonable request.

References

[1] J. Cao, M. Banu, Opportunities and challenges in metal forming for lightweighting: Review and future work, Journal of Manufacturing Science and Engineering 142 (2020) 1–24.

[2] S. Rosenthal, F. Maaß, M. Kamaliev, M. Hahn, S. Gies, A. E. Tekkaya, Lightweight in automotive components by forming technology, Automotive Innovation 3 (2020) 195–209.

[3] S. Zhang, A. Yuan, B. Wang, H. Zhang, Z. Wang, Influence of loading path on formability of 304 stainless steel tubes, Science China Technological Sciences 52 (2009) 2263–2268.

[4] J. Yan, H. Yang, M. Zhan, H. Li, Forming limits under multi-index constraints in NC bending of aluminum alloy thin-walled tubes with large diameters, Science China Technological Sciences 53 (2010) 326–342.

[5] M. Koç, T. Altan, An overall review of the tube hydroforming (THF) technology, Journal of Materials Processing Technology 108 (2001) 384–393.

[6] A. Alaswad, K. Benyounis, A. Olabi, Tube hydroforming process: A reference guide, Materials & Design 33 (2012) 328–339.

[7] C. Bell, J. Corney, N. Zuelli, D. Savings, A state of the art review of hydroforming technology: Its applications, research areas, history, and future in manufacturing, International Journal of Material Forming 13 (2020) 789–828.

[8] M. Koç, Hydroforming for advanced manufacturing, CRC Press, 2008.

[9] F. Zhang, J. Chen, J. Chen, J. Lu, G. Liu, S. Yuan, Overview on constitutive modeling for hydroforming with the existence of through-thickness normal stress, Journal of Materials Processing Technology 212 (2012) 2228–2237.

[10] A. Khalfallah, Z. Ktari, C. Leitão, J. V. Fernandes, New Mandrel Design for Ring Hoop Tensile Testing, Experimental Techniques (2021).

[11] Z. Ktari, C. Leitão, P. A. Prates, A. Khalfallah, Mechanical design of ring tensile specimen via surrogate modelling for inverse material parameter identification, Mechanics of Materials 153 (2021) 103673.

[12] J.-H. Kim, A. Serpantié, F. Barlat, F. Pierron, M.-G. Lee, Characterization of the post-necking strain hardening behavior using the virtual fields method, International Journal of Solids and Structures 50 (2013) 3829–3842.

[13] M. Nemat-Alla, Reproducing hoop stress–strain behavior for tubular material using lateral compression test, International Journal of Mechanical Sciences 45 (2003) 605–621.

[14] F. Bardi, S. Kyriakides, Plastic buckling of circular tubes under axial compression—part I: Experiments, International Journal of Mechanical Sciences 48 (2006) 830–841.

[15] F. Alhussainy, M. N. Sheikh, M. N. Hadi, Behaviour of small diameter steel tubes under axial compression, Structures 11 (2017) 155–163.

[16] J. Liu, H. Yang, H. W. Li, H. Li, S. Zhu, A new hybrid identification method for determining the material parameters of thin-walled tube under compressive stress state, Materials & Design 44 (2013) 49–58.

[17] E. Pavlina, C. Van Tyne, K. Hertel, Hydraulic bulge testing of dual phase steel tubes produced using a novel processing route, Journal of Materials Processing Technology 201 (2008) 242–246.

[18] D. Woo, P. Hawkes, Determination of stress/strain characteristics of tubular materials, Journal of the Institute of Metals 96 (1968) 357–359.

[19] S. Fuchizawa, Narazaki, H. Yuki, Bulge test for determining stress-strain characteristics of thin tubes, in: International Conference on Technology of Plasticity, International Academic Publishers, Beijing, 1993, pp. 488–493.

[20] M. Koç, Y. Aue-u lan, T. Altan, On the characteristics of tubular materials for hydroforming—experimentation and analysis, International Journal of Machine Tools and Manufacture 41 (2001) 761–772.

[21] L. Yang, C. Guo, Determination of stress–strain relationship of tubular material with hydraulic bulge test, Thin-Walled Structures 46 (2008) 147–154.

[22] P. Bortot, E. Ceretti, C. Giardini, The determination of flow stress of tubular material for hydroforming applications, Journal of Materials Processing Technology 203 (2008) 381–388.

[23] R. Velasco, N. Boudeau, Tube bulging test: Theoretical analysis and numerical validation, Journal of Materials Processing Technology 205 (2008) 51–59.

[24] T. Zribi, A. Khalfallah, H. BelHadjSalah, Experimental characterization and inverse constitutive parameters identification of tubular materials for tube hydroforming process, Materials & Design 49 (2013) 866–877.

[25] T. Sokolowski, K. Gerke, M. Ahmetoglu, T. Altan, Evaluation of tube formability and material characteristics: hydraulic bulge testing of tubes, Journal of Materials Processing Technology 98 (2000) 34–40.

[26] Y.-M. Hwang, Y.-K. Lin, T. Altan, Evaluation of tubular materials by a hydraulic bulge test, International Journal of Machine Tools and Manufacture 47 (2007) 343–351.

[27] B. Zhang, B. Endelt, L. Lang, Y. Zhao, S. Yan, K. B. Nielsen, An inverse strategy to determine constitutive parameters of tubular materials for hydroforming process, Chinese Journal of Aeronautics (2021) Accepted.

[28] Z. He, S. Yuan, Y. Lin, X. Wang, W. Hu, Analytical model for tube hydro-bulging test, part I: Models for stress components and bulging zone profile, International Journal of Mechanical Sciences 87 (2014) 297–306.

[29] N. Boudeau, P. Malécot, A simplified analytical model for post-processing experimental results from tube bulging test: Theory, experimentations, simulations, International Journal of Mechanical Sciences 65 (2012) 1–11.

[30] Y.-M. Hwang, Y.-K. Lin, Evaluation of flow stresses of tubular materials considering anisotropic effects by hydraulic bulge tests, Journal of

Engineering Materials and Technology 129 (2007) 414–421. Publisher: American Society of Mechanical Engineers Digital Collection.

[31] Y. M. Hwang, C. W. Wang, Flow stress evaluation of zinc copper and carbon steel tubes by hydraulic bulge tests considering their anisotropy, Journal of Materials Processing Technology 209 (2009) 4423–4428.

[32] A. H. B. Ouirane, R. Velasco, G. Michel, N. Boudeau, Error evaluation on experimental stress-strain curve obtained from tube bulging test, International Journal of Material Forming 3 (2010) 195–198.

[33] A. H. Ben Ouirane, N. Boudeau, R. Velasco, G. Michel, Error evaluation on experimental stress–strain curve obtained from tube bulging test, Thin-Walled Structures 49 (2011) 1217–1224.

[34] L. Vitu, N. Boudeau, P. Malécot, G. Michel, A. Buteri, Evaluation of models for tube material characterization with the tube bulging test in an industrial setting, International Journal of Material Forming 11 (2018) 671–686.

[35] T. Zribi, A. Khalfallah, H. B. Salah, A comparative study of the identification methods for tube hydroforming process, Key Engineering Materials 651-653 (2015) 169–174.

[36] A. Khalfallah, M. C. Oliveira, J. L. Alves, T. Zribi, H. Belhadjsalah, L. F. Menezes, Mechanical characterization and constitutive parameter identification of anisotropic tubular materials for hydroforming applications, International Journal of Mechanical Sciences 104 (2015) 91–103.

[37] Y. Ge, X. Li, L. Lang, Inverse approach to evaluate the tubular material parameters using the bulging test, Advances in Materials Science and Engineering 2015 (2015) 1–9.

[38] Y. Xu, L. C. Chan, Y. C. Tsien, L. Gao, P. F. Zheng, Prediction of work-hardening coefficient and exponential by adaptive inverse finite element method for tubular material, Journal of Materials Processing Technology 201 (2008) 413–418.

[39] E. Asaadi, P. S. Heyns, Flow stress identification of tubular materials using the progressive inverse identification method, Engineering Computations 33 (2016) 1472–1489.

[40] O. Silviu-Adrian, I. Mitelea, N. Simon, C. P. Lucian, Influence of laser beam power on the heterogeneous welded joints morphology of deformable aluminium alloys, Materials Today: Proceedings 45 (2021) 4349–4355.

[41] N. Tabrizian, H. Hansen, P. Hansen, R. Ambat, P. Møller, Influence of annealing and deformation on optical properties of ultra precision diamond turned and anodized 6060 aluminium alloy, Surface and Coatings Technology 204 (2010) 2632–2638.

[42] ASTM, Standard test methods for tension testing of metallic materials, Technical Report, 2013.

[43] L. Moreira Filho, H. Al-Quereshi, Unconventional tee forming on metal tubes, Journal of manufacturing sciences and engineering 107 (1985) 392–396.

[44] J. J. Moré, The Levenberg-Marquardt algorithm: Implementation and theory, Numerical Analysis 630 (1978) 105–116.

Chapter 6

Paper III

Identification of constitutive parameters for thin-walled aluminium tubes using a hybrid strategy

Bin Zhang, Benny Endelt, Lihui Lang, and Karl Brian Nielsen.

The paper has been published in the
Materials Today Communications Vol. 28(2021), p. 106270, 2021. DOI:
https://doi.org/10.1016/j.mtcomm.2021.102670

Materials Today Communications 28 (2021) 102670

Contents lists available at ScienceDirect

Materials Today Communications

journal homepage: www.elsevier.com/locate/mtcomm

Identification of constitutive parameters for thin-walled aluminium tubes using a hybrid strategy

Bin Zhang [a,*,1], Benny Endelt [a], Lihui Lang [b], Karl Brian Nielsen [c]

[a] Department of Materials and Production, Aalborg University, Aalborg 9220, Denmark
[b] School of Mechanical Engineering and Automation, Beihang University, Beijing 100083, China
[c] Department of Mechanical and Production Engineering, Aarhus University, Aarhus 8000, Denmark

ARTICLE INFO

Keywords:
Tubular material
Hydraulic bulge test
Theoretical analysis
Finite element method
Numerical optimization

ABSTRACT

The paper presents a hybrid strategy to determine constitutive parameters for thin-walled tubes based on experimental responses from hydraulic bulge tests. This developed procedure integrates the analytical model, finite element analysis and gradient-based optimization algorithm, where initial guesses of material parameters are generated quickly by a theoretical method, then they are input to an inverse framework integrating Gauss-Newton algorithm and finite element method. The solving for this inverse problem leads to a more accurate identification of material parameters by reducing the discrepancies between simulated results and experimental data. To evaluate its feasibility and performance, hydraulic bulge tests with different end-conditions for annealed 6060 and 5049 aluminium tubes are carried out. The strength coefficient and hardening exponent are determined using the hybrid strategy based on the collected measurements in the experiment. These material parameters are used to compare with those obtained by a single analytical model and inverse model. The comparison validates that the proposed hybrid strategy is not sensitive to starting points and can improve the calculation efficiency and determine more accurate constitutive parameters.

1. Introduction

With the latest development of computing power, finite element(FE) method has become a widely used and standard technique to model and investigate tube hydroforming processes in industry or science community [1,2]. It not only can help engineers and researchers to design desired products by analyzing stress and strain distribution and predicting the shape and size of deformed tubular specimens [3], but can evaluate tube damages and forming limits on the whole production cycle instead of trial and error method of physical experiments [4,5]. One of the most critical prerequisites for a successful FE modelling is the input data of accurate tubular material constitutive parameters, which can be obtained by different post-processing procedures for a variety of material testing methods and responses [6–9].

The hydraulic bulging test has proven to be a simple and effective method to determine the flow stress curve for tubular materials [10,11], which can reproduce deformation stress state in the tube forming operation and is a better alternative to evaluate the overall mechanical characteristics of tubes compared with the tensile test [12], hoop tension test [13,14], axial and lateral compression test [6,15]. Hydro-bulging equipment can construct flexible end-condition such as fixed ends [16], free ends [17,18] and forced ends [19] for tubular specimens and investigate their yielding and hardening behaviour under bi-axial and three-dimensional stress state [20]. During the test, the bugle diameter, thickness of meridian center point and corresponding liquid pressure are easily recorded. Then, theoretical models and fitting algorithms are used to further estimate the experimental data and determine the material stress-strain relationship.

Most of the existing analytical methods for modelling hydraulic bulge processes are based on the principle of membrane mechanics. Stress and strain tensors are determined separately by solving the force equilibrium equation and simplified plastic condition, and then these values are used to fit the assumed material model formula. Hwang et al. [18] propose a flow stress model in which stress components are derived based on force equilibrium and a plane stress hypothesis for deformed tubes, and strain components are calculated by assuming the bulge profile shape as an ellipse. Analytical models developed in subsequent works are similar to the classical Hwang model, where the stress formula

* Corresponding author.
E-mail address: zhangbin20100@outlook.com (B. Zhang).
[1] Address: Department of Materials and Production, Aalborg University, Fibigerstræde 16, Aalborg DK-9220, Denmark.

https://doi.org/10.1016/j.mtcomm.2021.102670
Received 19 May 2021; Received in revised form 19 July 2021; Accepted 19 July 2021
Available online 27 July 2021

in Hwang model is still used while the profile shape on the tube bulge region could be regarded as an circumference arc [21,22], spline function [17] and so on. It is obvious that all the above analytical models can guarantee the uniqueness and stability of the identified material parameters, but the application of geometrical and mechanical assumptions reduces the accuracy of these models.

Inverse modelling techniques can be used to estimate material constitutive parameters, which allows a more accurate parameter determination by eliminating the mechanical and geometrical hypothesis in classical theoretical analysis [23,24]. However, extensive research has been applied to determine the mechanical properties for sheet metals using different physical experiments [25–28] and limited work is performed for tubular materials. Based on various experimental tests, the inverse strategy combining corresponding FE models with different algorithms is developed to determine constitutive parameters for thin-walled tubes [29–32]. Although the utilization of inverse modelling method makes it possible to evaluate with better accuracy for responses from tube bulging tests, the introduction of FE models causes expensive calculation time [33]. Therefore, many scientists focus on improving the performance of optimization algorithms.

Classical gradient-based optimization algorithms like steepest descent, Gauss-Newton and Levenberg-Marquardt method, etc. [34] can solve the inverse problem with small residuals efficiently, but they are heavily dependent on the initial guesses and easily fall into the local minimum, especially in multi-objective optimization [35]. Another group of popular algorithms are called bioinspired approaches such as genetic algorithm, simulated annealing and so on which imitate some behaviours of natural and biological system and tends to find a global optimum for multi-objective optimization problems. However, one drawback for bioinspired algorithms is the requirement of a large number of function evaluations and this situation is particularly prominent in expensive FE model calculation [36]. The other type of way to solve inverse problem is meta-model based algorithms which use approximated model to replace sophisticated FE modelling. Response surface methodology, sequential kriging method, and neural networks are typical representatives of approximation models [33,37,38]. These algorithms not only can allow distributed and parallel calculations, but do not need the sensitivity analysis. One of the disadvantages of the approximation algorithm is that it only can get an approximate optimum rather than a real optimal result.

Several hybrid optimization strategies have been constructed to take advantages of selected algorithms and further improve the performance of inverse framework [30,35,39–43]. It is worth pointing out, a fuzzy logic-based approach is applied to choose the most reliable result from various material parameters calculated by common least square algorithms [40]. Ponthot et al. explore many possibilities of combining different gradient-based methods to determine material coefficients in hardening model based on cylindrical bar compression test [41]. A genetic algorithm is used to generate the initial points near the global minimums and then activate gradient-based algorithm to determine the optimum solution quickly while avoiding the local minimum trap [35]. Moreover, virtual orthogonal experiment [30], response surface design [33] and evolutionary alogirthm [42] also provide more possibilities for mapping searching space of design variables to perform inverse parameter identification process efficiently. This cascade strategy is still time-consuming because of the utilization of the global searching algorithm in its first stage.

This study aims to find the global optimum for tubular material parameters efficiently by making full use of two different types of hydraulic bulge tests with fixed and forced end-condition. The research advances and challenges are described in state of the art of Section 1. In this paper, a novel hybrid strategy combining theoretical analysis with inverse model is developed to determine constitutive parameters of tubular material, which characterizes with improved efficiency and accuracy. The structure and working principle of this new strategy are described in detail in Section 2. To validate the feasibility and performance of the proposed hybrid framework, two application cases on using this hybrid scheme to determine material properties of 5049 and 6060 aluminium tubes are presented in Section 3. In Section 4, identified material parameters using different models and their comparison for computational accuracy and efficiency are discussed. The main conclusions are drawn in Section 5.

2. The hybrid strategy

The developed hybrid scheme is a special framework for determining mechanical properties of tubular materials and combines theoretical analysis, FE model, optimization technique and responses from hydraulic bulge test, which can be divided into two stages. The purpose of the first stage is to produce the starting values in the vicinity of the optimal solution using a classical theoretical method named Hwang model [18]. Reasonable searching spaces can be found efficiently because of the simplicity and robustness of this analytical model. In the second stage, initial guesses from the first step will be imported into an inverse strategy which integrating FE model and Gauss-Newton algorithm to identify the final material parameters by reducing the error between experimental and simulated outputs. Gauss-Newton algorithm can converge to the minimum quickly near the global optimum solution and the introduction of FE models further improves the accuracy of results. Fig. 1 illustrates the flow chart of this hybrid strategy applied on the parameter identification for tubular materials.

2.1. Theoretical analysis

Hydraulic bulge test is an advanced material characterization technique where tubular specimens are deformed under hydraulic pressures with or without axial feeding forces, which can be divided into three categories, 1)free bulge test; 2)fixed bulge test; 3) forced bulge test, according to the different end-condition of tubular samples. The same theoretical analysis can be applied to both free and fixed bulging tests at the same time [44]. When considering the axial feeding force, the classical model needs to be updated.

The slab method can be used to analyse tube hydraulic bulge process with free or fixed ends by defining an equilibrium equation on a small element at tube pole. Fig. 2 shows a schematic diagram of the hydraulic bulge process and several important geometrical parameters are marked in this plot. Typical analytical models for tube hydraulic bulge process with free and fixed end-condition are derived from membrane theory. The stress in the radial direction can be ignored because of the small ratio of tube thickness to diameter. Based on the force equilibrium conditions, stress components along longitudinal and circumferential direction can be written as [18]:

$$\sigma_{\varphi} = \frac{P(R_{\theta o} - t)^2}{2t(R_{\theta o} - t/2)} \tag{1}$$

$$\sigma_{\theta} = \frac{P(R_{\theta o} - t)}{2t(R_{\varphi o} - t/2)}(2R_{\varphi o} - R_{\theta o} - t) \tag{2}$$

where t is the pole thickness at tube center under specified internal pressure P. $R_{\theta o}$ and $R_{\varphi o}$ are the curvature radius along meridian and circumferential direction at the center of tubes, which can be expressed as [44]:

$$R_{\varphi o} = \frac{L^2(R_0 + h)}{4h(2R_0 + h)} \tag{3}$$

$$R_{\theta o} = R_0 + h \tag{4}$$

in which R_0 is the initial outer radius, L is the length of the tube deformation zone and h is the bulge height. When these data are measured in the experiment, strain components in axial and hoop directions can be given as:

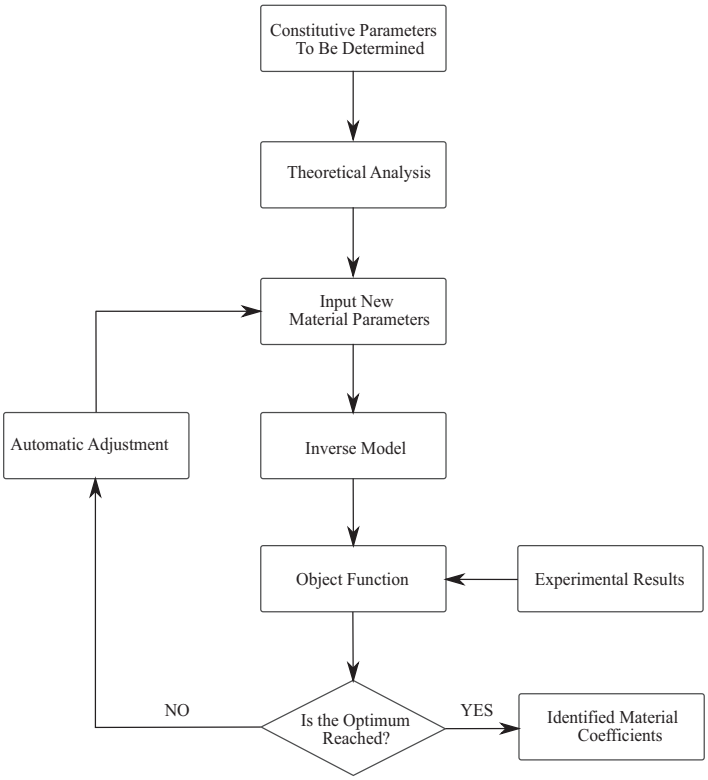

Fig. 1. Illustration of the flow chart for the proposed hybrid framework.

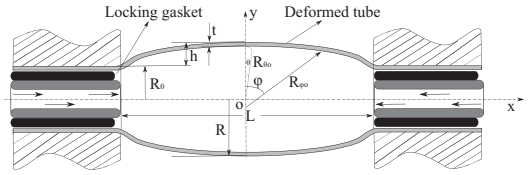

Fig. 2. Schematic diagram of the tube hydraulic bulge test with fixed end-condition.

$$\varepsilon_r = \ln \frac{t}{t_0} \tag{5}$$

$$\varepsilon_\theta = \ln \frac{(R_{\theta o} - t_0/2)}{(R_0 - t_0/2)} \tag{6}$$

Based on the volume constancy in metal plastic forming, the strain in longitudinal direction can be derived as:

$$\varepsilon_\varphi = -(\varepsilon_r + \varepsilon_\theta) \tag{7}$$

One-sided tube hydraulic bulge test with axial feeding force, which is illustrated in Fig. 3, can be used to characterize mechanical properties of tubular materials which are formed into complex components with angled branches such as T-shape, X-shape and Y-shape. Traditional slab methods are difficult to describe this forming process because of the poor symmetry of parts and the introduction of axial forces. Theoretical approaches based on energy balance provide a possibility to analyze this

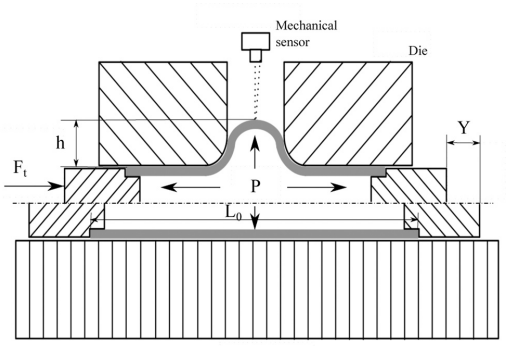

Fig. 3. Schematic diagram of the tube hydraulic bulge test with forced end-condition.

complex forming process [45]. Filho et al. [46] apply the upper bound method to calculate the total forming load for T-shape tube forming process using an elastomer as internal medium. Strano et al. [47] use a simple inverse approach based on energy balance to identify the strain-stress curve of tubular materials. Although the accuracy of the calculated parameters is low, but they can still be considered as the initial value of the inverse model.

In tube hydraulic bulge test with axial force, the tube deformation is

assumed as a plane strain state i.e. the longitudinal strain is zero. Strain components along radial and hoop direction can be written as [46]:

$$\varepsilon_r = \ln\frac{t}{t_0} \tag{8}$$

$$\varepsilon_\theta = -\varepsilon_r \tag{9}$$

According to the energy theory, the power balance can be written as [46]:

$$J* = \dot{W}_b + \dot{W}_i + \dot{W}_f \tag{10}$$

where J^* is the external power, $\dot{W}_b, \dot{W}_i, \dot{W}_f$ are additional power applied on internal pressure medium, internal power and contact surface friction power, respectively. The derivation and solution of the above equations can produce an approximate formula to calculate the flow stress as [46]:

$$\overline{\sigma}_t = \frac{\sqrt{3}(F_t L_0 - A_t P Y)}{\pi L_0[R_0^2 - (R_0 - t)^2 + cR_0(L_0 - Y + h)]} \tag{11}$$

in which L_0 is the initial length of a tube, F_t is the total external forming force, Y is the axial punch displacement, A_i is the area of punch cross section, c is the shear friction coefficient. It can be seen that more experimental data needs to be collected in tube hydraulic bulge test with axial feeding force.

According to the von Mises yield criterion, the effective stress and strain can be described as below:

$$\overline{\sigma} = \frac{1}{\sqrt{2}}\sqrt{(\sigma_r - \sigma_\theta)^2 + (\sigma_\theta - \sigma_\varphi)^2 + (\sigma_\varphi - \sigma_r)^2} \tag{12}$$

$$\overline{\varepsilon} = \frac{\sqrt{2}}{3}\sqrt{(\varepsilon_r - \varepsilon_\theta)^2 + (\varepsilon_\theta - \varepsilon_\varphi)^2 + (\varepsilon_\varphi - \varepsilon_r)^2} \tag{13}$$

Therefore, the equivalent stress and strain under different pressure levels in two types of hydraulic tests can be obtained using presented equations above.

2.2. FE analysis and constitutive model

LS-DYNA FE software is used to simulate tube hydraulic forming processes with or without axial compressive force. The tubular specimen is meshed with hexahedral solid elements and the dies are set as a rigid body. The contact friction between the workpiece and the die is described by Coulomb's law. Internal fluid pressure and punch feeding displacement are collected in the experiments and the recorded data is imported into FE models.

The constitutive model contains the yield criterion and hardening law, which can describe the mechanical behaviour of tubular materials. In our current research, the selected material is a fully annealed aluminium alloy which features isotropic properties. Thus, von Mises yield criterion and power isotropic hardening law are assigned to solid elements, which can be defined as:

$$\sigma = K\varepsilon^m \tag{14}$$

where K is the strength coefficient and m is the strain hardening exponent. These two values are also material parameters to be determined.

2.3. Objective function and constraint

An accurate determination of material parameters is very dependent on a reasonable cost function. The commonly used definition for objective functions are the sum of least square differences between simulated and experimental data, which proved to be a great success in parameter identification of metal forming processes [48,49]. However, some material parameters have different units or a wide magnitude of values, which can cause convergence difficulties or poor solution accuracy. In this research, the logarithm form is introduced to define the error between the experimental and calculated data and the sum of these values constitutes the objective function [50].

In free hydraulic bulge test, the bulge height and pole thickness are considered as a part of the optimization objective. Following the least square structure, the cost function can be defined as below:

$$f_1 = \alpha f_{11} + (1-\alpha) f_{12} \tag{15}$$

$$f11 = \sum_{i=1}^{n_1}\left[\omega_i \ln\left(1 + \frac{(h_i^{exp} - h_i^{sim})}{h_i^{exp}}\right)\right]^2 \tag{16}$$

$$f12 = \sum_{j=1}^{n_2}\left[\omega_j \ln\left(1 + \frac{(t_j^{exp} - t_j^{sim})}{t_j^{exp}}\right)\right]^2 \tag{17}$$

For hydraulic bulge test with axial force, more experimental data measured in the experiment need to be taken into the objective function in addition to the bulge height and thickness, which can be written as following:

$$f_2 = \alpha_1 f_{21} + \alpha_2 f_{22} + \alpha_3 f_{23} \tag{18}$$

$$f_{21} = \sum_{i=1}^{n_1}\left[\omega_i \ln\left(1 + \frac{(h_i^{exp} - h_i^{sim})}{h_i^{exp}}\right)\right]^2 \tag{19}$$

$$f22 = \sum_{j=1}^{n_2}\left[\omega_j \ln\left(1 + \frac{(t_j^{exp} - t_j^{sim})}{t_j^{exp}}\right)\right]^2 \tag{20}$$

$$f_{23} = \sum_{k=1}^{n_3}\left[\omega_k \ln\left(1 + \frac{(F_k^{exp} - F_k^{sim})}{F_k^{exp}}\right)\right]^2 \tag{21}$$

where h, t and F are the bulge height, pole thickness and axial feeding force, respectively. n is the number of recorded experimental data. ω is the weighted coefficient for different terms in the cost function, which can be expressed as:

$$\omega_i = N\frac{h_i^{exp}}{\sum_{i=1}^{n_1}\sum_{j=1}^{n_2}\sum_{k=1}^{n_3}(h_i^{exp} + t_j^{exp} + F_k^{exp})} \tag{22}$$

in which N is the total number of various experimental indicators. The remaining weighted coefficient in the cost function can be obtained by similar formulas.

In the hybrid framework, there are no many specified constraints on the material parameters because the flexibility and stability of this strategy needs to be verified. However, all constitutive parameters have to be ensured positive based on a real material behaviour. In the optimization process, the constraint that the strength coefficient and hardening exponent are larger than zero should be activated when the identified parameters are outside of the specified searching region.

2.4. Optimization method

A classical gradient-based method i.e. Gauss-Newton algorithm is used in the current study. The basic idea of Gauss-Newton algorithm [34] is to produce a quadratic approximation to the cost function at a given starting point. Then the approximated objective function will be minimized by an iterative procedure until the optimum point is found. When the Hessian matrix of the approximated function is positive definite, Gauss-Newton method can find the optimal solution with fewer iterations. However, the cost function is always so strongly nonlinear in parameter identification that causes some numerical convergence problems.

On the other hand, an initial point around the vicinity of the solution can produce a positive definite Hessian matrix and a good quadratic

function approximation to the objective function, where this algorithm can converge to the optimum point quickly. In order to improve the calculation speed and robustness of the algorithm, analytical model in Section 2.1 is used to generate the initial guesses at the neighborhood of the optimum and the application of trust region constraint instead of line search method enables it possible to solve a non-convex approximate quadratic function. In addition, the approximation of the Hessian matrix for the objective function is performed by the finite difference method. The structure of Gauss-Newton algorithm with trust region strategy is illustrated in Table 1.

3. Experimental procedure

3.1. Sample material and geometry

Two types of tubular materials are used in this study, one of which is the fully annealed 5049 aluminium alloy tube made in China whose outer diameter is 50.00 *mm* and thickness is 1.086 *mm*. The total length of tubular samples in the test is 300.00 *mm*. The other one is the thin-walled EN-AW 6060-O aluminium alloy tube with the dimension 32.00 *mm*×1.50 *mm*×150.00 *mm*(*diameter* × *thickness* × *length*). In order to improve the accuracy of the experimental data, all tested tubular samples are cut from the same batch of supplied tubes.

3.2. Testing tool and method

In order to verify the effectiveness of the proposed hybrid strategy, tube hydraulic bulge tests with and without axial feeding force are performed separately. Free hydraulic bugle tests for 5049-O aluminum tubes are carried out on an internal pressure press and a schematic diagram of this machine is illustrated in Fig. 4, where the tube ends are locked by a setup on this machine and the tube center part is freely expanded by the internal fluid pressure. Different pressure levels are applied on tested tubes and the bulge height and pole thickness are measured after deformation. The collected experimental data i.e. curves of the fluid pressure versus bulge height and pole thickness is used as the optimization objective in the developed hybrid framework.

One-sided hydraulic bulge tests with axial force for EN-AW 6060-O aluminium tubes are performed on an internal pressure-axial compression machine which is illustrated in Fig. 5. During the test, the axial feeding force from two punches and internal fluid pressure from an intensifier can be applied to tubular specimens at the same time. The filling height of the tube branch can be recorded online and the thickness at the top of specimens is measured after deformation. Besides, the axial compressive force and punch displacement are collected and imported into the hybrid strategy, which enable the simulation process more accurate and stable.

A remote high performance computer cluster named Hill is deployed to run FE simulations and solve the optimization design program, which is more powerful than a single computer in terms of computing performance. Hill cluster consists of five nodes and each node is running the Ubuntu GNU/Linux operating system which has 28 cores of Intel Xeon E5–2697 CPUs and 251*GB* of RAM. In the computation process, the number of CPUs and memory size are specified and set to the same to compare the running speed of different optimization strategies.

Table 1
The structure of Gauss-Newton algorithm with trust region strategy.

Step 0: The material parameters from theoretical analysis are given;
Step 1: If the cost function or its gradient at the current point satisfies the stopping criteria then stop; Step 2: Calculate the Jacobian matrix and the damping factor μ_0 in trust region strategy; Step 3: Approximately solve the equation $(J^TJ + \mu_0 I)s_k = -g$ and update the current material coefficients; Step 4: Generate the new damping factor μ_0 and repeat all steps until the optimum point is found.

4. Results and discussion

As shown above, two types of hydraulic tests for different tubular materials have been carried out to evaluate the effectiveness and robustness of the proposed hybrid framework. The experimental data and comparison results between this new strategy and other methods will be elaborated in this section.

4.1. Tube hydraulic test with fixed end-condition

The used material is thin-walled 5049-O aluminium alloy tube in free bulge test and the cut tubular specimens are expanded only under the internal fluid pressure. One deformed sample after the test is illustrated in Fig. 6 and the measured bulge height and pole thickness are partially shown in Fig. 7 and 8. The proposed hybrid strategy and inverse model are chosen as post-processing procedures to minimize the objective function for the experimental data. Identified material parameters and iteration information are presented in Table 2.

As can be observed from the results, two different strategies can reduce the value of the cost function to a very low level and determine the corresponding constitutive coefficients in the defined hardening model. Meanwhile, material parameters obtained by the hybrid framework can converge to the similar results even if the initial strength coefficient and hardening exponent are far from the optimal solution e.g. set 1 and 6. The inverse model determines the same optimal material parameters when the starting point is around the vicinity of the global minimum such as set 2, 3, and 4. However, it produces a local minimum e.g. set 1 and 5 when the starting point is not close to the optimum. Therefore, the hybrid framework is more flexible and stable than the single inverse model because the introduction of an analytical model make it to avoid the trap of local optimums. It can also be used to identify material coefficients in the constitutive model even though there is no information of input tubes for users.

In the parameter identification process, the local minimum can reduce the accuracy of the results. Figs. 7 and 8 illustrate the fitted curve of internal pressure versus the bulge height and pole thickness to the experimental data using different strategies. It is shown that the final optimized curve using the inverse model with bad initial points i.e. far from the optimum has a great gap to the measured bulge height and pole thickness because the application of gradient-based algorithm makes the iteration process locally convergent. The hybrid strategy and inverse model with good starting points can lead to a good match with the experimental result.

For a more accurate quantitative analysis, the concept of the average error is introduced to evaluate the discrepancy between the simulation and experiment, which can be written as $\psi = (D_{exp} - D_{sim})/D_{exp}$ where D_{exp} and D_{sim} are the experimental and calculated results, respectively. The predicted tube bulge profile from FE models using identified material parameters is compared with experimental data, which is plotted in Fig. 9. It can be observed that the simulated curve by the hybrid model has a good agreement with the measured data. The smallest average deviation 0.17% among 0.93%, 0.18%, 0.71% from the analytical model and inverse model with good and bad points also proves the point that the hybrid model seems to be the most accurate method in parameter identification problem. The biggest fitting error is generated by the analytical model because the mechanical and geometrical assumptions are made in the theoretical analysis.

Table 3 illustrates the comparison of CPU time using the hybrid strategy and inverse model. The initial set 5 are considered as an example, where the final material coefficients converge to the similar global optimums. It is possible to conclude that the hybrid strategy is more efficient than the single inverse model. 40 FE simulations are performed to meet the stopping criteria in the inverse model and the hybrid framework only take 32 FE model evaluations. Indeed, the total

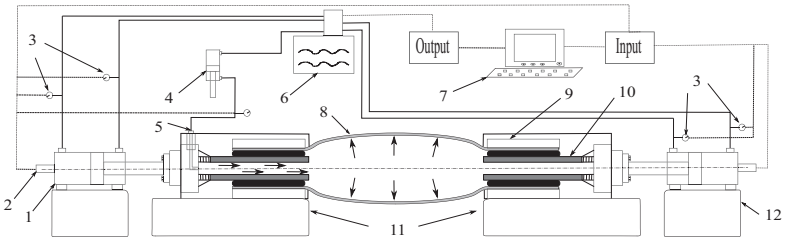

1. Hydraulic cylinder
2. Displacement transducer
3. Pressure sensor
4. Intensifier
5. Plug
6. Hydraulic power
7. Control system
8. Tubular specimen
9. Gasket
10. Mandrel
11. Slideway
12. Basement

Fig. 4. Schematic diagram of experimental setup for tube hydraulic test with fixed end-condition.

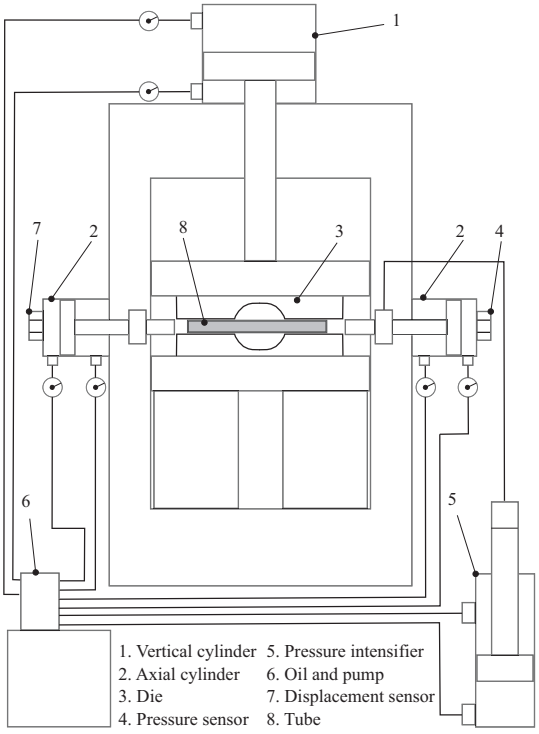

Fig. 5. Schematic diagram of experimental setup for tube hydraulic test with forced end-condition.

CPU time of 20% is reduced because of the application of this proposed hybrid strategy, where the analytical model can obtain a better searching space for design variables and reduce the iteration times for the second stage optimization process.

4.2. Tube hydraulic test with forced end-condition

In the hydraulic bulge test for 6060-O aluminium alloy tubes, the punch force and internal fluid pressure are exposed on the tubular specimens and the total punch axial feeding displacement is 36.00 *mm*. At the end of the experiment, recorded experimental results contain the axial displacement versus the filling height and punch force. The shape of the tubular sample before and after deformation is shown in Fig. 10. Based on the experimental data, material parameters in defined power hardening laws are identified using different methods, which are presented in Table 4.

Fig. 6. Illustration of the initial and deformed 5049-O aluminium tubes in hydraulic bulge test with fixed end-condition.

From the results, it can be seen that the hybrid model is more robust than the separate inverse model. The robustness of different methods can be estimated using the quality of the solution and the range of initial values. For the inverse model, different optimal solutions are obtained, which means that the cost function has several local minimums. Furthermore, the identified constitutive parameters from the initial set 2–7 converge to the similar values when the starting points are the vicinity of the optimum results. However, the identification process falls into the trap of local minimums when the initial values are far from the optimum solution, which can be seen from the set 1, 8. For the hybrid model, a wider range of initial values is used where the strength

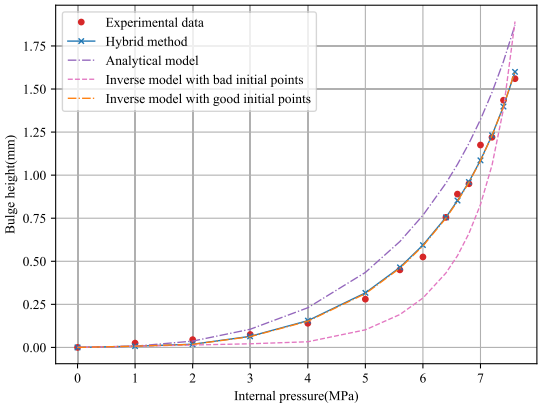

Fig. 7. Comparison of the internal pressure versus bulge height curve determined by different methods for 5049-O aluminium tubes.

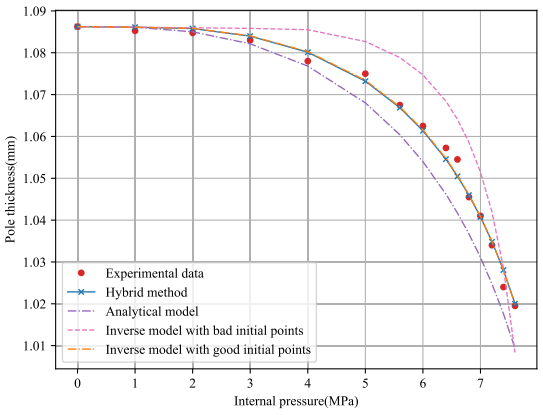

Fig. 8. Comparison of the internal pressure versus pole thickness curve determined by different methods for 5049-O aluminium tubes.

coefficient is from 100 to 1000 and hardening exponent is from 0.1 to 0.9. The identical material parameters are finally determined and this improvement can be attributed to the good searching space generated by the theoretical analysis in the first stage of the hybrid model.

The efficiency of different methods can be evaluated using calculation time i.e. the number of iterations. The computational cost of FE models dominates the total time in each iteration, so it can serve as a detailed evaluation criterion. It can be observed in Table 4 and considering the initial set 7 as an example, 28 evaluations of FE models(f-evaluation) are performed in the hybrid model. As a comparison, the inverse model needs 48 f-evaluations and converges to the final material parameters when the starting points are far from the optimum one. The quantitative evaluation of calculation time for these two methods is displayed in Table 3, where the hybrid model can save 42% of the running time. An iteration history for the objective function and its gradient, two design variables is presented in Figs. 11 and 12. It can be seen that these two methods can provide a stable parameter identification process while the hybrid model needs fewer iterations compared to

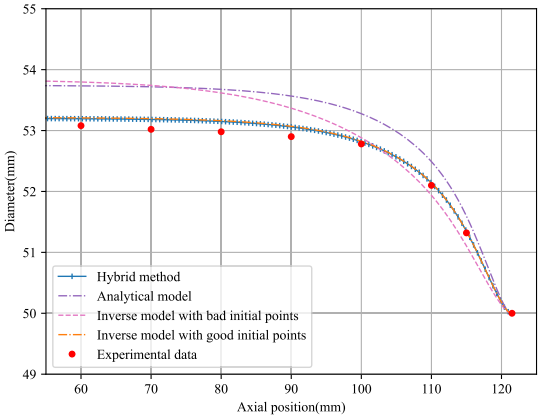

Fig. 9. Comparison of the axial position versus bulge shape profile curve determined by different methods for 5049-O aluminium tubes.

Table 3
Comparison of calculation time using different methods.

Hydraulic bulge test	Forced end-condition		Fixed end-condition	
	Hybrid model	Inverse model	Hybrid model	Inverse model
Number of CPU's	16	16	28	28
Memory(MB)	400	400	400	400
Number of FE model evaluation	28	48	32	40
Run time of each FE simulation(min)	14.63	14.63	12.41	12.41
The total time(h)	6.83	11.70	6.62	8.27

Table 2
Identified material parameters for 5049-O aluminium tubes based on hydraulic bulge test with fixed end-condition.

		Initial x_0				Optimum x*				
	set	K (MPa)	m	f (x_0)	f` (x_0)	K (MPa)	m	f (x*)	f` (x*)	Iteration
Inverse model	1	100.00	0.10	1.06E+ 2	8.47E+ 2	260.62	0.179	3.79E-1	7.27E+ 0	18
	2	300.00	0.20	1.16E+ 0	4.39E+ 1	380.17	0.311	1.28E-2	9.05E-1	10
	3	350.00	0.25	8.88E-1	3.52E+ 1	382.29	0.313	1.27E-2	6.30E-1	9
	4	400.00	0.30	5.35E-1	2.77E+ 1	380.89	0.312	1.27E-2	5.69E-1	10
	5	500.00	0.25	2.80E+ 0	1.16E+ 1	472.60	0.262	2.47E+ 0	1.66E+ 1	12
Hybrid model	1	100.00	0.10	1.06E+ 2	8.47E+ 2	383.32	0.313	1.27E-2	6.31E-1	8
	2	300.00	0.20	1.16E+ 0	4.39E+ 1	383.79	0.313	1.30E-2	1.35E+ 0	8
	3	350.00	0.25	8.88E-1	3.52E+ 1	382.63	0.312	1.29E-2	1.15E+ 0	8
	4	400.00	0.30	5.35E-1	2.77E+ 1	381.96	0.311	1.76E-2	4.62E+ 0	8
	5	500.00	0.25	2.80E+ 0	1.16E+ 1	382.09	0.312	1.28E-2	9.35E-1	8
	6	1000.00	0.90	8.35E+ 0	4.74E+ 1	382.46	0.313	1.29E-2	1.08E+ 0	8
Stable value						382.71	0.312			

Fig. 10. Illustration of the initial and deformed 6060-O aluminium tubes in hydraulic bulge test with forced end-condition.

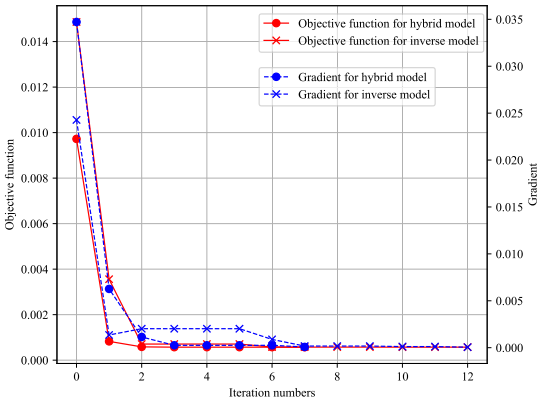

Fig. 11. Iteration history of the cost function and its gradient using initial set 7.

the inverse model. However, the computational efficiency of hybrid model has no significant improvements compared with the inverse model with good initial guesses.

Fig. 13 illustrates the comparison of the filling height versus axial displacement curve between experimental data and simulation results of FE models using identified constitutive parameters by different methods. It can be seen that the hybrid method leads to a good match between the simulated and experimental results as well as the inverse model with good initial points. Besides, a great gap can be observed when using the single analytical model and inverse model with bad initial guesses. On the other hand, the predicted punch force by FE models with material coefficients from different methods is compared with that recorded in the experiment, which is plotted in Fig. 14. It is found that the simulated results using the flow stress curve from the hybrid model and inverse model with good initial guesses have a small difference and can match the experimental data better than the analytical model and inverse model with bad starting points.

As an accuracy evaluation, the quantitative analysis for the deviation of the predicted bulge height and punch compressive force to experiment data are performed using the formula in Section 4.1. The average deviation of the filling height is 2.69% generated by the hybrid framework, which is the smallest value among 28.93%, 7.61%, 2.80% obtained by corresponding analytical model, inverse model with bad and good initial values. For the mean error of the punch force, the hybrid

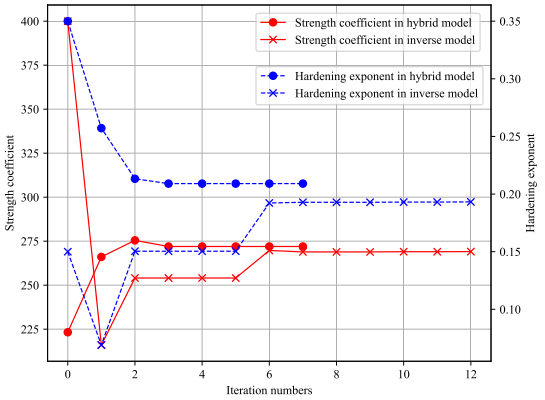

Fig. 12. Iteration history of two design variables using initial set 7.

Table 4
Identified material parameters for 6060-O aluminium tubes based on hydraulic bulge test with forced end-condition.

		Initial x_0				Optimum x*				
	set	K (MPa)	m	f (x_0)	f` (x_0)	K (MPa)	m	f (x^*)	f` (x^*)	Iteration
Inverse model	1	100.00	0.10	2.01E-1	9.18E-1	110.17	0.087	1.65E-3	2.39E-5	8
	2	150.00	0.15	4.14E-2	7.71E-2	271.44	0.204	5.69E-4	5.67E-5	9
	3	200.00	0.20	1.09E-2	5.43E-2	269.95	0.207	5.72E-4	7.96E-4	6
	4	250.00	0.25	1.99E-3	2.01E-2	271.73	0.206	5.70E-4	1.08E-4	7
	5	300.00	0.30	9.22E-4	3.36E-3	270.34	0.204	5.72E-4	3.54E-5	7
	6	400.00	0.40	6.12E-3	2.13E-2	271.25	0.202	5.71E-4	8.69E-6	8
	7	400.00	0.15	1.49E-2	2.43E-2	269.08	0.193	5.71E-4	5.13E-5	12
	8	1000.00	0.90	5.06E-2	2.55E-2	190.61	0.616	6.06E-4	8.57E-5	11
Hybrid model	1	100.00	0.10	2.00E-1	9.18E-1	271.98	0.209	5.70E-4	7.93E-5	7
	2	150.00	0.15	4.15E-2	7.70E-2	271.91	0.207	5.70E-4	1.12E-4	7
	3	200.00	0.20	1.09E-2	5.43E-2	269.92	0.209	5.73E-4	2.83E-5	7
	4	250.00	0.25	1.99E-3	2.01E-2	271.90	0.207	5.69E-4	1.11E-5	7
	5	300.00	0.30	9.22E-4	3.36E-3	270.59	0.201	5.70E-4	1.73E-5	7
	6	400.00	0.40	6.12E-3	2.13E-2	271.70	0.205	5.72E-4	7.15E-5	7
	7	400.00	0.15	1.49E-2	2.43E-2	271.23	0.200	5.70E-4	4.78E-6	7
	8	1000.00	0.90	5.06E-2	2.55E-2	270.94	0.210	5.71E-4	8.47E-5	7
Stable value						271.27	0.206			

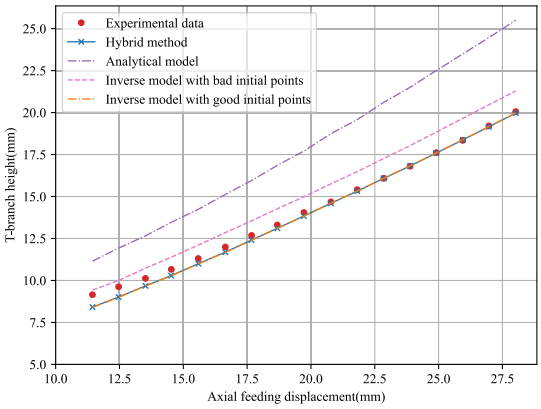

Fig. 13. Comparison of the axial displacement versus T-branch height curve determined by different identification methods for 6060-O aluminium tubes.

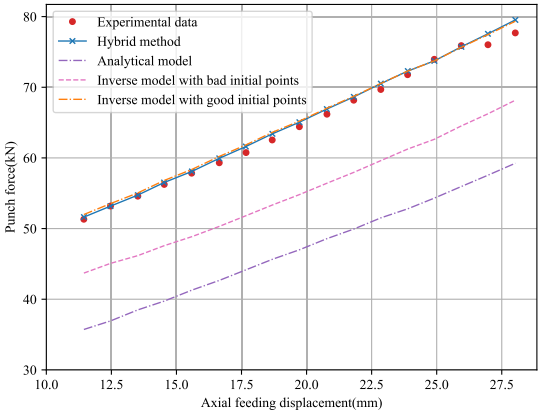

Fig. 14. Comparison of the axial displacement versus punch force curve determined by different identification methods for 6060-O aluminium tubes.

model and inverse model with good starting points present a better fitting with the 0.90% and 1.15% deviation. The other two methods with 27.33% and 14.72% error have a bad match to the experimental data. This quantitative analysis is consistent with observation in Fig. 13 and 14.

From these comparisons, it can be seen that the developed hybrid strategy can be used to determine material coefficients in constitutive models of the tubular metal and presents a more strong robustness and accuracy in parameter identification process compared with the other two methods. One possible reason is that the simplest theoretical model uses the plane strain or stress assumption and the tube profile shape is considered as a specific geometrical shape, whose two assumptions make it possible to quickly solve the equilibrium equation but reduce the accuracy of the solution. The inverse scheme is based on the incremental theory, which can obtain more accurate solutions but increase the model complexity and the computational cost. At the same time, the introduction of gradient-based algorithms makes it more dependent on the initial guesses.

5. Conclusion

A novel hybrid framework is developed to identify constitutive parameters of tubular materials, which combines the theoretical analysis, FE simulation and Gauss-Newton optimization algorithm. Hydraulic bulge tests with fixed and forced end-condition are carried on for annealed 5049 and 6060 aluminum alloy tubes separately to generate an experimental database and validate the feasibility and performance of the proposed inverse strategy. Material coefficients in Hollomon hardening law are determined using the hybrid scheme, inverse model and analytical method based on the experimental data. Through the analysis and comparison of obtained results, the following conclusions can be drawn: .

(1) Tube hydraulic bulge test with fixed and forced end-condition is suitable for characterization the mechanical properties of seamless thin-walled aluminium alloy tubes at different strain ranges. Strength coefficient K and hardening exponent m can be determined by means of three models described in this paper.
(2) The analytical model can achieve a fast parameter identification but the accuracy of the solution is low. Material parameters determined by the inverse model are more accurate than the theoretical analysis while the inverse model always converges to the local minimum and increases the computational cost when the initial guesses are far from the optimum points.
(3) The proposed hybrid strategy takes all advantages of the above two models and can obtain the global optimum efficiently, where the reasonable searching space around the vicinity of the global minimum is generated by an analytical model in the first stage then the optimal parameters are quickly determined using the trust region algorithm. The computation cost of the hybrid method can be saved by 20% compared with classical methods.
(4) Based on material parameters identified by three methods, the predicted bulge height, punch compressive force and pole thickness from FE simulations are used to compare with the experimental data. The results show that the simulated outputs using material parameters obtained by the hybrid scheme have a better agreement with the experimental data and the developed hybrid framework is more accurate than the other two models.

CRediT authorship contribution statement

Bin Zhang: Methodology, Software, Investigation, Formal analysis, Data curation, Writing – original draft, Visualization. **Benny Endelt:** Conceptualization, Methodology, Investigation, Writing – review & editing. **Lihui Lang:** Resources, Writing – review & editing. **Karl Brian Nielsen:** Supervision, Writing – review & editing.

Declaration of Competing Interest

The authors declare that they have no known competing financial interests or personal relationships that could have appeared to influence the work reported in this paper.

Data Availability

The raw data required to reproduce these findings can be available from the corresponding author upon reasonable request.

Acknowledgments

This work was partially supported by China Scholarship Council (CSC) (No. 201706080020) from the Ministry of Education of PR China and authors express their appreciation to CSC for their financial support.

References

[1] A. Alaswad, K. Benyounis, A. Olabi, Tube hydroforming process: a reference guide, Mater. Des. 33 (2012) 328–339.
[2] C. Bell, J. Corney, N. Zuelli, D. Savings, A state of the art review of hydroforming technology: its applications, research areas, history, and future in manufacturing, Int. J. Mater. Form. 13 (2020) 789–828.
[3] H. Ahmadi, M. Zohoor, Investigation of the effective parameters in tube hydroforming process by using experimental and finite element method for manufacturing of tee joint products, Int. J. Adv. Manuf. Technol. 93 (2017) 393–405.
[4] W. Volk, P. Groche, A. Brosius, A. Ghiotti, B.L. Kinsey, M. Liewald, L. Madej, J. Min, J. Yanagimoto, Models and modelling for process limits in metal forming, CIRP Ann. 68 (2019) 775–798.
[5] H. Zhu, Z. He, Y. Lin, K. Zheng, X. Fan, S. Yuan, The development of a novel forming limit diagram under nonlinear loading paths in tube hydroforming, Int. J. Mech. Sci. 172 (2020), 105392.
[6] M. Nemat-Alla, Reproducing hoop stress-strain behavior for tubular material using lateral compression test, Int. J. Mech. Sci. 45 (2003) 605–621.
[7] F. Bardi, S. Kyriakides, Plastic buckling of circular tubes under axial compression-part I: experiments, Int. J. Mech. Sci. 48 (2006) 830–841.
[8] L. Vitu, N. Boudeau, P. Malécot, G. Michel, A. Buteri, Evaluation of models for tube material characterization with the tube bulging test in an industrial setting, Int. J. Mater. Form. 11 (2018) 671–686.
[9] J. Yoon, J. Kim, H. Kim, C. Won, Y. Song, S.H. Park, Calibration of hoop stress in ring tensile test with Zircaloy-4 tube, J. Mech. Sci. Technol. 31 (2017) 4183–4188.
[10] D. Woo, P. Hawkes, Determination of stress/strain characteristics of tubular materials, J. Inst. Met. 96 (1968) 357–359.
[11] M. Koç, Y. Aue-u lan, T. Altan, On the characteristics of tubular materials for hydroforming-experimentation and analysis, Int. J. Mach. Tools Manuf. 41 (2001) 761–772.
[12] ASTM E8. Standard test methods for tension testing of metallic materials, Technical Report, 2013.
[13] H. Wang, P. Martin, Tube formability assessment for tube hydroforming, J. Mater. Manuf. 111 (2002) 880–889.
[14] A. Khalfallah, Z. Ktari, C. Leitão, J.V. Fernandes, New mandrel design for ring hoop tensile testing, Exp. Tech. (2021).
[15] F. Alhussainy, M.N. Sheikh, M.N. Hadi, Behaviour of small diameter steel tubes under axial compression, Structures 11 (2017) 155–163.
[16] B. Zhang, B. Endelt, L. Lang, Y. Zhao, S. Yan, K.B. Nielsen, An inverse strategy to determine constitutive parameters of tubular materials for hydroforming process, Chin. J. Aeronaut. (2021) Accepted.
[17] L. Yang, C. Ge, Determination of stress-strain relationship of tubular material with hydraulic bulge test, Thin Walled Struct. 46 (2008) 147–154.
[18] Y.-M. Hwang, Y.-K. Lin, T. Altan, Evaluation of tubular materials by a hydraulic bulge test, Int. J. Mach. Tools Manuf. 47 (2007) 343–351.
[19] X. Wang, W. Hu, S. Huang, R. Ding, Experimental investigations on extruded 6063 aluminium alloy tubes under complex tension-compression stress states, Int. J. Solids Struct. 168 (2019) 123–137.
[20] X. Cui, S. Yuan, Determination of mechanical properties of anisotropic thin-walled tubes under three-dimensional stress state, Int. J. Adv. Manuf. Technol. 87 (2016) 1917–1927.
[21] N. Boudeau, P. Malècot, A simplified analytical model for post-processing experimental results from tube bulging test: theory, experimentations, simulations, Int. J. Mech. Sci. 65 (2012) 1–11.
[22] R. Velasco, N. Boudeau, Tube bulging test: theoretical analysis and numerical validation, J. Mater. Process. Technol. 205 (2008) 51–59.
[23] O. Ghouati, J.-C. Gelin, A finite element-based identification method for complex metallic material behaviours, Comput. Mater. Sci. 21 (2001) 57–68.
[24] G. Rauchs, J. Bardon, Identification of elasto-viscoplastic material parameters by indentation testing and combined finite element modelling and numerical optimization, Finite Elem. Anal. Des. 47 (2011) 653–667.
[25] S. Schmaltz, K. Willner, Comparison of different biaxial tests for the inverse identification of sheet steel material parameters, Strain 50 (2014) 389–403.
[26] P.A. Prates, M.C. Oliveira, J.V. Fernandes, Identification of material parameters for thin sheets from single biaxial tensile test using a sequential inverse identification strategy, Int. J. Mater. Form. 9 (2016) 547–571.
[27] P.A. Prates, A.F.G. Pereira, N.A. Sakharova, M.C. Oliveira, J.V. Fernandes, Inverse strategies for identifying the parameters of constitutive laws of metal sheets, Adv. Mater. Sci. Eng. 2016 (2016) 1–18.
[28] A. Pereira, P. Prates, M. Oliveira, J. Fernandes, Inverse identification of the work hardening law from circular and elliptical bulge tests, J. Mater. Process. Technol. 279 (2020), 116573.
[29] Z. Ktari, C. Leitão, P.A. Prates, A. Khalfallah, Mechanical design of ring tensile specimen via surrogate modelling for inverse material parameter identification, Mech. Mater. 153 (2021), 103673.
[30] J. Liu, H. Yang, H.W. Li, H. Li, S. Zhu, A new hybrid identification method for determining the material parameters of thin-walled tube under compressive stress state, Mater. Des. 44 (2013) 49–58.
[31] T. Zribi, A. Khalfallah, H. BelHadjSalah, Experimental characterization and inverse constitutive parameters identification of tubular materials for tube hydroforming process, Mater. Des. 49 (2013) 866–877.
[32] A. Khalfallah, M.C. Oliveira, J.L. Alves, T. Zribi, H. Belhadjsalah, L.F. Menezes, Mechanical characterization and constitutive parameter identification of anisotropic tubular materials for hydroforming applications, Int. J. Mech. Sci. 104 (2015) 91–103.
[33] M.H.A. Bonte, A.H. van den Boogaard, J. Huétink, An optimisation strategy for industrial metal forming processes: modelling, screening and solving of optimisation problems in metal forming, Struct. Multidiscip. Optim. 35 (2008) 571–586.
[34] W. Sun, Y. Yuan, Optimization Theory and Methods: Nonlinear Programming, Springer, New York, 2006.
[35] B. Chaparro, S. Thuillier, L. Menezes, P. Manach, J. Fernandes, Material parameters identification: gradient-based, genetic and hybrid optimization algorithms, Comput. Mater. Sci. 44 (2008) 339–346.
[36] G.M. Kakandikar, V.M. Nandedkar, Sheet Metal Forming Optimization: Bioinspired Approaches, CRC Press, Boca Raton, 2018.
[37] C. Huang, A.E. Hami, B. Radi, Metamodel-based inverse method for parameter identification: elastic-plastic damage model, Eng. Optim. 49 (2017) 633–653.
[38] Y. Tsompanakis, N.D. Lagaros, G.E. Stavroulakis, Soft computing techniques in parameter identification and probabilistic seismic analysis of structures, Adv. Eng. Softw. 39 (2008) 612–624.
[39] M. Vaz, M.A. Luersen, P.A. Muñoz-Rojas, R.G. Trentin, Identification of inelastic parameters based on deep drawing forming operations using a global-local hybrid Particle Swarm approach, Comptes Rendus Mécanique 344 (2016) 319–334.
[40] M. Wójcik, A. Skrzat, Identification of Chaboche-Lemaitre combined isotropic-kinematic hardening model parameters assisted by the fuzzy logic analysis, Acta Mech. 232 (2021) 685–708.
[41] J.P. Ponthot, J.P. Kleinermann, A cascade optimization methodology for automatic parameter identification and shape/process optimization in metal forming simulation, Comput. Methods Appl. Mech. Eng. 195 (2006) 5472–5508.
[42] R. de Carvalho, R.A.F. Valente, A. Andrade-Campos, Optimization strategies for non-linear material parameters identification in metal forming problems, Comput. Struct. 89 (2011) 246–255.
[43] R.A.F. Valente, A. Andrade-Campos, J.F. Carvalho, P.S. Cruz, Parameter identification and shape optimization: an integrated methodology in metal forming and structural applications, Optim. Eng. 12 (2011) 129–152.
[44] Z. He, S. Yuan, Y. Lin, X. Wang, W. Hu, Analytical model for tube hydro-bulging test, part I: models for stress components and bulging zone profile, Int. J. Mech. Sci. 87 (2014) 297–306.
[45] K. Osakada, History of plasticity and metal forming analysis, J. Mater. Process. Technol. 210 (2010) 1436–1454.
[46] L. Moreira Filho, H. Al-Qureshi, Unconventional tee forming on metal tubes, J. Manuf. Sci. Eng. 107 (1985) 392–396.
[47] M. Strano, T. Altan, An inverse energy approach to determine the flow stress of tubular materials for hydroforming applications, J. Mater. Process. Technol. 146 (2004) 92–96.
[48] B. Endelt, J. Danckert, Identification of friction coefficients and hardening parameters using optimization methods coupled with a 3D finite element code, J. Mater. Process. Technol. 209 (2009) 4005–4010.
[49] B. Endelt, Least square optimization techniques applied on sheet metal forming - Inverse identification of constitutive parameters and optimization of process parameters, Ph.D. thesis, Aalborg University, Denmark, 2003.
[50] A. Andrade-Campos, R. de Carvalho, R. Valente, Novel criteria for determination of material model parameters, Int. J. Mech. Sci. 54 (2012) 294–305.

Chapter 7

Conclusions

The chapter covers a summary of published papers. This is followed by a statement of scientific contributions of this research. Finally some valuable future work is recommended.

7.1 Summary of papers

After the examination of the proposed research questions and corresponding hypotheses, three journal papers are produced based on the obtained experimental resource. The research results of these papers are summarized as below.

Paper I

Research question A proposed in section 3.1.1 has been tested in Paper I. In this paper, tube bulge tests with fixed-end condition for GB/T 5049-O aluminium are carried out on a flexible hydraulic forming press. The bulge height, pole thickness and bulge shape profile under distinct fluid pressure levels are collected during the test, see Fig. 7.1. An inverse scheme integrating FE model with an improved Levenberg-Marquardt algorithm is proposed to identify tubular material parameters through a minimization of the gap between computed and experimental results. Several sets of starting points are tested for the developed inverse strategy. Two different analytical models based on membrane theory and total strain principle are developed to describe and model the hydraulic bulge process and determine the strain-stress relationship of tested aluminium alloy. FE simulations of free bulging processes are conducted based on determined flow stress curves from distinct testing methods and models. Predicted pole thickness, bulge shape profile and bulge height by FE models are compared with measured values and

results calculated by the inverse strategy present a good agreement with experimental data.

Figure. 7.1. Hydro-bulged tubular samples at multiple pressure levels.

Paper II

In terms of research question B proposed in section 3.1.1, Paper II examines the hypothesis to solve this problem. In this paper, T-shape tube hydraulic bulge tests under axial compressive forces are carried out to identify the mechanical properties of EN AW 5049-O and 6060-O aluminium alloys. The punch displacement, filling height and axial feeding force are collected online during the experiment, see Fig. 7.2. An automatic inverse parameter identification framework combining FE method and optimization technique is developed to determine material coefficients by fitting calculated data to experimental results iteratively. Determined material parameters using the inverse model are compared to those identified using the analytical model and uni-axial tension test. The comparison shows that the predicted filling height and axial compressive force obtained by three types of methods are different and the smallest gap between calculated and experimental results is made by the inverse model.

Paper III

To figure out the research question C presented in section 3.1.1, paper III validate the hypothesis for this research question. A hybrid framework integrating a theoretical analysis, FE model and gradient-based optimization algorithm to identify material parameters for thin-walled metal tubes using obtained experimental data from hydro-bulging tests is developed. In this strategy, starting points of constitutive parameters are produced quickly using an analytical model, and then are imported into an inverse model integrating Gauss-Newton algorithm and FE method. The solving of this optimization problem can obtain more accurate material constitutive parameters

Figure. 7.2. Tubular sample before and after T-shape hydraulic bulge tests.

by decreasing the difference between simulated and experimental data. To assess its performance, hydraulic bulging tests with fixed and forced end-conditions for EN AW 6060 and GB/T 5049 aluminium tubes are performed. Mises yield criterion and Hollomon hardening model are used to describe the material behavior. Calculated material parameters are utilized to compare to those obtained by a single theoretical analysis or an inverse model. This comparison shows that the novel hybrid strategy is not sensitive to initial points and improve the computational efficiency and identify more accurate materials parameters.

7.2 Contributions

The main focus of this work is to develop an automatic parameter identification strategy to determine the flow stress data of tubular materials for hydroforming processes using hydraulic bulge tests. In order to verify the hypotheses to solve proposed research questions, physical experiments and modelling work have been performed. The following is a summary of the major scientific contributions:

- Tensile tests and hydraulic bulge tests with fixed or forced end-conditions are designed and performed to characterize mechanical properties of thin-walled metal tubes. Tube hydraulic bulge tests are more suitable for characterizing mechanical properties of tubular material compared with the tensile test, and the stress-strain data in a larger strain range

can be obtained in the bulge test under axial compressive forces.

- The novel inverse model combining FE models and gradient-based algorithms, total strain model and energy method are developed as three different parameter identification strategies to post-processing experimental resources from hydraulic bulge tests of tubular samples with different shapes. Analytical models, i.e., total strain model and energy method, are simple and efficient methods while the inverse model can determine more accurate material parameters.

- A more advanced hybrid strategy integrating analytical methods with inverse modelling techniques is developed, which combines the advantages of the above approaches and can find the global optimum efficiently. This generalized hybrid scheme has successfully handled all types of tube hydraulic bulge tests and has the potential to be extended more complex materials testing experiments.

7.3 Future work

Based on the analysis of the state of the art and experience of actual experiments and modelling work, the following research can be considered in the future:

Experimental setup A more flexible hydraulic press needs to be designed and manufactured, which can achieve multiple biaxial stress states, i.e., both tension-tension and tension-compression stress states, at the same time on one machine. In addition, the value of the applied axial feeding force can be controlled online accurately, which means that this machine can provide more rich and accurate the stress-strain data with different stress ratios Moreover, two stress states can be switched at any time during the test and deformation behavior of tubular materials under complex strain paths can be described.

Constitutive modelling For tube hydraulic bulge tests under monotonic loading conditions, the associated flow law based on simple yield criteria and the isotropic hardening model can be used to describe material characteristics. For tubular materials tests under complex strain paths, traditional associated plastic constitutive relationship can not meets the accuracy requirements in the simulation of advanced metal forming processes and a novel non-associated flow rule based on an anisotropic yield criterion and kinematic hardening model should be established to subject the loading conditions.

Optimization strategy The proposed hybrid strategy can avoid local minimum points and converge to the global optimum solution efficiently in the parameter identification process, but the tedious calculation of FE models is still time-consuming and increase the total computational cost. A meta-model generated by the response surface method can be constructed to replace the original and expensive FE model. The simplified meta-model is simple to calculate and significantly reduce the total run time. Furthermore, it will make online control of metal forming processes possible when the accuracy of the generated meta-model is good enough.

Appendix A: Gradient-based optimization algorithms for nonlinear least squares problems

General overview

Various optimization methods have been developed to solve the nonlinear least squares problems in the relevant mathematical literature, in which four classical algorithms are coded using Python programming language in this chapter. In order to measure their reliability and efficiency, a relatively large set of testing functions have been defined. The final numerical experiments results show the characteristics of these four algorithms in solving different problems, which further provides computational experiences for the algorithm selection in solving practical engineering problems.

Gradient-based optimization algorithms

The process optimization and parameter identification in the field of metal forming can be treated as mathematical programming problems, in which the objective function always is reformulated as the form of nonlinear least squares and can be written as the following [144]:

$$f(\mathbf{x}) = \frac{1}{2}\mathbf{r}^T(\mathbf{x})\mathbf{r}(\mathbf{x}) = \frac{1}{2}\sum_{i=1}^{m} r_i^2(\mathbf{x}) \tag{A.1}$$

where $\mathbf{x} = [x_1, x_2, ..., x_n]^T$ represent a design variable in the n-dimensional space. $\mathbf{r}(\mathbf{x}) = [r_1(\mathbf{x}), r_2(\mathbf{x}), ..., r_m(\mathbf{x})]^T$ is the residual function from $\mathbb{R}^m$ to $\mathbb{R}^n$

and r_i is the *ith* component from the residual vector function. The first partial derivative of the residual function can be defined as:

$$\boldsymbol{J}(\mathbf{x}) = \begin{bmatrix} \frac{\partial r_1}{\partial x_1} & \frac{\partial r_1}{\partial x_2} & \cdots & \frac{\partial r_1}{\partial x_n} \\ \frac{\partial r_2}{\partial x_1} & \frac{\partial r_2}{\partial x_2} & \cdots & \frac{\partial r_2}{\partial x_n} \\ \vdots & \vdots & \ddots & \vdots \\ \frac{\partial r_m}{\partial x_1} & \frac{\partial r_m}{\partial x_2} & \cdots & \frac{\partial r_m}{\partial x_n} \end{bmatrix} \tag{A.2}$$

Therefore, the gradient and Hessian of the objective function can be written as:

$$\boldsymbol{g}(\mathbf{x}) = \sum_{i=1}^{m} r_i(\mathbf{x}) \nabla r_i(\mathbf{x}) = \boldsymbol{J}^T(\mathbf{x}) \mathbf{r}(\mathbf{x}) \tag{A.3}$$

$$\boldsymbol{G}(\mathbf{x}) = \boldsymbol{J}^T(\mathbf{x}) \boldsymbol{J}(\mathbf{x}) + \boldsymbol{S}(\mathbf{x}) \tag{A.4}$$

$$\boldsymbol{S}(\mathbf{x}) = \sum_{i=1}^{m} r_i(\mathbf{x}) \nabla^2 r_i(\mathbf{x}) \tag{A.5}$$

According to two-term Taylor's expansion, the quadratic model of $f(\mathbf{x})$ around the neighbour of x_k can be expressed as:

$$\begin{aligned} m_k(\mathbf{x}) = & \frac{1}{2} \mathbf{r}^T(\mathbf{x}_k) \mathbf{r}(\mathbf{x}_k) + (\boldsymbol{J}^T(\mathbf{x}_k) \mathbf{r}(\mathbf{x}_k))^T (\mathbf{x} - \mathbf{x}_k) \\ & + \frac{1}{2} (\mathbf{x} - \mathbf{x}_k)^T (\boldsymbol{J}^T(\mathbf{x}_k) \boldsymbol{J}(\mathbf{x}_k) + \boldsymbol{S}(\mathbf{x}_k)) (\mathbf{x} - \mathbf{x}_k) \end{aligned} \tag{A.6}$$

Therefore, the derived formula to solve Eq. (A.1) based on Newton-Raphson method can be written as:

$$\mathbf{x}_{k+1} = \mathbf{x}_k - (\boldsymbol{J}^T(\mathbf{x}_k) \boldsymbol{J}(\mathbf{x}_k) + \boldsymbol{S}(\mathbf{x}_k))^{-1} \boldsymbol{J}(\mathbf{x}) \mathbf{r}(\mathbf{x}) \tag{A.7}$$

Eq. (A.6) is approximated to the objective function and the nonlinear least squares problems can be solved when the Hessian matrix is calculated analytically or numerically. The second order term $\boldsymbol{S}(\mathbf{x})$ in the Hessian matrix is key problem because Jacobian matrix is relatively convenient or inexpensive to obtain. More efforts is made to explore possibilities to neglect or approximate the second derivative of the residual function according to distinct properties, i.e. zero, small and large residual, of nonlinear least squares problems. Four commonly used gradient-based methods will be demonstrated in this chapter, i.e. Gauss-Newton [154], Levenberg-Marquardt [155], modified Levenberg-Marquardt [156], adaptive Quasi-Newton algorithms [157].

Gauss-Newton algorithm

Gauss-Newton(GN) algorithm is the simplest method, i.e. the Newton-Raphson method with line search strategy, for minimizing the objective function with the form of nonlinear least squares. It has been proved that this method gets quadratic convergence when solving zero and small residual least squares problems. In this method, the second order term $\boldsymbol{S}(\mathbf{x})$ is neglected and Hessian matrix is replaced by the first order term. Thus, Eq.(A.7) can be rewritten as below:

$$\mathbf{x}_{k+1} = \mathbf{x}_k - (\boldsymbol{J}^T(\mathbf{x}_k)\boldsymbol{J}(\mathbf{x}_k))^{-1}\boldsymbol{J}(\mathbf{x})\mathbf{r}(\mathbf{x}) \tag{A.8}$$

It can be observed that GN method only needs to calculate the first order derivative of the residual function but it is not convergent if $\boldsymbol{S}(\mathbf{x}_k)$ is relatively large to $\boldsymbol{J}^T(\mathbf{x}_k)\boldsymbol{J}(\mathbf{x}_k)$. Another weakness of GN method is that the Jacobian matrix $\boldsymbol{J}$ has to be full rank at all iterations.

Levenberg-Marquardt algorithm

Levenberg-Marquardt(LM) algorithm [158, 159] is proposed to avoid one of disadvantages of GN method where the step size is not a descent direction when Jacobian matrix $\boldsymbol{J}(\mathbf{x})$ is rank-deficient. It can also be seen as a combination of GN method with the trust region strategy, in which a damping parameter μ is introduced to approximate the second order term $\boldsymbol{S}(\mathbf{x})$. The value of damping parameter is greater than zero and this ensures the Hessian matrix is positive definite in every iteration. Hence, Eq.(A.7) in LM method can be expressed as:

$$\mathbf{x}_{k+1} = \mathbf{x}_k - (\boldsymbol{J}^T(\mathbf{x}_k)\boldsymbol{J}(\mathbf{x}_k) + \mu\boldsymbol{I})^{-1}\boldsymbol{J}(\mathbf{x})\mathbf{r}(\mathbf{x}) \tag{A.9}$$

where $\boldsymbol{I}$ is the identity matrix. It can be observed that LM method takes all advantages of GN and steepest descent algorithm. When the value of μ is relatively large, LM method switch to steepest descent method. It will be good when initial points are far from the solution. If μ is small, the step size is closer to GN step and this method presents quadratic convergence when the iterated points is around the neighbor of the optimum. The initial choice is suggested by this following strategy [160],

$$\mu_0 = \tau \cdot max\{\boldsymbol{J}^T(\mathbf{x}_0)\boldsymbol{J}^T(\mathbf{x}_0)\} \tag{A.10}$$

where $\mathbf{x}_0$ is the initial guess for design variables and τ is chosen by users from the range $[10^{-6}, 1]$. During the iteration, the update of μ is controlled by a gain ratio ρ ,

$$\rho = \frac{f(\mathbf{x}_k) - f(\mathbf{x}_k + \mathbf{h}_k)}{m_k(\mathbf{0}) - m_k(\mathbf{h}_k)} \tag{A.11}$$

in which $\mathbf{h}_k$ is the current searching step. Hence, the updating strategy of the damping parameter μ can be expressed as:

$$\begin{aligned} &\textbf{if} \quad \rho > 0 \\ &\qquad \mu = \mu \cdot \{1/3, 1-(2\rho-1)^3\};\ v = 2 \\ &\textbf{else} \\ &\qquad \mu = \mu \cdot v;\ v = 2v \end{aligned} \tag{A.12}$$

where the value of v is generally set as 2.0. When ρ is greater than zero, the current m_k is a good approximation to the objective function and μ can be decreased such that the next step is GN step with the quadratic convergence. If the value of ρ is negative, the m_k is a poor approximation to $f(\mathbf{x}_k)$ and the step length should be reduced by increasing the value of μ.

Modified Levenberg-Marquardt algorithm

The poorly scaled issue may appear in solving nonlinear least squares problems, primarily due to a substantial numerical gap of the magnitude of design variables. This situation will lead to numerical convergence difficulties or inaccurate solutions. Modified Levenberg-Marquardt(m-LM) has been suggested to address this issue [156]. In this method, a scaling diagonal matrix is taken into account to reduce the effects of poorly scaling. This matrix can collect some information related to the size of each component in design variable vectors and enable the algorithm invariant with scaling. It can be updated from iteration to iteration as below:

$$\begin{aligned} &\mathbf{D}_k = diag(d_1^k, ..., d_m^k) \\ &d_i^0 = \|\partial_i \mathbf{r}(\mathbf{x}_0)\| \\ &d_i^k = max(d_i^{k-1}, \|\partial_i \mathbf{r}(\mathbf{x}_k)\|),\ k \geq 1 \end{aligned} \tag{A.13}$$

where $\mathbf{D}_k$ is the scaling matrix with positive entries. Based on Eq. (A.7), the step in m-LM method can be defined as:

$$\mathbf{x}_{k+1} = \mathbf{x}_k - (\boldsymbol{J}^T(\mathbf{x}_k)\boldsymbol{J}(\mathbf{x}_k) + \mu \boldsymbol{D}^T(\mathbf{x}_k)\boldsymbol{D}(\mathbf{x}_k))^{-1}\boldsymbol{J}(\mathbf{x})\mathbf{r}(\mathbf{x}) \tag{A.14}$$

This m-LM step formula is analogous with Eq. (A.9) except for the second order term in Hessian matrix. Therefore, the damping parameter μ can be updated using the same strategy.

Adaptive Quasi-Newton algorithm

GN and LM methods present the slow linear convergence rate when the residual function $\mathbf{r}(\mathbf{x})$ is highly nonlinear or handling large residual problems. Quasi-Newton(QN) algorithm provides another possibility to obtain

superlinear convergence rate for these cases because it takes into account the secant approximation of the second order term in Hessian matrix. Dennis et al. [157] combine this QN method and trust region strategy to improve its performance further. Hence, Eq. (A.7) in QN method can be rewritten as:

$$\mathbf{x}_{k+1} = \mathbf{x}_k - (\boldsymbol{J}^T(\mathbf{x}_k)\boldsymbol{J}(\mathbf{x}_k) + \mathbf{B}_k + \mu\boldsymbol{I})^{-1}\boldsymbol{J}(\mathbf{x})\mathbf{r}(\mathbf{x}) \tag{A.15}$$

where $\mathbf{B}_k$ presents the *kth* approximation of the second order term in Hessian matrix and can be updated by the following formula:

$$\begin{aligned}\mathbf{B}_{k+1} = \mathbf{B}_k + \frac{(\mathbf{y}_k - \mathbf{B}_k\mathbf{h}_k)\mathbf{v}_k^T + \mathbf{v}_k^T(\mathbf{y}_k - \mathbf{B}_k\mathbf{h}_k)^T}{\mathbf{h}_k^T\mathbf{v}_k} \\ - \frac{\mathbf{h}_k^T(\mathbf{y}_k - \mathbf{B}_k\mathbf{h}_k)}{(\mathbf{h}_k^T\mathbf{v}_k)^2}\mathbf{v}_k\mathbf{v}_k^T\end{aligned} \tag{A.16}$$

in which

$$\begin{aligned}\mathbf{h}_k &= \mathbf{x}_{k+1} - \mathbf{x}_k \\ \mathbf{y}_k &= \boldsymbol{J}_{k+1}^T\mathbf{r}_{k+1} - \boldsymbol{J}_k^T\mathbf{r}_{k+1} \\ \mathbf{v}_k &= \boldsymbol{J}_{k+1}^T\mathbf{r}_{k+1} - \boldsymbol{J}_k^T\mathbf{r}_k\end{aligned} \tag{A.17}$$

It should be noted that zero matrix is applied to $\mathbf{B}_0$, which means NQ step is equivalent with LM method at first iteration. Moreover, in order to reduce the effects of $\mathbf{B}_k$ when the optimization approaching a zero residual solution, the sizing factor λ_k is multiplied $\mathbf{B}_k$ before its update, where

$$\lambda_k = min\{\frac{\mathbf{h}_k^T\mathbf{y}_k}{\mathbf{h}_k^T\mathbf{B}_k^T\mathbf{h}_k}, 1\} \tag{A.18}$$

The introduction of λ_k ultimately improves the efficiency of the algorithm and the accuracy of the optimum solution.

Stopping criteria

The four different methods shown above are the core part in the algorithm and can be used to determine the appropriate step size. In addition, the stopping criteria also plays an important role to terminate the iteration process. Firstly, the gradient of the cost function $f(\mathbf{x})$ should be equal zero when reaching the global minimizer and the following criterion is satisfied,

$$\|\boldsymbol{g}(\mathbf{x}_k)\| \leq \varepsilon_1 \tag{A.19}$$

Secondly, the iteration process will be terminated when the change of design vectors is relatively small,

$$\|\mathbf{x}_{k+1} - \mathbf{x}_k\| \leq \varepsilon_2(\|\mathbf{x}_k\| + \varepsilon_2) \tag{A.20}$$

in which ε_1 and ε_2 are small positive real number. Finally, a safeguard value k_{max} must be set by the users in any algorithm,

$$k \leq k_{max} \tag{A.21}$$

The introduction of k_{max} can avoid an infinite iteration loop when the first two criteria do not come into effect.

Based on the computing formula of step length and stopping criteria, the overall algorithm is implemented below.

Algorithm 1: Methods for nonlinear least squares problems

Input: Starting point $\mathbf{x}_0$;
Damping parameter τ and v;
Termination value ε_1 and ε_2;
Safeguard value k_{max}
Output: Optimum point $\mathbf{x}_*$
Initialize $k = 0$, $\mathbf{x} = \mathbf{x}_0$;
$\mu_0 = \tau \cdot max\{\boldsymbol{J}^T(\mathbf{x})\boldsymbol{J}^T(\mathbf{x})\}$;
$stop = (\boldsymbol{g} \leq \varepsilon_1)$;
while *(***not** *stop) **and** (*$k \leq k_{max}$*)* **do**
  $k = k + 1$;
  Solve $(\boldsymbol{J}^T\boldsymbol{J} + \boldsymbol{S})\mathbf{h} = -\boldsymbol{g}$ {Appropriate formula is selected from Eqs.(A.8),(A.9),(A.14) and (A.15)};
  if $\boldsymbol{h} \leq \varepsilon_2(\|\boldsymbol{x}\| + \varepsilon_2)$ **then**
    Stop;
  else
    $\mathbf{x}_{new} = \mathbf{x} + \mathbf{h}$;
    $\rho = (f(\mathbf{x}_k) - f(\mathbf{x}_k + \mathbf{h}_k))/(m_k(\mathbf{0}) - m_k(\mathbf{h}_k))$;
    if $\rho \geq 0$ **then**
      $\mathbf{x} = \mathbf{x}_{new}$;
      $\mu = \mu \cdot \{1/3, 1 - (2\rho - 1)^3\} \quad v = 2$;
      Update gradient and Hessian matrix;
    else
      $\mu = \mu \cdot v$;
      $v = 2v$;
      end
    end
  end

Table 1. Numerical results for GN method

No.	m	n	ε_1	ε_2	k_{max}	*Itr.*	*Stop*
1	2	2	1E-10	1E-14	5000	3	1
2	2	2	1E-8	1E-10	5000	16	1
3	2	2	1E-10	1E-12	5000	13	1
4	20	4	1E-6	1E-8	5000	Failed	-
5	33	5	1E-10	1E-10	5000	Failed	-
6	6	4	1E-6	1E-6	5000	Failed	-
7	3	3	1E-6	1E-8	5000	Failed	-
8	15	3	1E-6	1E-8	5000	Failed	-
9	3	3	1E-8	1E-12	5000	Failed	-
10	16	3	1E-8	1E-12	5000	Failed	-

Results from numerical experiments

All benchmark problems for testing the above four algorithms are recommended by Moré et al. [161] and Endelt et al. [133]. Both standard and random starting points are generated to measure the robustness and efficiency. The selected testing functions are listed below:

1. Rosenbrock function
2. Freudenstein and Roth function
3. Powell badly scaled function
4. Brown and Dennis function
5. Osborne 1 function
6. Wood function
7. Box 3-dimensional function
8. Bard function
9. Helical valley function
10. Meyer function

Numerical results have been collected in four tables for different algorithms, i.e. GN, LM, mLM and QN methods. From the results, it can be observed that classical GN method presents the fewer iteration times and quicker convergence rate when solving simple and linear cost functions, such

Table 2. Numerical results for LM method

No.	m	n	ε_1	ε_2	τ	*Itr.*	*Stop*
1	2	2	1E-10	1E-14	1E-6	22	1
2	2	2	1E-8	1E-10	1E-1	22	2
3	2	2	1E-10	1E-12	1E-15	70	1
4	20	4	1E-6	1E-8	1E-2	21	2
5	33	5	1E-10	1E-10	1E-4	161	2
6	6	4	1E-6	1E-6	1E-9	3739	2
7	3	3	1E-6	1E-8	1E-1	1709	1
8	15	3	1E-6	1E-8	1E-9	58	1
9	3	3	1E-8	1E-12	1E-6	331	1
10	16	3	1E-8	1E-12	1E-6	4995	2

Table 3. Numerical results for mLM method

No.	m	n	ε_1	ε_2	τ	*Itr.*	*Stop*
1	2	2	1E-10	1E-14	1E-6	18	1
2	2	2	1E-8	1E-10	1E-1	20	1
3	2	2	1E-10	1E-12	1E-15	68	1
4	20	4	1E-6	1E-8	1E-2	5000	3
5	33	5	1E-10	1E-10	1E-4	118	2
6	6	4	1E-6	1E-6	1E-9	5000	3
7	3	3	1E-6	1E-8	1E-1	5000	3
8	15	3	1E-6	1E-8	1E-9	7	2
9	3	3	1E-8	1E-12	1E-6	2569	2
10	16	3	1E-8	1E-12	1E-6	3446	2

Table 4. Numerical results for QN method

No.	m	n	ε_1	ε_2	τ	*Itr.*	*Stop*
1	2	2	1E-10	1E-14	1E-3	49	1
2	2	2	1E-8	1E-10	1E-6	33	2
3	2	2	1E-10	1E-12	1E-1	179	1
4	20	4	1E-6	1E-8	1E-2	40	2
5	33	5	1E-10	1E-10	1E-4	380	2
6	6	4	1E-6	1E-6	1E-9	3768	3
7	3	3	1E-6	1E-8	1E-1	3173	1
8	15	3	1E-6	1E-8	1E-9	44	2
9	3	3	1E-8	1E-12	1E-6	31	2
10	16	3	1E-8	1E-12	1E-6	5000	3

function number 1, 2 and 3 compared to other methods. However, it encounters the numerical issue where the Jacobian matrix is rank-deficient when solving nonlinear objective functions $4 - 10$.

From the perspective of robustness, LM method is proven to have the best performance because it solves almost all test functions, although sometimes more iterations are required. It should be noted that mLM algorithm requires fewer number of iteration for poorly scaled problems compared to classical LM algorithm and functions number 5, 8 and 10 demonstrate this point. QN method performs better when solving large residual problems or highly nonlinear cost function, such as problems number 4 and 9.

Summary

Four classical methods for nonlinear least squares problems have been reviewed and tested by a relatively large set of function libraries. From the practice of numerical experiments, the following conclusions can be drawn. Firstly, simple GN method is recommended for zero residual problems and the cost function is close to linear. Secondly, On large residual problems with highly nonlinear function, QN method needs fewer iteration times. Finally, LM-type algorithms presents strong robustness and and inexpensive computing cost and is recommended for general small residual problems.

Appendix B: Automatic optimization framework implemented in Python

The Automatic Optimization Framework(AUTOPT) is implemented by Python programming language, which can run any operating system such as Windows, Linux, Unix and macOS without further codes modification and compilation. Python supports multiple programming paradigms and procedural programming is used in this framework. It should be noted that all codes are based on the Python 3.0 which is not completely backward compatible with Python 2.0.

LS-DYNA, LS-Reader and gradient-based optimization algorithm are the main components of this framework, where LS-DYNA is a general-purse FE software capable of modelling and solving metal forming processes. LS-Reader is designed as a special Python package for reading and extracting the binary data from LS-DYNA. Gradient-based optimization tool provides the interface and environment to specify the input design parameters and post-processing the simulated data from LS-Reader.

The first step of this framework is to define the initial values for FE simulation and optimization, and the detailed codes are shown in Fig. B.1. Key process parameters and simulation time in FE simulation, damping parameters, weighted factors, and stopping criteria for optimization tools can be specified in this part. The collected experimental data is further read and handled in a unified format.

In the second step of this coded framework, the built FE model for metal forming processes is called to obtain the prediction results. Then LS-Reader converts the acquired binary data into decimal data and the objective function is formulated using the sum of least square error between computed and experimental data. The corresponding code is shown in Fig. B.2.

At the final and core part of this framework, the optimization tool is launched to calculate the Jacobian and Hessian matrix of the cost function

```python
#import Python packages
import numpy as np
import os
import itertools
import matplotlib.pyplot as plt
from numpy.linalg import inv,eig,matrix_rank
from datetime import datetime
import pdb
#special packages for LS-DYNA
from lsreader import D3plotReader
from lsreader import DataType
from lsreader import D3P_Parameter
from lsreader import BinoutReader
from lsreader import BINOUT_DataType
from lsreader import BINOUT_IdType
#define simulation parameters
tt = 0.021 #simulation time
exp_thic_pole = 1.18 #pole thickness
disp = 36.03 #punch displacement
fric_coe = 0.10 #friction coefficient
#define optimization starting points
iternum = 49 #the safeguard value
tao = 1E-3 #damping parameter
v = 2 #
step = 0 #iteration number
alpha  = 0.60 #weighted factor for filling height
alpha1 =  0.05 #for the thickness
alpha2 =  0.30 #distance between tube and die
alpha3 =  0.05 #punch force
eps1 = 1e-5 #stoping criteria1
eps2 = 1e-3 #stoping criteria1
xk = np.array([[400.00],[0.300]])#starting design parameters
```

Figure. B.1. The first part in the automatic optimization framework coded by Python.

```python
#run the simulation and collect the post data
print("Launch the **********************LS-DYNA*************************")
os.system('dyna_d i= T_tube_umat_half.k ncpu=-28 > dyna.temp')
print("The calculation of LS-DYNA is over and launch the LS-Reader to read binout and d3plot")
#read the binout file using lsreader
br = BinoutReader('./binout')
dr = D3plotReader('d3plot')
res = BinoutReader.is_valid('./binout')
print('The current directory is', cwd, end='; \n')
print('Check path: the path for binout file is',res,end='. \n')
#get number of branch in binout file
num_branch = br.get_data(BINOUT_DataType.BINOUT_NUM_BRANCH)
print("The number of branch in binout file is", num_branch,end='; \n')
#list branches in binout file
branches = br.get_data(BINOUT_DataType.BINOUT_BRANCHES)
for branch in branches:
    print("The branch in binary files is", branch, end='. \n')
#get number of id in rcforc branch
forc_num_id = br.get_data(BINOUT_DataType.BINOUT_RCFORC_NUM_ID)
print("The number of id in",branches[1],'is',forc_num_id,end=";\n")
#list all ids in rcforc branch
forc_ids = br.get_data(BINOUT_DataType.BINOUT_RCFORC_IDS)
print("List all ids in",branches[1],end='; \n')
for forc_id in forc_ids:
    print(forc_id, end=',')
print("Therefore, the last id in the branch",branches[1],"is",forc_id,end='. \n')
#get the number of components in rcforc branch
forc_num_component = br.get_data(BINOUT_DataType.BINOUT_RCFORC_NUM_COMPONENT)
print("The number of components in the branch",branches[1],'is',forc_num_component,end='; \n')
```

Figure. B.2. The second part in the automatic optimization framework coded by Python.

based on the finite difference approximation. New design parameters can be obtained using GN or LM algorithm and then stopping criteria evaluate whether the iteration process will be terminated. The Python code is summarized in Fig. B.3.

```
J = np.array(np.zeros((len(f0),len(xk))))#define the initial Jacobian matrix
for m in range(len(f0)):
    fx = f0
    mse = mse + fx[m,0]**2
    for n in range(len(xk)):
        J[m,n] = (hst[m,n] - fx[m,0])
H = J.T@J + u*D.T@D#define the Hessian matrix
dx = -inv(H)@J.T@fx

xk_tmp = xk.copy()
xk_tmp = xk_tmp + dx

#The criterion 1 based on the gradient
if np.linalg.norm(J.T@fx, ord =np.inf) <= eps1:
    print('The criteria NO.1 works at step', step)
    print('The initial point is', np.array([[iteration_data[0,1]],\
        [iteration_data[0,2]],[iteration_data[0,3]]]))
    print("The optimum point is ",xk)
    break
#The criterion 2 based on the step size
if np.linalg.norm(dx) <= eps2*(np.linalg.norm(xk)+eps2):
    print('The criteria NO.2 works at step',step)
    print('The initial point is', np.array([[iteration_data[0,1]],\
        [iteration_data[0,2]],[iteration_data[0,3]]]))
    print("The optimum point is ",xk)
    break
```

Figure. B.3. The final part in the automatic optimization framework coded by Python.

At Materials Processing Group in Aalborg University, a remote computer cluster running Ubuntu 14.04 LTS operating system is deployed to handle all FE simulations and numerical optimization subroutines used in this research. As shown in Fig. B.4, this cluster consists of five nodes and each node is configured with two CPUs of Intel Xeon E5-2697V3 and 251G memory. Its deployment also provides a reliable and efficient hardware foundation for the scientific computing power required in this thesis.

Figure. B.4. The computer cluster deployed at Materials Processing Group in Aalborg University.

Appendix C: Preform optimization in a two-stage sheet hydroforming

General overview

A two-stage hydroforming process has been designed to form a cylindrical cup having small radii. In this process, the intermediate preform shape formed at the first stage has a great influence on the forming quality of final parts at the second stage. The developed framework based on gradient descent strategy and FE modelling is extended to determine the optimum preform shape and geometry, in which parametric modeling technique will be used to model the preform geometry with a simple mathematical formula of two design variables, and it is embedded in the FE solver LS-DYNA to make the optimization automatic totally. Finally, the numerical experiment of this two-stage hydroforming validates its feasibility and performance.

Process principle and modelling

The two-stage hydroforming process is combined hydromechanical deep drawing with hydraulic stretch forming process. In the first stage, a hydromechanical deep drawing is used to form a three-dimensional preform with a specified bulge and this stage is divided into four steps as shown in Fig. C.1. The preform presents some features with large punch corner radius and specified shaped bulge at cup bottom which gathers materials for the second-stage forming.

Four steps are illustrated in Fig. C.1, a: filling the counter pressure pot and inserting the blank; b: closing the upper binders and loading the blank holder force; c: start the hydromechanical deep drawing with the punch force, the blank holder force and the counter pressure; d: when punch reaching the

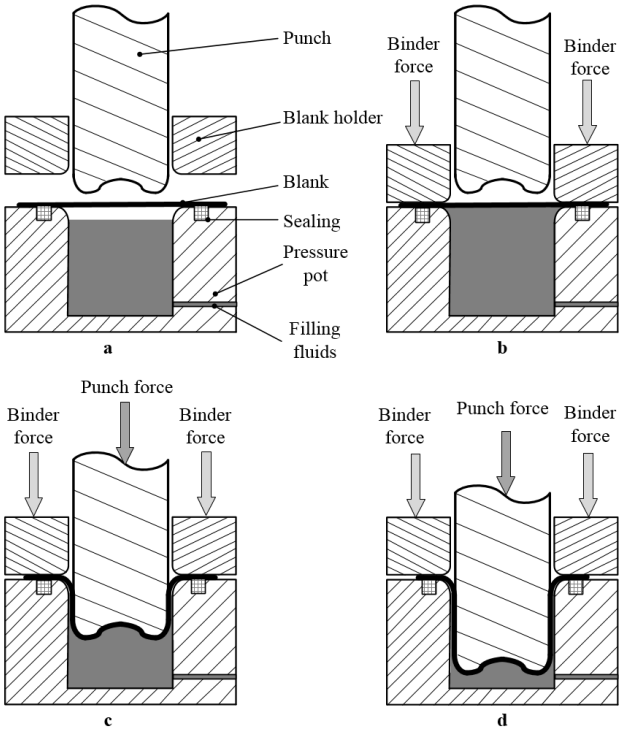

Figure. C.1. The first stage in two-stage hydroforming process

bottom, calibrating the workpiece by forming against the shaped punch with high counter pressure. This is four steps in first step of two-stage hydroforming process for parts having small radii.

In the second stage, the corner radius of three-dimensional preform is decreased further by the hydraulic stretch forming. As shown in Fig. C.2, this stage follows the next steps. a: put the preformed blank on the right place; b: close the upper binder, champ the preform tightly, and fill the counter pressure pot; c: form the small corner radii under hydraulic stretch forming with counter fluids pressure and blank holder force; d: calibrate and reduce the small radius further at workpiece corner by forming against the female die with high counter pressure.

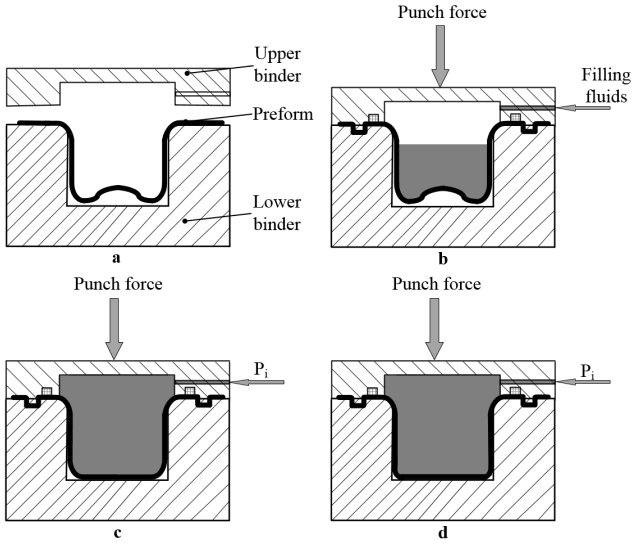

Figure. C.2. The second stage in two-stage hydroforming process

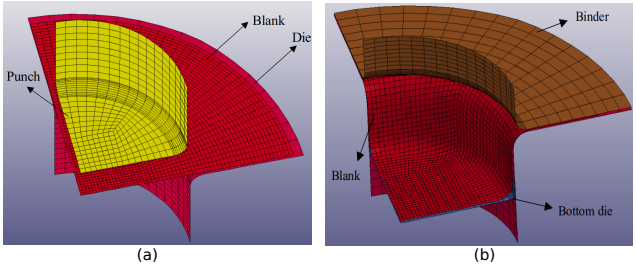

Figure. C.3. FE model of two-stage hydroforming process: (a) first stage, and (b) second stage.

The simulation of the two-stage process was performed using the FE

software LS-DYNA, and a quarter of the model is shown in Fig. C.3. The punch, die, and blank holder were set to rigid materials, and the elasto-plastic material with isotropic hardening model was used to define the flow chararteristics of blank. Materials behavior follows the Hollomon plastic flow strain hardening relation. Shell elements (Belytschko-Tsay) with five through-thickness integration points were utilized in the mesh of the workpiece. Friction between the blank and tools were modeled using the Coulomb friction law, and a friction coefficient(0.1) was set at the contacting interfaces. The pot pressure was set as a compressive stress along the normal direction applied on the blank and obeys a load mask curve which was defined using different loading path. The mesh size for the blank was chosen such that six elements at least lie on the corner radius region.

Preform design and analysis

Two kinds of shaped preforms have been designed, and the first stage hydromechanical deep drawing is used to form them. The preform cross sections are shown in Fig. C.4.

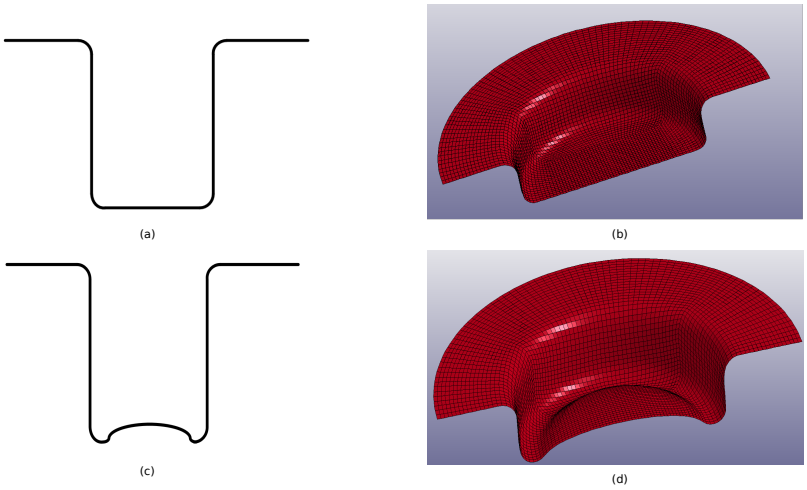

Figure. C.4. Schematic diagram of preform shape in the first stage: (a)cross section of flat preform, (b) 3D diagram of flat preform, (c) cross section of convex preform, and (d) 3D diagram of convex preform.

For the flat preform, in the forming of small radius, the blank region around the small radius has contacted with the die as shown in Fig. C.5, which causes high friction between the part and the die, and ultimately leading to the severely thinning of parts. However, when using convex three-dimensional preforms, the forming mechanism at small radius region will be

changed. It can not only reduce the pressure of hydraulic stretch forming, but also reduce the excessive thinning of radius corners. The reason why the preform enable hydraulic loads be much less can be described by a force analysis. As shown in Fig. C.6, the area 1 of preform will be flattened under internal high pressure, which generates an additional push force to move the metal towards the rounded corners. In this way, the fluids pressure is less than that required for the pure bulging and the thrust force is closely related to the bulge height, friction coefficient, and fluids pressure.

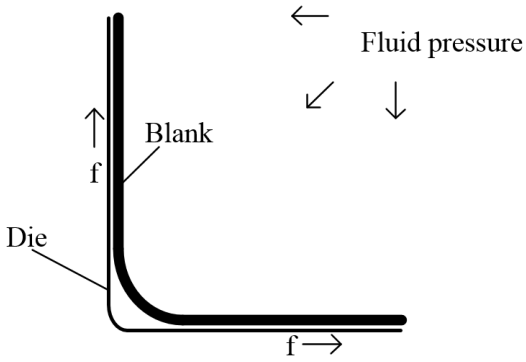

Figure. C.5. Force diagram when forming small radii with flat preform.

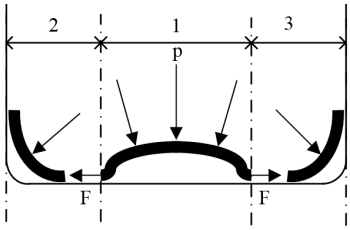

Figure. C.6. Force diagram when forming small radii with convex preform.

Moreover, the convex preform can make the plastic deformation more uniform at corner radius region and the reason behind it can be explained by metal flow rules. As demonstrated in Fig. C.6, preforms make the metal materials at region 1 and 2, 3 contact die almost simultaneously. In this way, it can reduce the friction force between cup bottom and die, and the material flow to the corner radius easily. Furthermore, plasticity deformation is evenly distributed in these two regions and avoid the deformation concentration at radius corner. Therefore, this method make the thickness distribution of components more uniform and avoids excessive thinning or fracture of radii.

Preform automatic optimization

The key research question aims to find the suitable preform shape. The developed framework combing the FE model and optimization techniques has been extend to determine the optimum three-dimensional preform geometry in this two-stage hydroforming process. Its objective is to improve the part thickness profile and avoid the risk of wrinkles.

Design variables

Parametric modeling of three-dimensional preforms requires a complex mathematical expression. To simplify the problem, its cross section can be used to generate a three-dimensional preform by rotation owing to the asymmetric. The cross section of preforms are shown in Fig. C.7 where the bulge shape can be expressed by two parameters r_1 and r_2, so the design variable can be expressed as $\mathbf{r} = [r_1, r_2]^T$.

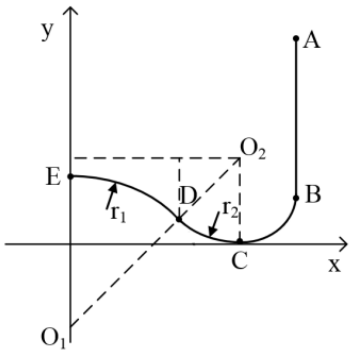

Figure. C.7. Parametric modelling of convex preform.

Objective function

Generally, fracture always appear at the punch corner of a component having small radius, because there is a severe thinning at this region. In order to characterize the forming quality of a part, the thinning ratio φ_i of an ith element can be defined as,

$$\varphi_i = \frac{t_i - t_0}{t_0} \tag{C.1}$$

where t_0 is initial shell thickness and t_i is the shell thickness of the ith element after plastic deformation. Therefore, the forming quality of an entire component can be represented by a set of thinning rates of specified elements on this part, as shown in Fig. C.8. However, the preform has different effects on

the different regions of a component, so the weight factor should be assigned to thinning rate of each different region. The objective function is sums of thinning ratio squares for selected elements and can be given below,

$$f = \sum_{i=1}^{m} (\omega_i \varphi_i)^2 \tag{C.2}$$

where ω_i is the weight factor of the ith element, and m is the number of elements selected on the part.

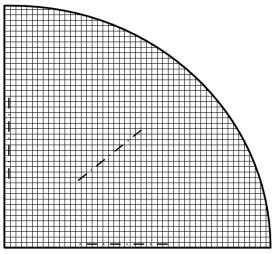

Figure. C.8. The specified elements marked by dashed line.

Results and discussion

There are two types of preform shapes with a flat and convex bulge, in which the preform with a flat bottom can be taken as a comparison. Firstly, the two-stage hydroforming process is simulated using these two preforms, and the simulation results are shown in Fig. C.9. It can be seen that the most serious thinning occurs in the part bottom area where connection to the punch corner radius region, because the material is stretched to the radius corner when forming the small radius. The thinning rate at this area with convex preform is more serious than that with flat preform, which means that convex shape do not reduce the thinning rate at punch corner radius, even leads to more serious thinning. Therefore, it is necessary to optimize the preform geometry and shape.

The initial point $\mathbf{r} = [80.00, 20.00]^T$ and the bugle shape is convex. After 14 times optimization, the preform geometry has been changed dramatically to $\mathbf{r} = [60.97, 4.77]^T$. Fig. C.10 shows that the iteration process for the objective function. The cost function decrease dramatically to 4.71 from initial 8.22, which means there is an improvement for the thinning rate at the cup bottom.

The thickness distribution of the cup with initial and optimum preform is demonstrated in Fig. C.11. It can be observed that the thinning rate at the punch corner region is improved enormously reducing to 24% from 33%.

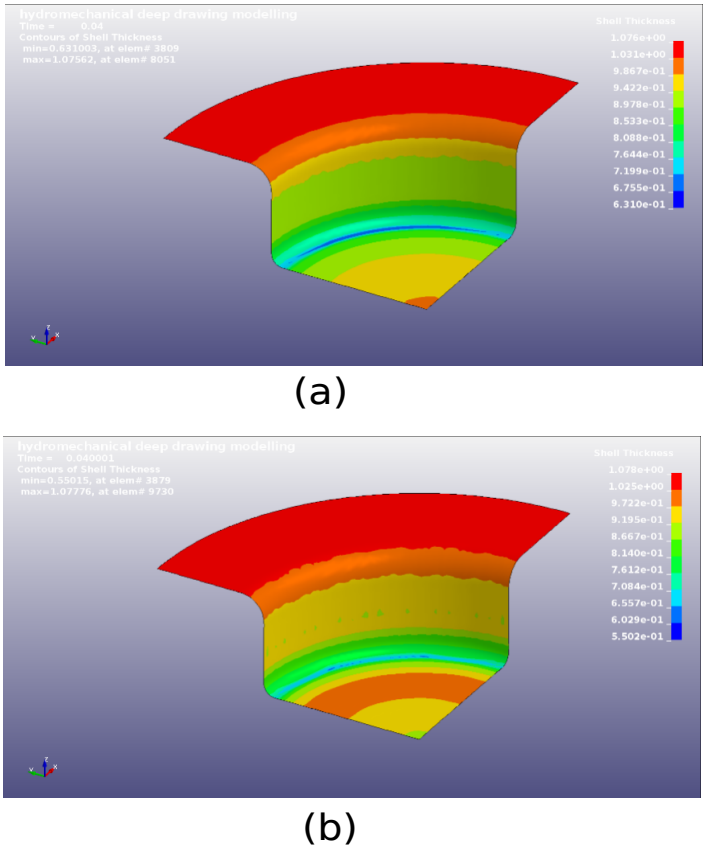

Figure. C.9. Thickness distribution using: (a)flat preform, and (b)convex preform.

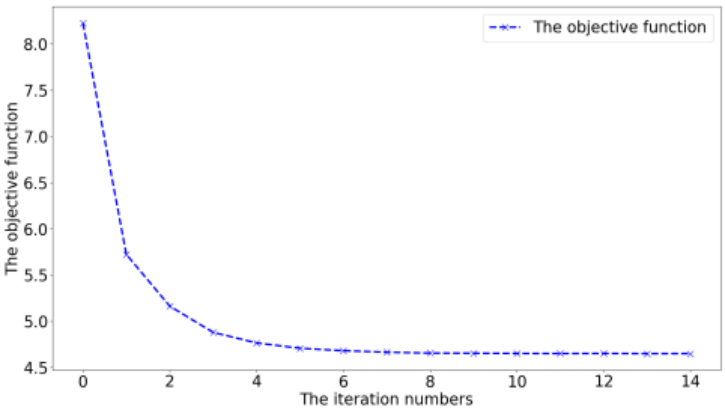

Figure. C.10. Iteration history of the objective function.

However, a disadvantage of the preform is that the thickness nonuniformity become more serious at the cup bottom. One reason for this is that the region adjacent to the sharp corner accumulate more materials from bulge, especially at the center of the bulge, so it leads to the extreme thinning of this region.

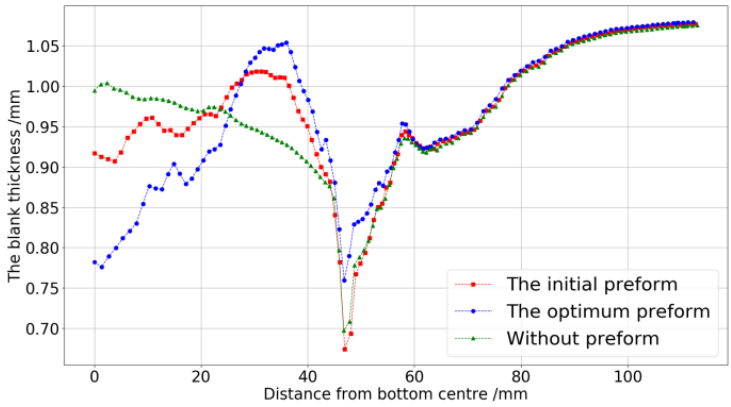

Figure. C.11. Comparison of thickness distribution using flat, initial and optimized preforms.

Summary

The developed framework has been extended to determine the optimal preform in a two-stage hydroforming process. The following conclusions are drawn:

1) The two-stage hydroforming process has the capability of forming the blank into complex shaped parts with sharp radii.

2) The height and bulge cross section of the preform can change the part thickness distribution, and not all preforms will improve thinning rate of the part. It depends heavily on the geometry and shape of the preform.

3) The proposed framework can determine the optimum intermediate preform in a multi-stage metal forming processes. Optimum convex preform can reduce thinning at the punch corner radius and increase the nonuniformity of thickness distribution at the part bottom.

Bibliography

[1] Shijian Yuan. Fundamentals and processes of fluid pressure forming technology for complex thin-walled components. *Engineering*, 7(3):358–366, 2021.

[2] Kailun Zheng, Jing-Hua Zheng, Zhubin He, Gang Liu, Denis J. Politis, and Liliang Wang. Fundamentals, processes and equipment for hot medium pressure forming of light material tubular components. *International Journal of Lightweight Materials and Manufacture*, 3(1):1–19, 2020.

[3] Muammer Koç and Taylan Altan. An overall review of the tube hydroforming (THF) technology. *Journal of Materials Processing Technology*, 108(3):384–393, 2001.

[4] A. Alaswad, K.Y. Benyounis, and A.G. Olabi. Tube hydroforming process: A reference guide. *Materials & Design*, 33:328–339, 2012.

[5] Colin Bell, Jonathan Corney, Nicola Zuelli, and David Savings. A state of the art review of hydroforming technology: Its applications, research areas, history, and future in manufacturing. *International Journal of Material Forming*, 13(5):789–828, 2020.

[6] Ch. Hartl. Research and advances in fundamentals and industrial applications of hydroforming. *Journal of Materials Processing Technology*, 167(2-3):383–392, 2005.

[7] M. Tolazzi. Hydroforming applications in automotive: A review. *International Journal of Material Forming*, 3(1):307–310, 2010.

[8] Myoung-Gyu Lee, Yannis P Korkolis, and Ji Hoon Kim. Recent developments in hydroforming technology. *Proceedings of the Institution of Mechanical Engineers, Part B: Journal of Engineering Manufacture*, 229(4):572–596, 2015.

[9] P. Venkateshwar Reddy, B. Veerabhadra Reddy, and P. Janaki Ramulu. Evolution of hydroforming technologies and its applications — A review. *Journal of Advanced Manufacturing Systems*, 19(4):737–780, 2020.

[10] Muammer Koç. *Hydroforming for advanced manufacturing*. Woodhead Publishing Limited, England, 2008.

[11] N. Boudeau, A. Lejeune, and J.C. Gelin. Influence of material and process parameters on the development of necking and bursting in flange and tube hydroforming. *Journal of Materials Processing Technology*, 125-126:849–855, 2002.

[12] Ken-ichi Manabe and Masaaki Amino. Effects of process parameters and material properties on deformation process in tube hydroforming. *Journal of Materials Processing Technology*, 123(2):285–291, 2002.

[13] P. Groche, R. Steinheimer, and D. Schmoeckel. Process stability in the tube hydroforming process. *CIRP Annals*, 52(1):229–232, 2003.

[14] Vasile Adrian Ceclan, Nicolae Balc, Sorin Grozav, Paul Bere, and Cristina Stefana Borzan. Quality of the hydroformed tubular parts. *Advanced Engineering Forum*, 8-9:215–224, 2013.

[15] Vasile Ceclan and Sorin Grozav. Determination of the force required for the hydroforming of al 99,5. In *3rd International Scientific Conference on Innovative Technologies in Engineering Production (ITEP)*, volume 244, page 01003, 2018.

[16] Muhammad Ali Ablat and Ala Qattawi. Numerical simulation of sheet metal forming: a review. *The International Journal of Advanced Manufacturing Technology*, 89(1-4):1235–1250, 2017.

[17] Bryan J. Macdonald. Finite element simulation of hydroforming processes. *Journal of the Japan Society for Technology of Plasticity*, 53(614):176–182, 2012.

[18] P.F. Bariani, T. Dal Negro, and S. Bruschi. Testing and modelling of material response to deformation in bulk metal forming. *CIRP Annals*, 53(2):573–595, 2004.

[19] S. Bruschi, T. Altan, D. Banabic, P.F. Bariani, A. Brosius, J. Cao, A. Ghiotti, M. Khraisheh, M. Merklein, and A.E. Tekkaya. Testing and modelling of material behaviour and formability in sheet metal forming. *CIRP Annals*, 63(2):727–749, 2014.

[20] H Vegter and Y An. Mechanical testing for modeling of the material behaviour in forming simulations. In *Proceedings of the 7th International Conference and Workshop on Numerical Simulation of 3D Sheet Metal Forming Processes(NUMISHEET)*, Interlaken, Switzerland, 2008.

[21] Chong Li, Daxin E, Jingwen Zhang, and Ning Yi. Investigation of the geometry of metal tube walls after necking in uniaxial tension. *Metals*, 7(3):100, 2017.

[22] Rich Davies, Glenn Grant, Darrell Herling, Mark Smith, Bob Evert, Steve Nykerk, and Jeff Shoup. Formability investigation of aluminum extrusions under hydroforming conditions. SAE Technical Paper, 2000.

[23] Woo-Jin Song, Seong-Chan Heo, Tae-Wan Ku, Jeong Kim, and Beom-Soo Kang. Evaluation of effect of flow stress characteristics of tubular material on forming limit in tube hydroforming process. *International Journal of Machine Tools and Manufacture*, 50(3):753–764, 2010.

[24] Bin Zhang, Benny Endelt, Lihui Lang, Yang Zhao, Shu Yan, and Karl Brian Nielsen. An inverse strategy to determine constitutive parameters of tubular materials for hydroforming process. *Chinese Journal of Aeronautics*, Accepted, 2021.

[25] ASTM E8. Standard test methods for tension testing of metallic materials. ASTM International, 2013.

[26] Jian Cao and Mihaela Banu. Opportunities and challenges in metal forming for lightweighting: Review and future work. *Journal of Manufacturing Science and Engineering*, 142(11):1–24, 2020.

[27] Feifei Zhang, Jun Chen, Jieshi Chen, Jian Lu, Gang Liu, and Shijian Yuan. Overview on constitutive modeling for hydroforming with the existence of through-thickness normal stress. *Journal of Materials Processing Technology*, 212(11):2228–2237, 2012.

[28] Dr Petersen, Re Link, H Wang, R Bouchard, R Eagleson, P Martin, and Wr Tyson. Ring hoop tension test (RHTT): A test for transverse tensile properties of tubular materials. *Journal of Testing and Evaluation*, 30(5):382–391, 2002.

[29] L. Jiang, J.J. Jonas, K. Boyle, and P. Martin. Deformation behavior of two Mg alloys during ring hoop tension testing. *Materials Science and Engineering: A*, 492(1-2):68–73, 2008.

[30] Zhubin He, Shijian Yuan, Gang Liu, Jia Wu, and Weiwei Cha. Formability testing of AZ31B magnesium alloy tube at elevated temperature. *Journal of Materials Processing Technology*, 210(6):877–884, 2010.

[31] Mk Samal, Ks Balakrishnan, J Parashar, Gp Tiwari, and S Anantharaman. Estimation of transverse tensile behavior of Zircaloy pressure tubes using ring-tensile test and finite element analysis. *Proceedings of the Institution of Mechanical Engineers, Part C: Journal of Mechanical Engineering Science*, 227(6):1177–1186, 2013.

[32] Chris P. Dick and Yannis P. Korkolis. Mechanics and full-field deformation study of the Ring Hoop Tension Test. *International Journal of Solids and Structures*, 51(18):3042–3057, 2014.

[33] Tarek M. A. A. El-Bagory, Maher Y. A. Younan, and Ibrahim M. Alarifi. Failure analysis of Ring Hoop Tension Test (RHTT) specimen under different loading conditions. In *ASME Pressure Vessels and Piping Conference (PVP 2018)*, Prague, Czech Republic, 2018.

[34] S.S. Panicker, K.S. Prasad, G. Sawale, S. Hazra, B. Shollock, and S.K. Panda. Warm redrawing of AA6082 sheets and investigations into the effect of aging heat treatment on cup wall strength. *Materials Science and Engineering: A*, 768:138445, 2019.

[35] E. J. Walsh and D. O. Adams. Development and evaluation of the quadrant ring test method. *Experimental Mechanics*, 48(3):319–326, 2008.

[36] Ali Khalfallah, Zied Ktari, Carlos Leitão, and José Valdemar Fernandes. New mandrel design for ring hoop tensile testing. *Experimental Techniques*, pages 1–19, 2021.

[37] Gerhard Gutscher, Hsien-Chih Wu, Gracious Ngaile, and Taylan Altan. Determination of flow stress for sheet metal forming using the viscous pressure bulge (VPB) test. *Journal of Materials Processing Technology*, 146(1):1–7, 2004.

[38] Mahmoud Nemat-Alla. Reproducing hoop stress–strain behavior for tubular material using lateral compression test. *International Journal of Mechanical Sciences*, 45(4):605–621, 2003.

[39] Vincent Busser, Marie-Christine Baietto-Dubourg, Jean Desquines, Christian Duriez, and Jean-Paul Mardon. Mechanical response of oxidized Zircaloy-4 cladding material submitted to a ring compression test. *Journal of Nuclear Materials*, 384(2):87–95, 2009.

[40] Gayan Rathnaweera, Yvonne Durandet, Dong Ruan, and Shigeaki Kinoshita. Characterizing the material properties of a tube from a lateral compression test. *International Journal of Protective Structures*, 2(4):465–475, 2011.

[41] J. Liu, H. Yang, H. W. Li, H. Li, and S. Zhu. A new hybrid identification method for determining the material parameters of thin-walled tube under compressive stress state. *Materials & Design*, 44:49–58, 2013.

[42] Laurent Bizet, Ludovic Charleux, Pascale Balland, and Laurent Tabourot. Influence of heterogeneities introduced into the modelling of a ring compression test. *Archives of Civil and Mechanical Engineering*, 17(2):365–374, 2017.

[43] Hui Chen and Li Xun Cai. Unified ring-compression model for determining tensile properties of tubular materials. *Materials Today Communications*, 13:210–220, 2017.

[44] S.R. Guillow, G. Lu, and R.H. Grzebieta. Quasi-static axial compression of thin-walled circular aluminium tubes. *International Journal of Mechanical Sciences*, 43(9):2103–2123, 2001.

[45] Faez Alhussainy, M. Neaz Sheikh, and Muhammad N.S. Hadi. Behaviour of small diameter steel tubes under axial compression. *Structures*, 11:155–163, 2017.

[46] F.C. Bardi and S. Kyriakides. Plastic buckling of circular tubes under axial compression—part I: Experiments. *International Journal of Mechanical Sciences*, 48(8):830–841, 2006.

[47] Jean Legendre, Philippe Le Grognec, Cédric Doudard, and Sylvain Moyne. Analytical, numerical and experimental study of the plastic buckling behavior of thick cylindrical tubes under axial compression. *International Journal of Mechanical Sciences*, 156:494–505, 2019.

[48] Tohid Ghanbari Ghazijahani, Hui Jiao, and Damien Holloway. Plastic buckling of dented steel circular tubes under axial compression: An experimental study. *Thin-Walled Structures*, 92:48–54, 2015.

[49] Mehdi Imaninejad, Ghatu Subhash, and Adam Loukus. Influence of end-conditions during tube hydroforming of aluminum extrusions. *International Journal of Mechanical Sciences*, 46(8):1195–1212, 2004.

[50] D.M. Woo and P.J. Hawkes. Determination of stress/strain characteristics of tubular materials. *Journal of the Institute of Metals*, 96(12):357–359, 1968.

[51] D.M. Woo. Tube-bulging under internal pressure and axial force. *Journal of Engineering Materials and Technology*, 95(4):219–223, 1973.

[52] D. M. Woo and A. C. Lua. Plastic deformation of anisotropic tubes in hydraulic bulging. *Journal of Engineering Materials and Technology*, 100(4):421–425, 1978.

[53] S. Fuchizawa, M. Narazaki, and H. Yuki. Bulge test for determining stress-strain characteristics of thin tubes. In *4th International Conference on Technology of Plasticity*, Beijing, China, 1993.

[54] Yeong-Maw Hwang and Yi-Kai Lin. Evaluation of flow stresses of tubular materials considering anisotropic effects by hydraulic bulge tests. *Journal of Engineering Materials and Technology*, 129(3):414–421, 2007.

[55] T Sokolowski, K Gerke, M Ahmetoglu, and T Altan. Evaluation of tube formability and material characteristics: hydraulic bulge testing of tubes. *Journal of Materials Processing Technology*, 98(1):34–40, 2000.

[56] Muammer Koç, Yingyot Aue-u lan, and Taylan Altan. On the characteristics of tubular materials for hydroforming—experimentation and analysis. *International Journal of Machine Tools and Manufacture*, 41(5):761–772, 2001.

[57] M Strano and T Altan. An inverse energy approach to determine the flow stress of tubular materials for hydroforming applications. *Journal of Materials Processing Technology*, 146(1):92–96, 2004.

[58] Yeong-Maw Hwang, Yi-Kai Lin, and Taylan Altan. Evaluation of tubular materials by a hydraulic bulge test. *International Journal of Machine Tools and Manufacture*, 47(2):343–351, 2007.

[59] Y. M. Hwang and C. W. Wang. Flow stress evaluation of zinc copper and carbon steel tubes by hydraulic bulge tests considering their anisotropy. *Journal of Materials Processing Technology*, 209(9):4423–4428, 2009.

[60] Yeong-Maw Hwang, Yi-Kai Lin, and Han-Chieh Chuang. Forming limit diagrams of tubular materials by bulge tests. *Journal of Materials Processing Technology*, 209(11):5024–5034, 2009.

[61] Lianfa Yang and Cheng Guo. A simple experimental tooling with internal pressure source used for evaluation of material formability in tube hydroforming. *Journal of Materials Processing Technology*, 180(1-3):310–317, 2006.

[62] L. Fllice, L. Fratini, and F. Micari. A simple experiment to characterize material formability in tube hydroforming. *CIRP Annals*, 50(1):181–184, 2001.

[63] Lianfa Yang and Cheng Guo. Determination of stress–strain relationship of tubular material with hydraulic bulge test. *Thin-Walled Structures*, 46(2):147–154, 2008.

[64] P. Bortot, E. Ceretti, and C. Giardini. The determination of flow stress of tubular material for hydroforming applications. *Journal of Materials Processing Technology*, 203(1-3):381–388, 2008.

[65] E. Ceretti, D. Braga, and C. Giardini. Steel and copper flow stress determination for THF applications. *International Journal of Material Forming*, 1(1):309–312, 2008.

[66] Raphaël Velasco and Nathalie Boudeau. Tube bulging test: Theoretical analysis and numerical validation. *Journal of Materials Processing Technology*, 205(1-3):51–59, 2008.

[67] Nathalie Boudeau and Pierrick Malécot. A simplified analytical model for post-processing experimental results from tube bulging test: Theory, experimentations, simulations. *International Journal of Mechanical Sciences*, 65(1):1–11, 2012.

[68] Abdel Hakim Ben Ouirane, Nathalie Boudeau, Raphaël Velasco, and Gérard Michel. Error evaluation on experimental stress–strain curve obtained from tube bulging test. *Thin-Walled Structures*, 49(10):1217–1224, 2011.

[69] Ali Khalfallah, Temim Zribi, and Hedi Belhadj Salah. Application of tube hydroforming in square cross-section die for inverse identification method validation. *Key Engineering Materials*, 554-557:966–973, 2013.

[70] Ali Khalfallah, Marta Cristina Oliveira, José Luís Alves, Temim Zribi, Hédi Belhadjsalah, and Luís Filipe Menezes. Mechanical characterization and constitutive parameter identification of anisotropic tubular materials for hydroforming applications. *International Journal of Mechanical Sciences*, 104:91–103, 2015.

[71] Zhubin He, Shijian Yuan, Yanli Lin, Xiaosong Wang, and Weilong Hu. Analytical model for tube hydro-bulging test, part I: Models for stress components and bulging zone profile. *International Journal of Mechanical Sciences*, 87:297–306, 2014.

[72] Zhubin He, Shijian Yuan, Yanli Lin, Xiaosong Wang, and Weilong Hu. Analytical model for tube hydro-bulging tests, part II: Linear model for pole thickness and its application. *International Journal of Mechanical Sciences*, 87:307–315, 2014.

[73] T. Kuwabara, M. Ishiki, M. Kuroda, and S. Takahashi. Yield locus and work hardening behavior of a thin-walled steel tube subjected to combined tension-internal pressure. *Journal de Physique IV*, 105:347–354, 2003.

[74] T Kuwabara. Anisotropic plastic deformation of extruded aluminum alloy tube under axial forces and internal pressure. *International Journal of Plasticity*, 21(1):101–117, 2005.

[75] Toshihiko Kuwabara and Fuminori Sugawara. Multiaxial tube expansion test method for measurement of sheet metal deformation behavior under biaxial tension for a large strain range. *International Journal of Plasticity*, 45:103–118, 2013.

[76] H. Y. Li, X. S. Wang, S. J. Yuan, Q. B. Miao, and Z. R. Wang. Typical stress states of tube hydroforming and their distribution on the yield ellipse. *Journal of Materials Processing Technology*, 151(1):345–349, 2004.

[77] Y Korkolis and S Kyriakides. Inflation and burst of anisotropic aluminum tubes for hydroforming applications. *International Journal of Plasticity*, 24(3):509–543, 2008.

[78] Yannis P. Korkolis and Stelios Kyriakides. Inflation and burst of aluminum tubes. Part II: An advanced yield function including deformation-induced anisotropy. *International Journal of Plasticity*, 24(9):1625–1637, 2008.

[79] Yannis P. Korkolis and Stelios Kyriakides. Path-dependent failure of inflated aluminum tubes. *International Journal of Plasticity*, 25(11):2059–2080, 2009.

[80] Xiaosong Wang, Weilong Hu, Shoujun Huang, and Rui Ding. Experimental investigations on extruded 6063 aluminium alloy tubes under complex tension-compression stress states. *International Journal of Solids and Structures*, 168:123–137, 2019.

[81] Y Lin, G Chu, Z He, S Yuan, and Y Yan. Complex stress-strain relations of tubular materials studied with a flexible hydroforming system. *Journal of Testing and Evaluation*, 45(4):1130–1138, 2017.

[82] Zhubin He, Kun Zhang, Yanli Lin, and Shijian Yuan. An accurate determination method for constitutive model of anisotropic tubular materials with DIC-based controlled biaxial tensile test. *International Journal of Mechanical Sciences*, 181:105715, 2020.

[83] Kun Zhang, Zhubin He, Kailun Zheng, and Shijian Yuan. Experimental verification of anisotropic constitutive models under tension-tension and tension-compression stress states. *International Journal of Mechanical Sciences*, 178:105618, 2020.

[84] Haihui Zhu, Zhubin He, Yanli Lin, Kailun Zheng, Xiaobo Fan, and Shijian Yuan. The development of a novel forming limit diagram under nonlinear loading paths in tube hydroforming. *International Journal of Mechanical Sciences*, 172:105392, 2020.

[85] Vadim V. Silberschmidt. *Mechanics of materials in modern manufacturing methods and processing techniques*. Elsevier Limited, Netherlands, 2020.

[86] Abdel Hakim Ben Ouirane, Raphaël Velasco, Gérard Michel, and Nathalie Boudeau. Error evaluation on experimental stress-strain curve obtained from tube bulging test. *International Journal of Material Forming*, 3(1):195–198, 2010.

[87] Ludovic Vitu, Nathalie Boudeau, Pierrick Malécot, Gérard Michel, and Aurélien Buteri. Evaluation of models for tube material characterization with the tube bulging test in an industrial setting. *International Journal of Material Forming*, 11(5):671–686, 2018.

[88] B. Yang, W.G. Zhang, and S.H. Li. Analysis and finite element simulation of the tube bulge hydroforming process. *The International Journal of Advanced Manufacturing Technology*, 29(5):453–458, 2006.

[89] W. J. Song, J. Kim, and B. S. Kang. Experimental and analytical evaluation on flow stress of tubular material for tube hydroforming simulation. *Journal of Materials Processing Technology*, 191(1-3):368–371, 2007.

[90] H. S. Kim, Michael Sumption, H. Lim, and E. W. Collings. Analysis of materials properties of niobium tube from the results of a virtual bulge test. In *Joint Conference on Transactions of the Cryogenic Engineering Conference (CEC)/International Cryogenic Materials Conference (ICMC)*, volume 1435, pages 305–312, Spokane, Washington, USA, 2012.

[91] H Kim, M Sumption, H Lim, and E Collings. Evaluation of mechanical properties of tubular materials with hydraulic bulge test for superconducting radio frequency (SRF) cavities. *IEEE Transactions on Applied Superconductivity*, 23(3):3500604, 2013.

[92] Jianwei Liu, Xinyu Liu, Lianfa Yang, and Huiping Liang. Determination of flow stress of thin-walled tube based on digital speckle correlation method for hydroforming applications. *The International Journal of Advanced Manufacturing Technology*, 69(1-4):439–450, 2013.

[93] H.S. Kim, M.D. Sumption, M.A. Susner, H. Lim, and E.W. Collings. Bulge testing of copper and niobium tubes for hydroformed RF cavities. *Materials Science and Engineering: A*, 654:13–20, 2016.

[94] E.J. Pavlina, C.J. Van Tyne, and K. Hertel. Hydraulic bulge testing of dual phase steel tubes produced using a novel processing route. *Journal of Materials Processing Technology*, 201(1-3):242–246, 2008.

[95] M. Saboori, H. Champliaud, J. Gholipour, A. Gakwaya, J. Savoie, and P. Wanjara. Evaluating the flow stress of aerospace alloys for tube hydroforming process by free expansion testing. *The International Journal of Advanced Manufacturing Technology*, 72(9):1275–1286, 2014.

[96] Yang Lianfa, Wang Ninghua, and Jia Huijie. Determination of material parameters of welded tube via digital image correlation and reverse engineering Technology. *Materials and Manufacturing Processes*, 31(3):328–334, 2016.

[97] Kai Wu, Xiaoxing Li, Yulong Ge, and Shangwen Ruan. Determination of tubular material parameters in bulging test with three-dimensional digital image correlation method. *The International Journal of Advanced Manufacturing Technology*, 96(5-8):2091–2099, 2018.

[98] Shijian Yuan, Wencai Xie, Yanli Lin, and Zhubin He. Analytical model and testing method for equivalent stress-strain relation of anisotropic thin-walled steel tube. *Journal of Testing and Evaluation*, 47(2):775–790, 2019.

[99] Guolin Hu and Chunrong Pan. Investigation of the plastic hardening of metal thin-walled tube under pulsating hydraulic loading condition. *Journal of Mechanical Science and Technology*, 34(11):4743–4751, 2020.

[100] L. Yang, Y. Fu, Y. He, J. Ma, and J. Guo. Determination of constitutive relationships of tubular materials at various strain rates using hydro-bulging experiments. *Experimental Techniques*, 44(1):127–136, 2020.

[101] Yulong Ge, Xiaoxing Li, and Lihui Lang. Inverse approach to evaluate the tubular material parameters using the bulging test. *Advances in Materials Science and Engineering*, 2015:1–9, 2015.

[102] Jianwei Liu, Xinyu Liu, Lianfa Yang, Guolin Hu, and Huijie Jia. Constructing curvilinear equation of bulging profile for tube based on digital speckle correlation method(In Chinese). *Forging & Stamping Technology*, 39(4):31–35, 2014.

[103] Jing Li and Lianfa Yang. Comparison of constitutive relationships of tubes established using uniaxial tensile tests and tube hydroforming experiments. In *10th International Conference and Workshop on Numerical Simulation of 3D Sheet Metal Forming Processes (NUMISHEET)*, volume 734, 2016.

[104] Karl Brian Nielsen. *Sheet metal forming simulation using explicit finite element methods*. PhD thesis, Aalborg University, Denmark, 2000.

[105] Zhenfan Wang and Xianghua Liu. *Energy principle and it's application in metal forming(In Chinese)*. Science Press, Beijing, 2009.

[106] L.A. Moreira Filho and H.A. Al-Quereshi. Unconventional tee forming on metal tubes. *Journal of Manufacturing Science and Engineering*, 107(4):392–396, 1985.

[107] L.A. Moreira Filho, J.C. Menezes, and H.A. Al-Qureshi. Analysis of unconventional tee forming on metal tubes. *Journal of Materials Processing Technology*, 45(1-4):383–388, 1994.

[108] Cristiano Roberto Martins Foli, Miguel Ângelo Menezes, and Lindolfo Araújo Moreira Filho. Alternative process for unconventional forming of junction in thin-walled metal tubes. In *17th International Congress of Mechanical Engineering*, 2003.

[109] Cristiano Roberto Martins Foli, Miguel Ângelo Menezes, and Lindolfo Araújo Moreira Filho. Influence of the yielding criterion on total forming force in metallic junctions using elastomers. *Journal of Materials Processing Technology*, 179(1-3):61–66, 2006.

[110] Cristiano Roberto Martins Foli, Miguel Ângelo Menezes, and Lindolfo Araújo Moreira Filho. Finite element analysis of the total forming force of thin-walled metallic tube junctions employing elastomers. In Andreas Öchsner, Lucas F. M. da Silva, and Holm Altenbach, editors, *Materials with Complex Behaviour II*, volume 16, pages 419–431. Springer, Berlin, Heidelberg, 2012.

[111] J. C. Gelin and O. Ghouati. An inverse method for material parameters estimation in the inelastic range. *Computational Mechanics*, 16(3):143–150, 1995.

[112] J. C. Gelin and O. Ghouati. The inverse approach for the determination of constitutive equations in metal forming. *CIRP Annals*, 44(1):189–192, 1995.

[113] Omar Ghouati and Jean-Claude Gelin. A finite element-based identification method for complex metallic material behaviours. *Computational Materials Science*, 21(1):57–68, 2001.

[114] N. Distéfano. On the identification problem in linear viscoelasticity. *ZAMM - Zeitschrift für Angewandte Mathematik und Mechanik*, 50(11):683–690, 1970.

[115] Robert H. Iding, Karl S. Pister, and Robert L. Taylor. Identification of nonlinear elastic solids by a finite element method. *Computer Methods in Applied Mechanics and Engineering*, 4(2):121–142, 1974.

[116] Edward I-Ho Lin and Jerome L. Sackman. Identification of the dynamic properties of nonlinear vicoelastic materials and the associated wave propagation problem. *International Journal of Solids and Structures*, 11(10):1145–1159, 1975.

[117] P Pedersen and P.S Frederiksen. Identification of orthotropic material moduli by a combined experimental/numerical method. *Measurement*, 10(3):113–118, 1992.

[118] Giancarlo Gioda and Shunsuke Sakurai. Back analysis procedures for the interpretation of field measurements in geomechanics. *International Journal for Numerical and Analytical Methods in Geomechanics*, 11(6):555–583, 1987.

[119] Kenneth T. Kavanagh. Extension of classical experimental techniques for characterizing composite-material behavior. *Experimental Mechanics*, 12(1):50–56, 1972.

[120] MAN Max Hendriks. *Identification of the mechanical behavior of solid materials*. PhD thesis, Eindhoven University of Technology, Netherlands, 1991.

[121] C.W.J. Oomens, M.R.v. Ratingen, J.D. Janssen, J.J. Kok, and M.A.N. Hendriks. A numerical-experimental method for a mechanical characterization of biological materials. *Journal of Biomechanics*, 26(4-5):617–621, 1993.

[122] Jean-Loup Chenot, E Massoni, and JL. Fourment. Inverse problems in finite element simulation of metal forming processes. *Engineering Computations: Int J for Computer-Aided Engineering*, 13(2-4):190–225, 1996.

[123] Robertt A. F. Valente, António Andrade-Campos, José F. Carvalho, and Paulo S. Cruz. Parameter identification and shape optimization: An integrated methodology in metal forming and structural applications. *Optimization and Engineering*, 12(1-2):129–152, 2011.

[124] Éric Markiewicz, Bertrand Langrand, and Delphine Notta-Cuvier. A review of characterisation and parameters identification of materials constitutive and damage models: From normalised direct approach to most advanced inverse problem resolution. *International Journal of Impact Engineering*, 110:371–381, 2017.

[125] P. A. Prates, A. F. G. Pereira, N. A. Sakharova, M. C. Oliveira, and J. V. Fernandes. Inverse strategies for identifying the parameters of constitutive laws of metal sheets. *Advances in Materials Science and Engineering*, 2016:1–18, 2016.

[126] P A Prates, J V Fernandes, M C Oliveira, and N A Sakharova. Inverse analysis methodology on metal sheets for constitutive parameters identification. *International Journal of Materials Engineering Innovation*, 4(2):101–116, 2013.

[127] S. Schmaltz and K. Willner. Comparison of different biaxial tests for the inverse identification of sheet steel material parameters: Comparison of different biaxial tests for the inverse identification. *Strain*, 50(5):389–403, 2014.

[128] Hamdi Aguir, Hédi BelHadjSalah, and Ridha Hambli. Parameter identification of an elasto-plastic behaviour using artificial neural networks–genetic algorithm method. *Materials & Design*, 32(1):48–53, 2011.

[129] L. C. Reis, P. A. Prates, M. C. Oliveira, A. D. Santos, and J. V. Fernandes. Inverse identification of the Swift law parameters using the bulge test. *International Journal of Material Forming*, 10(4):493–513, 2017.

[130] P.-A. Eggertsen and K. Mattiasson. On the modelling of the bending–unbending behaviour for accurate springback predictions. *International Journal of Mechanical Sciences*, 51(7):547–563, 2009.

[131] A. F. G. Pereira, P. A. Prates, N. A. Sakharova, M. C. Oliveira, and J. V. Fernandes. On the identification of kinematic hardening with reverse shear test. *Engineering with Computers*, 31(4):681–690, 2015.

[132] Q. Yin, C. Soyarslan, A. Güner, A. Brosius, and A.E. Tekkaya. A cyclic twin bridge shear test for the identification of kinematic hardening parameters. *International Journal of Mechanical Sciences*, 59(1):31–43, 2012.

[133] Benny Endelt. *Least square optimization techniques applied on sheet metal forming - Inverse identification of constitutive parameters and optimization of process parameters*. PhD thesis, Aalborg University, Denmark, 2003.

[134] Benny Endelt and Joachim Danckert. Identification of friction coefficients and hardening parameters using optimization methods coupled with a 3D finite element code. *Journal of Materials Processing Technology*, 209(8):4005–4010, 2009.

[135] T. Zribi, A. Khalfallah, and H. Belhadjsalah. Inverse method for flow stress parameters identification of tube bulge hydroforming considering anisotropy. *International Journal of Mechatronics and Manufacturing Systems*, 4(5):441–453, 2011.

[136] Temim Zribi, Ali Khalfallah, and Hedi BelHadjSalah. Experimental characterization and inverse constitutive parameters identification of tubular materials for tube hydroforming process. *Materials & Design*, 49:866–877, 2013.

[137] Ali Khalfallah. Experimental and numerical assessment of mechanical properties of welded tubes for hydroforming. *Materials & Design*, 56:782–790, 2014.

[138] Erfan Asaadi and P. Stephan Heyns. Flow stress identification of tubular materials using the progressive inverse identification method. *Engineering Computations*, 33(5):1472–1489, 2016.

[139] M. H. A. Bonte, A. H. van den Boogaard, and J. Huétink. An optimisation strategy for industrial metal forming processes: Modelling, screening and solving of optimisation problems in metal forming. *Structural and Multidisciplinary Optimization*, 35(6):571–586, 2008.

[140] Y. Xu, L. C. Chan, Y. C. Tsien, L. Gao, and P. F. Zheng. Prediction of work-hardening coefficient and exponential by adaptive inverse finite element method for tubular material. *Journal of Materials Processing Technology*, 201(1):413–418, 2008.

[141] Ganesh M. Kakandikar and Vilas M. Nandedkar. *Sheet metal forming optimization: Bioinspired approaches*. CRC Press, Boca Raton, 2018.

[142] Jasbir Arora. *Introduction to optimum design*. Elsevier, Cambridge, 2016.

[143] P. Landkamer, B. Söhngen, P. Steinmann, and K. Willner. On gradient-based optimization strategies for inverse problems in metal forming. *GAMM-Mitteilungen*, 40(1):27–50, 2017.

[144] Wenyu Sun and Yaxiang Yuan. *Optimization theory and methods: Nonlinear programming*. Springer, New York, 2006.

[145] A. Andrade-Campos, S. Thuillier, P. Pilvin, and F. Teixeira-Dias. On the determination of material parameters for internal variable thermoelastic–viscoplastic constitutive models. *International Journal of Plasticity*, 23(8):1349–1379, 2007.

[146] J. P. Ponthot and J. P. Kleinermann. A cascade optimization methodology for automatic parameter identification and shape/process optimization in metal forming simulation. *Computer Methods in Applied Mechanics and Engineering*, 195(41-43):5472–5508, 2006.

[147] J F Carvalho, P S Cruz, R A F Valente, and A Andrade-Campos. An integrated methodology for parameter identification and shape optimization in metal forming and structural applications. In *International Conference on Engineering Optimization*, Rio de Janeiro, Brazil, 2008.

[148] Y. Tsompanakis, N. D. Lagaros, and G. E. Stavroulakis. Soft computing techniques in parameter identification and probabilistic seismic analysis of structures. *Advances in Engineering Software*, 39(7):612–624, 2008.

[149] Changwu Huang, Abdelkhalak El Hami, and Bouchaïb Radi. Metamodel-based inverse method for parameter identification: elastic–plastic damage model. *Engineering Optimization*, 49(4):633–653, 2017.

[150] D. Y. Li, Y. H. Peng, and J. L. Yin. Optimization of metal-forming process via a hybrid intelligent optimization technique. *Structural and Multidisciplinary Optimization*, 34(3):229–241, 2007.

[151] B.M. Chaparro, S. Thuillier, L.F. Menezes, P.Y. Manach, and J.V. Fernandes. Material parameters identification: Gradient-based, genetic and hybrid optimization algorithms. *Computational Materials Science*, 44(2):339–346, 2008.

[152] R. de Carvalho, R. A. F. Valente, and A. Andrade-Campos. Optimization strategies for non-linear material parameters identification in metal forming problems. *Computers & Structures*, 89(1-2):246–255, 2011.

[153] Miguel Vaz, Marco A. Luersen, Pablo A. Muñoz-Rojas, and Robson G. Trentin. Identification of inelastic parameters based on deep drawing forming operations using a global–local hybrid Particle Swarm approach. *Comptes Rendus Mécanique*, 344(4-5):319–334, 2016.

[154] Jorge Nocedal and Stephen J. Wright. *Numerical optimization*. Springer, New York, 2nd edition, 2006.

[155] Kaj Madsen, Nielen Hans Bruun, and Ole Tingleff. Methods for non-linear least squares problems. Technical Report IMM3215, Technical University of Denmark, Denmark, 2004.

[156] Jorge J. Moré. The Levenberg-Marquardt algorithm: Implementation and theory. *Numerical Analysis*, 630:105–116, 1978.

[157] John E. Dennis, David M. Gay, and Roy E. Walsh. An adaptive nonlinear least-squares algorithm. *ACM Transactions on Mathematical Software*, 7(3):348–368, 1981.

[158] Kenneth Levenberg. A method for the solution of certain non-linear problems in least squares. *Quarterly of Applied Mathematics*, 2(2):164–168, 1944.

[159] Donald W. Marquardt. An algorithm for least-squares estimation of nonlinear parameters. *Journal of the Society for Industrial and Applied Mathematics*, 11(2):431–441, 1963.

[160] Hans Bruun Nielsen. Damping parameter in Marquardt's method. Technical Report IMM-REP-1999-05, Technical University of Denmark, Denmark, 1999.

[161] Jorge J. Moré, Burton S. Garbow, and Kenneth E. Hillstrom. Testing unconstrained optimization software. *ACM Transactions on Mathematical Software*, 7(1):17–41, 1981.

ISSN (online): 2446-1636
ISBN (online): 978-87-7573-950-9

AALBORG UNIVERSITY PRESS